TERBLANCHE, DEON ETIENNE

DIGITAL SIGNAL PROCESSING OF DATA FROM CONVENTIONAL WEATHER RADAR: THE DISPLACE METHOD

PhD UP 1996

DIGITAL SIGNAL PROCESSING OF DATA FROM CONVENTIONAL WEATHER RADAR: THE DISPLACE METHOD

DEON ETIENNE TERBLANCHE

A thesis submitted in partial fulfilment of
the requirements for the degree

PHILOSOPHIAE DOCTOR (METEOROLOGY)

in the

FACULTY OF ENGINEERING

UNIVERSITY OF PRETORIA

November 1996

THESIS SUMMARY

Digital signal processing of data from conventional weather radar: The DISPLACE method

Deon Etienne Terblanche

Supervisor: Professor Johan van Heerden
Department: Civil Engineering
University: University of PRETORIA
Degree: Philosophiae Doctor (Meteorology)

Keywords: signal processing, radar, meteorology, rainfall, storm, data acquisition, stream flow, cloud seeding, rain gauges, ground clutter.

The ability of radar to probe large volumes of the atmosphere at high resolution, providing real-time data at a radar site, has advantages in studies relating to hydrology and meteorology. The information obtained from radar is comparable to that from a X-ray image as the radar beam penetrates clouds, seeing the precipitation that reveals their inner structures. The advantages of using radar to measure rainfall over large areas has been demonstrated during recent devastating floods in South Africa. During the last decade, the South African Weather Bureau (SAWB) has made a large investment in a network of weather radars. Radar also plays an important role in the National Precipitation Research Programme's (NPRP) rainfall stimulation research funded by the Water Research Commission (WRC) and the SAWB. The emphasis of this research is moving away from the relative radar measurements between seeded and non-seeded storms of randomized seeding experiments. The focus is now on absolute radar measurements needed in area experiments. The continuous upgrading of the equipment, improvements in methods used to process the data and calibrate the equipment are crucial to optimise the benefits of this investment. The latest addition to the weather radar infrastructure in South Africa has been the acquisitioning of an MRL-5 dual-wavelength radar by the WRC in 1994.

This thesis describes the development, testing and implementation of a new, improved method to process the output from a weather radar's logarithmic receiver. The processing method, called DISPLACE, has proven to have many applications, and is computationally efficient and accurate. Its applications include the processing of digitized logarithmic receiver output in order to simulate different receiver transfer functions, the processing of multi-parameter radar measurements and the filtering of ground clutter. It facilitates the computation of CAPPI's (Constant Altitude Plan Position Images) and radar-rainfall accumulation. The thesis also deals with the upgrading of South African weather radars since about 1990 through the in-house developed radar data acquisition system and the procedures established to ensure accurate calibrations. In addition, the hydrometeorological infrastructure deployed in the Bethlehem research area is used in an integrated manner to verify data obtained using the new method. This work is well timed to address the needs that are now emerging in South Africa and clearly illustrate the role the NPRP (National Precipitation Research Programme) played in reviving radar meteorology. The DISPLACE method is proving that the potential of conventional weather radar has not been fully exploited. It has also stimulated the interest of young technicians and scientists in the field of radar meteorology. This augurs well for the future use of weather radar in South Africa, both in the field of rainfall stimulation and as an integral part of systems designed to forecast and to help manage the effects of severe weather conditions.

SAMEVATTING VAN DIE PROEFSKRIF

Digitale seinverwerking vir konvensionele weerradardata: Die DISPLACE metode
Deon Etienne Terblanche

Promotor: Professor Johan van Heerden
Departement: Siviele Ingenieurswese
Universiteit: Universiteit van PRETORIA
Graad: Philosophiae Doctor (Weerkunde)

Sleutelwoorde: seinverwerking, radar, weerkunde, reënval, storm, dataversameling, stroomvloei, wolkbestroiing, reënmeters, grondgeruis.

Radar se vermoë om intyds groot volumes van die atmosfeer teen hoë resolusie af te tas het voordele vir weerkundige en hidrologiese studies. Die inligting wat met behulp van 'n radar verkry word, kan vergelyk word met die van 'n X-straal foto aangesien die radarstraal wolke deurdring en in die proses neerslag waar neem om sodoende hul interne strukture bloot te lê. Die voordele van radarbepaalde reënval oor groot areas is gedurende onlangse vloede in Suid-Afrika bevestig. Gedurende die afgelope dekade het die Suid-Afrikaanse Weerburo (SAWB) 'n radarnetwerk teen groot kapitale uitleg tot stand gebring. Radar speel ook 'n belangrike rol in die Nasionale Neerslag Navorsingsprogram (NPRP) wat deur die Waternavorsingskommissie (WNK) en die SAWB befonds word om reënvalstimulering te ondersoek. Die klêm van hierdie navorsing is besig om te verskuif van die relatiewe radarmetings tussen bestrooide en nie-bestrooide storms in ewekansige eksperimente. Die fokus is nou op absolute metings vir area-eksperimente. Die volgehoue opgradering van die toerusting, verbeterde metodes vir dataverwerking en kalibrasies is dus van kardinale belang om die volle waarde van dié belegging te ontgin. Die nuutste toevoeging tot die radar infrastruktuur is die MRL-5 dubbel-golflengte radar wat in 1994 deur die WNK aangekoop is.

Hierdie proefskrif beskryf die ontwikkeling, toetse en implementering van 'n nuwe, verbeterde verwerkingsmetode vir die uitset van 'n weerradar se logaritmiese ontvanger. Die veelsydige verwerkingstegniek staan as DISPLACE bekend. Dit is berekeningseffektief en lewer akkurate resultate. Spesifieke aanwendings sluit die verwerking van logaritmiese ontvanger uitsette om verskillende oordragsfunksies te simuleer, die verwerking van multiparameter radargegewens en die demping van grondgeruis in. Dit vergemaklik ook die transformasie van radardata na CAPPI formaat en die akkumulasie van radar-reënvalvelde. Die proefskrif beskryf verder die radar opgraderings met behulp van die plaaslik ontwikkelde radardata-versamelingstelsel asook die verbeterde kalibrasiemetodes wat sedert 1990 in Suid-Afrika in gebruik is. Verder word die hidro-weerkundige infrastruktuur, wat in die Bethlehem area ontplooi is, op 'n geïntegreerde wyse gebruik om data te toets wat met die nuwe metode versamel is. Hierdie werk is aangepak om aan die behoeftes wat tans in Suid-Afrika ontwikkel, te voldoen. Dit dui ook op die sentrale rol wat die NPRP in die herlewing van radarweerkunde in ons land gespeel het. Die DISPLACE tegniek bewys dat die volle potensiaal van konvensionele weerradar nog nie ten volle ontgin is nie en het belangstelling in radarweerkunde by verskeie jong tegnici en wetenskaplikes geprikkel. Dit is 'n positiewe teken vir die optimale gebruik van weerradar in die toekoms, beide as deel van die reënvalstimuleringsnavorsing en as 'n geïntegreerde deel van stelsels om die impakte van hewige weerkundige verskynsels beter te bestuur en te voorspel.

ACKNOWLEDGEMENT

I wish to express my appreciation to the following organisations and persons who made this thesis possible:

- This thesis is based on research conducted as part of the National Precipitation Research Programme (NPRP) of the South African Weather Bureau and the Water Research Commission. Permission to use the material is gratefully acknowledged.

- The Commission for Administration through the South African Weather Bureau (Department of Environment Affairs and Tourism) for financial support.

- The following persons are gratefully acknowledged for their assistance during the course of the study:

  Mr Gerhard Schulze
  Dr George Green
  Mr Farren Hiscutt
  Mr Dennis Dicks
  Dr Graeme Mather
  Mr Piet du Toit
  Me Marion Mittermaier
  Mr Karel de Waal
  Mr Hein Pienaar
  Mr Nico Kroese
  Mr Steve Edwards
  Mr Henning Viljoen

- Professor Johan van Heerden, my supervisor, for his guidance and support.

- A special thanks to my wife Monica and daughter Rochelle whose encouragement and love makes all the difference.

TABLE OF CONTENTS

5. THEORETICAL STUDIES AND APPLICATIONS

6. CASE STUDIES AND RESULTS

7. CONCLUSIONS AND RECOMMENDATIONS

LIST OF TABLES

LIST OF FIGURES

LIST OF SYMBOLS AND ACRONYMS

A	instantanoues echo amplitude
A_e	effective antenna cross-section
A_p	effective antenna efficiency cross-section
A_t	target cross-sectional area
c	speed of light
C	radar constant
D	drop diameter
dBZ	decibel reflectivity
f	microwave frequency
f_d	Doppler frequency
f_r	Pulse Repetition Frequency (PRF)
$f_{d\,max}$	maximum Doppler frequency
G	antenna gain
h	pulse length
k	number of independent samples
k_I	number of equivalent independent samples
k'	number of correlated samples
K	attenuation rate
$\|K\|^2$	related to the complex index of refraction, m, through $K=(m^2-1)/(m^2+2)$
L_m	microwave loss within radar system
L_r	receiver bandwidth loss
L_a	atmospheric loss
m	complex index of refraction
P_i	incident power per unit area
P_r	received power
$\overline{P_r}$	average received power
P_t	peak transmitted power
P_σ	target intercepted power
r	range
r_o	radius of spherical scatterer
r_{max}	maximum unambiguous range
R	rainfall rate
S	backscattered power per unit area at antenna
T_s	pulse repetition time
V	radial velocity
V_{max}	maximum unambiguous velocity
V_m	contributing volume
Z	reflectivity factor
Z_{DR}	differential reflectivity
Z_e	effective reflectivity factor
Z_H	horizontally polarized reflectivity
Z_V	vertically polarized reflectivity
η	radar reflectivity
θ	horizontal beamwidth
λ	wavelength

$\rho( )$	autocorrelation coefficient
σ	Backscattering cross-section
σ_i	backscattering cross-section of a single target
σ^2	variance
σ_a^2	variance due to different dropsize fall speeds
σ_b^2	variance due to beam broadening
σ_r^2	variance due to antenna rotation
σ_s^2	variance due to wind shear
σ_t^2	variance due to turbulence
σ_v^2	velocity variance
σ_x^2	variance of the linear detected received signal for precipitation
σ_y^2	variance of the linear detected composite received signal (ground clutter and precipitation)
τ	pulse duration
$\tau_{0.01}$	decorrelation time
ϕ	vertical beamwidth

ACC	Antenna control card
ATI	Area-Time Integral
BEWMEX	Bethlehem Weather Modification Experiment
BPRP	Bethlehem Precipitation Research Project
CAPPI	Constant Altitude Plan-Position Indicator
COHO	Coherent Oscillator
CSIR	Council for Scientific and Industrial Research
DISPLACE	Digital signal processing for logarithmic, linear and quadratic responses
DSD	Dropsize distribution
DSP	Digital Signal Processor
DWAF	Department of Water Affairs and Forestry
NPRP	National Precipitation Research Programme
PAWS	Programme to Augment Water Supplies
PEP	Precipitation Enhancement Programme
PRF	Pulse Repetition Frequency
Radar	Radio detection and ranging
RCC	Radar Control Card
RDAS	Radar Data Acquisition System
RDF	Radio Direction Finding
RVPC-1	Version 1 of the Radar Video Processor Card
RVPC-2	Version 2 of the Radar Video Processor Card
SAWB	South African Weather Bureau
STALO	Stable local oscillator
TITAN	Thunderstorm Identification, Tracking And Nowcasting
UHF	Ultra High Frequency
VHF	Very High Frequency
VP	Digitized video processor value
WRC	Water Research Commission

CHAPTER 1

BACKGROUND AND INTRODUCTION

1.1 THE BACKGROUND TO THIS STUDY

The weather-radar infrastructure in South Africa represents a capital investment of about twenty million Rand. The South African Weather Bureau (SAWB) operates nine Enterprise C-band radars. The Water Research Commission (WRC) owns a Pacer C-band radar and a Russian built MRL-5 dual-wavelength radar.

Since the beginning of this decade the National Precipitation Programme (NPRP) was central to most basic radar meteorological research and development in South Africa. The SAWB's radar group in Pretoria concentrated on networking the radars and developing operational forecasting aids. The NPRP, in contrast, focussed on improving the performance of the radars that they operated. This included modernizing the processing, display and storage of radar data and doing thorough performance testing. As NPRP personnel are actively using radar data as part of the precipitation enhancement research programme, they are in a position to identify areas where improvements can be made. As co-programme leader of the NPRP, the author is in the fortunate position to be actively involved in both the technical and scientific aspects of the developments. The fact that the NPRP's research is developing towards area experiments means that radars have an increasingly important role to play. As part of the preparations for area experiments, extended rain-gauge networks were deployed for radar-rain-gauge comparisons. The capable and dedicated technical personnel of the NPRP ensured that the upgrades were implemented successfully for quality data collection. These data provided the opportunity to show potential users the benefits of radar technology and of the NPRP's radar development (Terblanche et al., 1993).

An in-house developed radar data acquisition system (RDAS) was introduced on all meteorological radars in South Africa. At this stage, two overseas radars have been upgraded in a similar manner. The system made a large contribution to the SAWB networking efforts and led to standard radar formats and calibration methods across the country. This is a unique accomplishment. Radar data is now being used as input to hydrological models and is also beginning to form an integral part of managing reservoirs, especially during floods. The infrastructure and continuous developments of the NPRP is central to the revival of radar meteorology in South Africa. This was timely as, by the beginning of the 1990's, the small group of NPRP researchers were the only people actively using radar. Radar meteorology is now seen as a multifaceted technology that can benefit science and the people of South Africa.

The essence of this thesis is the development, implementation and testing of a new digital signal processing method which is ideal for radar data processing. This method is called *DISPLACE*, an acronym coined by the author for *di*gital *s*ignal *p*rocessing for *l*ogarithmic, line*ar* and quadratic *re*sponses. This acronym also describes the processing concept whereby displacement values are applied to data values in order to simulate more complex mathematical operations. Secondary to this, the applications of *DISPLACE* are shown using the NPRP's hydrometeorological infrastructure and research tools. The timing

of the work should be viewed against the background of the needs that are now emerging from the precipitation enhancement research programme and the hydrometeorological community in South Africa.

1.2 A SHORT HISTORY OF THE USE OF RADAR IN METEOROLOGY

Leading up to, and during World War 2, radar was developed primarily to detect and determine the range and position of aircraft for military applications. The acronym radar, for radio detection and ranging, was coined in the 1940's. Through increased output power, improved sensitivity and refinements to antennae and receivers, this technology soon found applications in other fields including meteorology. The radar beam penetrates clouds, seeing the precipitation that reveals their internal structures. A thorough treatment of the development and use of radar in meteorology can be found in Atlas (1990). Textbooks on the theory and applications of weather radar are those by Atlas (1964), Skolnik (1970, 1981), Battan (1973) and Doviak and Zrnic (1984).

1.2.1 An International Perspective

At least four countries - France, Britain, the USA and the former USSR - claim the credit for the invention of radar. However, radar in the sense that we understand it today, is an American invention. In 1923 two American scientists, Breit and Tuve (1926), used radar principles to establish that the height of the ionosphere was approximately 160 km.

The United Kingdom played a leading role in the development of radar as a military device. As the war clouds gathered during the late 1930's it was clear to the British that they would be on the front line. Finding a method for the detection of approaching enemy bombers was becoming more and more pressing. The radio physicist Watson-Watt successfully demonstrated to the British Government the use of radar principles in 1936, utilising a shortwave radio transmitter, to detect aircraft. This lead to the development and deployment of a series of radar stations (known as RDF units (Radio Direction Finding)) along the east coast of England by early 1939. These radars remained in operation without major changes throughout World War 2. At the outbreak of the War, Britain, Germany and the United States had radar systems for aircraft detection and warning, anti-aircraft fire control and airborne search using frequencies in the VHF and UHF bands. Churchill, in his World War 2 memoirs, refers to the 'decisive role' played by radar in the outcome of the War.

The highly secret invention of the resonant cavity magnetron at the University of Birmingham in Britain paved the way for the development of microwave (centrimetric) radar. The first working examples (S-band) were produced in the middle of 1940. This technology was provided to the USA shortly thereafter. Enemy intelligence failed to discover even the use of these frequencies until mid-1943, giving the Allies a decisive advantage, especially in the airborne offensive against the German U-boats. It was using radar operating at these wavelengths that storms and precipitation were observed the first time. The first reported radar observation of a rain shower was made in Britain in February 1941.

The foundations for radar meteorology were laid by Ryde (1941), while working at the General Electric Research Laboratories in England. The research was in anticipation of the widespread use of micro-wave radar and the effects weather would have at these short wavelengths. Their work included theoretical and observational studies on the reflectivity and attenuation of rain and hail as a function of precipitation rate and wavelength, as well as studies of the 'bright band'. Therefore, they provided the base for the quantitative relationship between reflectivity and rain intensity.

Quantitative measurements of precipitation gained momentum after World War 2 with the work of Marshall et al. (1947) and Marshall and Palmer (1948) from the Stormy Weather Group in Canada. They showed that the rain rate and radar reflectivity could be related by a simple power law, called a Z-R relationship, which assumes an exponential drop size distribution (DSD). Although measurements around the world soon proved that a wide range of Z values could represent the same rain rate, the universal Z-R relationship suggested by Marshall and Palmer did however invigorate radar measurements and research. The M-P exponential drop size distribution has held its own throughout the years as the simplest accurate description of average drop spectra.

The use of radar to improve short range weather forecasting was soon apparent. It is not surprising that the USA played a major role in this regard as damage to property and the loss of life due to severe weather are common in North America. The Thunderstorm Project, conducted in Florida and Ohio during 1946 and 1947, using radar as an important observational tool, provided new insight into convective storms (Byers and Braham, 1949). Another event of major historical significance was the first documented account of the 'hook' echo that coincided with a tornado in Illinois in April 1953. This observation led to the almost immediate formation of the Texas Tornado Warning Network, a cooperative radar project. A network of conventional S-band weather radars (WSR-57) was established in the USA and led to the extensive use of radar by the National Weather Service between 1960 and 1990. The Digital Video Processor (DVIP) unit, developed towards the late 1960's, made digital data collection possible. Even before the introduction of the NEXRAD (Next Generation Weather Radar - S-band Doppler) network in the USA towards the late 1980's, it was stated that 80 percent of all severe weather warnings issued by the US National Weather Service were based on radar observations.

The first meteorological observations using Doppler radar were made in May 1953 at the Cavendish Laboratory in England. The measured Doppler spectrum (in the vertical) in a shower agreed with the spectrum expected from a model drop-size distribution, but the measured spectrum was displaced by an amount consistent with a down draft of 2 m s^{-1}. In June 1958 wind speeds of up to 92 m s^{-1} were measured in a tornado for the first time in Kansas. The limitations on data processing capabilities limited the full utilization of Doppler radar up to about 1965. Prior to this date, although its applications in meteorology was amply demonstrated, it remained a "laboratory" tool, since the data analysis was tedious and labour intensive. After 1965 developments came rapidly as breakthroughs were made in data processing. With the introduction of pulse-pair processing and the fast Fourier transform (Radar Conference in 1972), Doppler radar research, was well launched by 1975. The capabilities of Doppler radar are coming of age in the NEXRAD network.

The importance of polarimetry in radar was immediately evident after the early investigations of the ionosphere by Breit and Tuve (1926) and therefore formed an essential

component of the very first radars. Although the significance of polarization was evident from the early stages of research it received little attention through the 1960's, compared to other radar research opportunities. Early work by Atlas (1951) formed the basis for the differential reflectivity concepts further developed by Seliga and Bringi (1976) which shed light on the sizes of the hydrometeors due the axial ratio dependency on size. Some of the early meteorological observations using polarization techniques were those carried out at the Massachusetts Institute of Technology (MIT) around 1955. In both the USSR and Canada contributions were also made during the 1950's and 1960's. Throughout this period studies relating to quantitative reflectivity and rain rate measurements, the structure of precipitating systems and the development of Doppler techniques dominated.

1.2.2 A South African Perspective

The first South African radar was built in 1939 under the leadership of Dr Basil Schonland of the Bernard Price Institute of Geophysical Research at the University of the Witwatersrand. Hewitt (1975) gave an interesting account of these early years of radar in South Africa. Just before World War 2, the British Government notified Commonwealth countries, in extreme secrecy, of the RDF system. They invited senior scientists to the United Kingdom to acquaint them with the principles involved. Each country could then assist with the introduction of these systems in their own countries. Although no one went from South Africa, Dr Schonland and his Institute (which now fell under the Department of Defence), obtained some rather vague documents on the principles involved. They set out, using local components, to build South Africa's first radar. It generated about 5 kW of transmitter power, had a pulse length of twenty microseconds, a pulse repetition frequency of 50 Hz and a wavelength of about 3.5 m. The antenna consisted of an aerial system producing a beam width of about thirty degrees. The first radar echo was observed on 16 December 1939 and was thought to be from the Northcliff Water Tower in Johannesburg.

Upgraded and modified versions of this radar saw service at the four South African ports, East Africa and the Middle East. They were used for the detection of aircraft during the first few years of the War in the hands of the Special Signals Services. For the first two or three years of the War, South Africa relied on the locally designed and built equipment for its coastal defence. The first microwave radars, supplied by the Royal Navy, were installed on Signal Hill and at Cape Point during 1943 to monitor shipping movements.

After the war, in 1946, a couple of junior members of Dr Schonland's team formed the basis of the Telecommunications Research Laboratory of the Council for Scientific and Industrial Research (CSIR) of which he was the first president. The CSIR, in association with the South African Air force and the Weather Bureau and inspired by the then recent cloud seeding results in the USA, conducted a glaciogenic seeding experiment on the Highveld in an attempt to enhance rainfall during the summer of 1947/1948 (CSIR, 1948). An X-band radar based at the Laboratory's premises in Johannesburg was used to monitor the seeding effects - one of the first times radar was utilized in this role.

These early cloud seeding tests stimulated the interest at the CSIR in the formation of ice in clouds, the nature of atmospheric freezing nuclei and the supercooling of water. This later led to studies of hailstones and the storms that produce them. The study of lightning also played an

important role and radar was used during the 1950's in some of the pioneering studies (Hewitt 1953 and 1957; Miles 1952 and 1953). All this work ultimately led to the acquisition, in 1970, of a Mitsubishi S-band weather radar which was installed at Houtkoppen, near Johannesburg. A large number of documented studies was done using data collected by this system (Held and Carte, 1973; Carte and Held, 1978; and Held 1978 and 1982). Severe hail-producing storms over the Highveld were documented which highlighted some of the differences between these storms and storms in other parts of the world. One was the lack here of large steady-state storms which occur in the Northern Hemisphere. These studies also showed that the measurement of the airflow patterns in and around storms was crucial to the better understanding of these storms.

The CSIR upgraded the S-band radar to a Doppler system to obtain information on the internal flow patterns of storms by the measurement of radial velocities of the meteorological scatterers (Dicks et al, 1987). They followed the same route with a C-band radar installed in Pretoria in the late 1980's to perform South Africa's first dual Doppler convective cloud studies (Held and Gomes, 1992). Funding for the project was terminated before a third radar could be commissioned, thus effectively ending the CSIR's important contribution to Doppler studies (Carte, 1992). In his thesis, Hodson (1993) concluded the radar-rainfall studies conducted at the CSIR.

The Weather Bureau started using radar for upper-air balloon tracking in 1952/53 using British made GL3 S-band radars initially installed in Pretoria and Maun, Botswana. Similar systems were later introduced at the weather offices in Cape Town, Durban and Alexander Bay. The Pretoria GL3 set was modified in 1959 to provide PPI's and was thereafter used for the observation of storms (du Toit, 1996 - personal communication). In the second half of the 1950's a Decca X-band weather radar was installed at the then Jan Smuts Airport. During 1962 two Selenia X-band weather radars were purchased, the one for Pretoria and the other for Durban while a third one was installed at Port Elizabeth in 1963. These radars were used for weather observations and balloon tracking. In the first half of 1964 a Mitsubishi RC 4B C-band radar was installed in Bloemfontein and used for meteorological observations before being moved to Bethlehem in 1971 as part of the Bethlehem Weather Modification Experiment (BEWMEX). An introduction to this programme, listing the equipment in use in the early years, is given in Harrison (1974). Fleischer (1980) compiled a report on the radar storm observations in the north-eastern Free State from data collected by this system during the 1978/79 summer season.

The Enterprise WSR-81 C-band radar, installed in Bethlehem during 1982, has been used for the acquisition of reflectivity data from weather targets in volume-scan mode as part of the research effort into precipitation enhancement. The radar was used to monitor the effects of glaciogenic cloud seeding, complementing the data acquired by three instrumented research aircraft. Analyses carried out on data captured by this radar include studies of first echoes and storm climatologies (Steyn and Bruintjes, 1990; Mather and Terblanche, 1993); radar responses of glaciogenic cloud seeding (Krauss et al, 1987; Gagin et al, 1986); the effects of evaporation of precipitation between cloud base and the ground (Rosenfeld, 1988) and the rainfall yield from convective storms (Rosenfeld and Gagin, 1989).

This all formed part of the glaciogenic seeding experiments conducted in the Bethlehem area during the 1980's when the name of the project was changed to the Bethlehem Precipitation research Project (BPRP). In the same period the WRC, contracting CloudQuest, carried out the

Programme to Augment Water Supplies (PAWS) in the Nelspruit area. Data collected with a Pacer C-band radar were used extensively in the evaluation of this glaciogenic seeding experiment. This radar was also used in a previous operational hail suppression programme in the same area. A thorough description of this programme and its results are given by Mather et al. (1996). During the course of PAWS, Mather (1989) developed a radar based method that discriminates between water drops or recently frozen riming water drops and low density graupel particles, using the WRC's Learjet research aircraft.

In 1990 the National Precipitation Research Programme (NPRP) was formed, formalizing co-operation between the BPRP and CloudQuest. Rapid progress was made after the formation of the NPRP. A milestone was the development of hygroscopic flares for cloud seeding (Mather and Terblanche, 1994 and 1996). Radar continued to play a central role in the research and the addition of the MRL-5 radar to the NPRP's responsibilities in 1994 provided an additional impetus. Since 1995 the NPRP's research has led to a gradual shift away from randomized seeding experiments to area experiments. In area experiments the role of radar becomes even more important for compiling accurate estimates of area rainfall. Furthermore, in these experiments absolute measurements are important. This contrasts with the emphasis on relative measurements between seeded and non-seeded storms in a randomized experiment.

Although most of the South African uses of radar were limited to reflectivity and Doppler measurements, Hodson and Peter (1964) made an early contribution to radar polimetry. Through observations they proved that raindrops fall as oblate spheroids and that hail could be identified. They were probably on the right track to discover how to use dual-polarization measurements for better estimates of rainfall and precipitation type.

Much of South Africa suffers from critical shortages of water. Not only is the average annual rainfall over the country significantly less than the global average but marked inter-annual variations in precipitation are common. Competition for the available water is growing from the demands of a growing population, expanding industrial and agricultural sectors, and from the need to maintain a healthy environment. Weather related damage from hailstorms, lightning strikes and flooding are not uncommon features. It is clear that the financial implications of South Africa's weather and water-related challenges will have an increasing impact on the country's economy. Research into the atmospheric processes involved in precipitation formation and investigations into methods to control and forecast these processes are vital as rainfall is our major source of fresh water.

Weather radar provides us with a means to probe and study the eccentricities and vagaries of our weather. Despite its limitations, which are often overemphasised, radar is effective in estimating rainfall over wide areas and is an indispensable tool for thunderstorm research and forecasting. The decline in interest and involvement in this research field in South Africa towards the end of the 1980s, has to be reversed if these challenges are to be addressed (Carte, 1992). The dual-wavelength MRL-5 forms an important part of the revival that is now taking place in radar meteorology in South Africa.

1.3 A GUIDE TO THE THESIS

The remaining chapters in the thesis deal with the theory of radar, the meteorological target and radar-rainfall measurement (Chapter 2). This is followed by a description of the Bethlehem research area and its infrastructure. The upgrades performed on the Enterprise and MRL-5 radars, the calibration procedures and modes of operation of the two radars as well as the checks carried out to verify their performance, are described (Chapter 3). Thereafter the DISPLACE method of processing radar data is derived (Chapter 4), the DISPLACE applications are developed and the implementations and performance tests are presented (Chapter 5). This is followed by case studies, illustrating the method's applications using S-band data collected during convective storm and general rain conditions (Chapter 6). In conclusion the impact of this new method on radar meteorology and its role in optimizing the use of the existing conventional weather radar infrastructure is summarised (Chapter 7). Some recommendations for the future are also given.

Chapters 1 and 2 provide the background and necessary theory for interpreting later chapters. The references in these two chapter provide additional background. Chapters 4, 5 and 6 form the core of this thesis.

CHAPTER 2

RADAR THEORY

2.0 INTRODUCTION

The first section of this chapter gives a short overview of weather radar and the principles involved, including those of Doppler measurements. In the next section the radar equation is derived in the form familiar to meteorologists. This is followed by a discussion on the signal statistics of precipitation scatterers. In the last section of the chapter, the relationship between radar measurements and rainfall is discussed, highlighting some of the methods used. As the classic Marshall-Palmer Z-R relationship will be used exclusively in this thesis, its origins will be dealt with in more detail.

This chapter gives the theoretical background to the chapters that follow. It provides the necessary information regarding the radar equation, the returned signal properties of precipitation scatterers and the relationship between radar reflectivity and rainfall.

2.1 THE METEOROLOGICAL RADAR

A conventional radar, also called a non-coherent radar (because the phase of the returning radar wave with respect to the phase of the transmitted wave is not taken into account), consists of the following main components:

- A transmitter, which produces power at microwave frequencies
- An antenna, which radiates the focused power and receives the backscattered signal
- A receiver, which detects, amplifies and transforms the received signals into video form, and
- A processing and display unit that performs averaging on the individual received samples and displays the results.

The radar transmitter generates short pulses of high frequency (f), short wavelength (λ) electromagnetic waves which are focused by a high gain steerable antenna into a narrow beam. The longer wavelengths (0.01 to 0.1 m) in the microwave band of the electromagnetic spectrum are used by weather radar. A set of letter designations exists for the frequency bands commonly used in radar; see Table 2.1 (Skolnik, 1970). The original code letters (P, L, S, X and K) were introduced during World War 2 for purposes of secrecy but some are still widely used.

Table 2.1 Radar frequency - wavelength bands.

Nomenclature	Frequency range
VHF	30 - 300 MHz
UHF	300 - 1000 MHz
P-band	230 - 1000 MHz
L-band	1 - 2 GHz
S-band	2 - 4 GHz
C-band	4 - 8 GHz
X-band	8 - 12.5 GHz
Ku-band	12.5 GHz - 18 GHz
K-band	18 - 26.5 GHz
Ka-band	26.5 - 40 GHz
Millimetre	> 40 GHz

These electromagnetic waves are Electric **E** and Magnetic **H** force fields (vectors) that propagate at the speed of light, c, and interact with matter along their paths. The frequency (f) and wavelength (λ) of these waves are uniquely related to the speed of light through:

$$c = \lambda f = 3 \times 10^8 \text{ m s}^{-1} \qquad (2.1)$$

Due to the large range of powers dealt with in radar systems, e.g. 10^{-13} W (minimum detectable signal) to 10^6 W (transmitted power), it is common to express power ratios in terms of decibels (dB) and power in terms of decibels with respect to a milliwatt (dBm).

The amplitude of the returned signal bears a relationship to losses due to propagation to the target and the target size, composition and temperature. Target range is measured in terms of the time taken for the pulse to travel to the target and back at the speed of light. The location of the target is then given by the antenna's azimuth and elevation at the time the echo is received. The maximum usable range of a radar is determined by the pulse repetition frequency (PRF) which is denoted by f_r. The maximum unambiguous range is given by $r_{max} = c/2f_r$. During the time interval between transmission of successive pulses of the radar, the returned signal is sampled (and digitized) at discrete time intervals. These intervals divide the sampled range into a number of range samples each representing a volume defined by the pulse length in range (h/2) and the angular width of the antenna beam (θ and ϕ).

The radar receiver output signal (video signal) depends on the transfer function applied to the signal amplitude at the receiver input port. Common receiver transfer functions are quadratic, linear and logarithmic and their characteristics will be discussed further in Section 2.3.

The choice of the radar transmitting frequency is a very important consideration in that the shorter wavelengths allow better resolution of the scatterers but suffer greater attenuation due to propagation. Thus the X-band pulse can detect smaller precipitating particles than the S-band pulse but suffers an appreciable amount of attenuation, a factor of some 100 times that of the S-band in heavy rain (Doviak and Zrnic, 1984). To illustrate this point: observing by radar at X-band frequencies a distant storm which is optically obscured by a nearer dense storm would return a two way attenuated signal far below that which would be the true representation of the water content in the sampled distant volume. An S-band signal, while not containing the same resolution, would not suffer any appreciable attenuation.

In addition, the frequency also determines the statistical properties of samples taken from the received signal and therefore must be taken into account when processing these samples (See Section 2.3).

Although this thesis deals with conventional radars, a short description is given of the important principles of Doppler radar as it is of relevance to later sections. These are normally coherent radars which measure the shift in microwave frequency caused by moving targets. To ensure that this can be done, either the STALO - COHO (Stable Local Oscillator - Coherent Oscillator) principle is used with a magnetron based transmitter, or a Klystron tube based transmitter is used. The latter produces pulses that are coherent. The Doppler shift frequency and the radial target velocity - positive being away from the radar - are related through:

$$f_d = -\frac{2V}{\lambda} \tag{2.2}$$

The maximum Doppler shift frequency is limited by the radar's PRF, f_r :

$$f_{d\max} = \pm \frac{f_r}{2} \tag{2.3}$$

and this also determines a maximum Doppler velocity, called the maximum unambiguous velocity, that can be measured:

$$V_{\max} = \pm f_r \frac{\lambda}{4} \tag{2.4}$$

Therefore, in Doppler radar there is a trade-off between the maximum unambiguous velocity and the maximum unambiguous range. As a meteorological target is non-coherent, a Doppler radar can in addition to the average radial Doppler velocity also measure the Doppler velocity variance σ_V^2. This is related to the relative movement of the scatterers in the contributing volume and is also influenced by the characteristics of the radar. σ_V^2 can be considered as a sum of the variances contributed by each of the following factors:

$$\sigma_V^2 = \sigma_s^2 + \sigma_b^2 + \sigma_r^2 + \sigma_d^2 + \sigma_t^2 \tag{2.5}$$

where: σ_s variance due to wind shear,
σ_b variance due to beam broadening,
σ_r variance due to antenna rotation,
σ_d variance due to different drop size fall speeds,
σ_t variance due to turbulence.

Sirmans and Doviak (1973), using the WSR-57 S-band radar, calculated the contribution from each of these factors and found that the contributions from shear and turbulence dominate.

Battan (1973) pointed out that the variance of the Doppler velocity spectrum within a radar sample volume is closely related to the frequency of the sampled received power from this volume. This relationship will be looked at in more detail in Section 2.3.

2.2 THE RADAR EQUATION

In deriving the radar equation the approach used by Battan (1973) is closely followed. Radars normally employ antennae that are highly directional, in order to concentrate the transmitted power into a narrow beam. The gain, G of the antenna is a measure of the ratio of power per unit area along the axis of the radar beam to the isotropic value. A target at range r with a cross-sectional area A_t, will therefore intercept an amount of power, P_σ equal to:

$$P_\sigma = \frac{P_t G A_t}{4\pi r^2} \tag{2.6}$$

where P_t is the power during the brief period the transmitter is operating.

Assuming that the target radiates all incident power isotropically, i.e. it does not absorb any power, the power intercepted by the radar antenna will be given by:

$$P_r = \frac{P_t G A_t A_e}{(4\pi)^2 r^4} \tag{2.7}$$

where A_e is the effective cross section of the antenna.

Based on theoretical considerations, the gain of a circular parabolic antenna reflector, can be approximately related to the aperture of the antenna by:

$$G = \frac{8\pi A_p}{3\lambda^2} \tag{2.8}$$

where $A_e = 2/3\ A_p$. It is assumed that the antenna efficiency, which depends on the efficiency of the feed and the antenna illumination, is 2/3.

By substituting (2.8) in (2.7) we now get:

$$P_r = \frac{P_t G^2 \lambda^2 A_t}{(4\pi)^3 r^4} \cong \frac{P_t A_p^2 A_t}{9\pi\lambda^2 r^4} \tag{2.9}$$

However, in practice there are no targets that scatter isotropically and therefore it is necessary to introduce a function, σ, called the back scattering cross section. This is defined as "the area intercepting that amount of power, which, if scattered isotropically, would return to the receiver an amount of power equal to that actually received". It can be written as:

$$\sigma P_i = 4\pi r^2 S \tag{2.10}$$

where P_i is the power per unit area incident on the target at range r and S is the backscattered power per unit area at the antenna.

From (2.10) and (2.9), a general radar equation, for any single target, can be written:

$$P_t = \frac{P_t G^2 \lambda^2 \sigma_i}{(4\pi)^3 r^4} \tag{2.11}$$

In (2.11), σ_i represents the backscattering cross section of a single scatterer. We need the instantaneous backscattering cross section of all particles - e.g. raindrops - that fill the volume, V_m, defined by the beam width and pulse length of the radar set. The backscattered signal voltage from a volume of randomly distributed scatterers is the sum of the signals scattered by each of the scatterers, with the phase of each signal taken into account. This quantity varies from one reflected pulse to the next as will be discussed in Section 2.3. It is therefore necessary to average the received power over a large number of independent samples to obtain an averaged received power:

$$\overline{P_r} = \frac{P_t G^2 \lambda^2}{(4\pi)^3 r^4} \sum_{i=0}^{n} \sigma_i \tag{2.12}$$

where the summation is carried out over the entire volume V_m.

The quantity V_m is approximately given by:

$$V_m = \pi \left(r\frac{\theta}{2} \right) \left(r\frac{\phi}{2} \right) \frac{h}{2} \tag{2.13}$$

where θ and ϕ are the horizontal and vertical widths of the beam at the one-way half-power (3 dB) points. A radial distance, h/2, is used as we are only interested in those scatterers that contribute to the instantaneous received power. The power backscattered by particles at a range (r + h/2) from the front of the outgoing pulse of length h will arrive at the antenna at the same time as the power backscattered by particles at range r from the rear of the outgoing pulse.

From (2.12) it now follows that:

$$\overline{P_r} = \frac{P_t G^2 \lambda^2 \theta \phi h}{512 \pi^2 r^2} \sum_{vol} \sigma_i \qquad (2.14)$$

The factor $\sum_{vol} \sigma_i$ represents a summation of σ over a unit volume and is called the radar reflectivity, η.

Till now it has been assumed that the antenna gain is uniform within its 3 dB limits, which is not true. A Gaussian beam shape assumption (Probert-Jones, 1962) can be introduced to modify (2.14) to:

$$\overline{P_r} = \frac{P_t G^2 \lambda^2 \theta \phi h}{512 (2 \ln 2) \pi^2 r^2} \sum_{vol} \sigma_i \qquad (2.15)$$

The Probert-Jones correction therefore compensates for a $16/\pi^2$ overestimation in the antenna gain that would occur otherwise.

The Rayleigh scattering law - where the spherical scatterer is small compared to the radar wavelength (about 0.1λ is small enough) - relates the backscattering cross section to the sphere radius r_o by:

$$\sigma = 64 \frac{\pi^5}{\lambda^4} |K|^2 r_o^6 \qquad (2.16)$$

with $K = (m^2-1)/(m^2+2)$ where m is the complex index of refraction of the sphere. Considering raindrops with diameters D, and by introducing a new quantity, Z, the reflectivity factor:

$$Z = \sum_{vol} D^6 = \int N(D) D^6 dD \qquad (2.17)$$

where *N(D)dD* denotes the number of scatterers per unit volume with diameters within *dD*. For raindrops, *N(D)* is the drop-size distribution (DSD).

By substituting (2.16) and (2.17) in (2.15) and using $h=c\tau$, with c the speed of light and τ the pulse duration, the well known meteorological radar equation is obtained:

$$\overline{P_r} = \frac{\pi^3 C}{1024 \ln 2}\left[\frac{P_t \tau G^2 \theta \phi}{\lambda^2}\right]\left[\frac{|K|^2 Z}{r^2}\right] \tag{2.18}$$

The first term in brackets represents the radar parameters and the second term in brackets the target parameters.

In practice three explicit loss factors should be included in (2.18), which gives us the equation of Smith (1986):

$$\overline{P_r} = \frac{\pi^3 C}{1024 \ln 2}\left[\frac{P_t \tau G^2 \theta \phi L_m L_r}{\lambda^2}\right]\left[\frac{|K|^2 Z L_a}{r^2}\right] \tag{2.19}$$

with L_m microwave loss within the radar system, associated with transmission through waveguide, antenna and radome.

L_r receiver loss due to the frequency bandwidth characteristics of the receiver (Doviak and Zrnic, 1984).

L_a atmospheric loss, due to attenuation by gasses and any particulate that may be present along the propagation path.

In logarithmic form, (2.19) can be written as:

$$10 \log Z = 10 \log \overline{P_r} + 20 \log r - C \tag{2.20}$$

The quantity 10 log Z is called the reflectivity factor in dBZ, 10 log $\overline{P_r}$ the received power in dBm (decibels relative to a milliwatt) and C the radar constant which includes all the constants and losses in the equation. The logarithmic version of the equation is useful because of the wide ranges over which $\overline{P_r}$ and Z vary.

Whenever the Rayleigh approximation does not apply due to some of the scatterers being in the Mie scattering region, as when measuring thunderstorm precipitation using short-wavelength radar ($\lambda < 10$ cm), it is accepted practice to refer to the equivalent reflectivity factor, Z_e.

2.3 SIGNAL STATISTICS OF METEOROLOGICAL SCATTERERS

The precipitation particles contained within the radar target are in continuous motion due to many factors, such as wind velocity and turbulence, as mentioned before. These targets are therefore non-coherent, in contrast to a solid object like a metal sphere, that is regarded as a coherent target. Consecutive samples from the same volume of precipitation particles therefore exhibit a large and characteristic variance.

The theory of fluctuating echoes from randomly distributed particles was developed by Marshall and Hitschfeld (1953). They showed that the instantaneous echo amplitude A (corresponding to linear detection), echo intensity A^2 (quadratic detection) and echo intensity level log A^2 (logarithmic detection), have the following probability distributions:

$$P(A)\,dA = \frac{2A}{\overline{A^2}} e^{-A^2/\overline{A^2}}\,dA, \tag{2.21}$$

$$P(A^2)\,dA^2 = \frac{1}{\overline{A^2}} e^{-A^2/\overline{A^2}}\,dA^2 \tag{2.22}$$

$$P(\log A^2)\,d\log A^2 = \frac{1}{M\overline{A^2}} \exp\left[\frac{\log A^2}{M} - \frac{1}{\overline{A^2}} e^{(\log A^2)/M}\right] d\log A^2 \tag{2.23}$$

For a meaningful interpretation of the fluctuating echoes, averaging over a number (k) of independent samples (P_i) is necessary to reduce the standard deviation (or variance) to within acceptable limits. It has for example been found that if 25 independent samples from a quadratic receiver are averaged, the measured $\overline{P_r}$ would be within 40 % (-2.2 dB to 1.5 dB) of the correct $\overline{P_r}$ 95% of the time. These discrepancies are close to the experimental errors involved in the measurement of $\overline{P_r}$. However, it has become the rule of thumb to try and reduce the variance in measured $\overline{P_r}$ to 1 dB. Independent samples are obtained from the same volume at time intervals which correspond to the time for the scatterers to reshuffle to a new state, or from adjacent volumes in range separated by a distance of at least h/2. The time interval restraint, when obtaining independent samples from the same volume, determines a dwell time in excess of that available to scan a large volume of space rapidly. A reduction of the required dwell time can therefore be achieved, at the expense of spatial resolution, by consecutively range averaging a number of independent range samples (Smith, 1995) into what we call *bin*s. In addition, these *bin*s are time averaged over a number of PRF pulses, essentially from the same *bin* volumes, but slightly displaced in azimuth due to the antenna rotation, to form what we refer to as *ray*s of averaged *range bin*s. The time averaging will be called time-azimuth averaging if done while the antenna is rotating.

When a number of samples (k′) that are not completely independent (due to sampling a volume at a rate higher than that needed to obtain complete reshuffling of the scatterers, or using range samples with dimensions < h/2 are used for averaging, the number of equivalent independent samples, k_p, is used to determine the variance reduction. The inverse of the equivalent number of time samples (called the variance reduction factor), is given by Sirmans and Doviak (1973):

$$(k_I)^{-1} = \sum_{m=-(k'-1)}^{k'-1} \frac{k'-|m|}{k'^2} \rho(mT_s) \tag{2.24}$$

where

$$\rho(mT_s) = \exp\left(-\frac{16\pi^2\sigma_v^2 (mT_s)^2}{\lambda^2} \right) \tag{2.25}$$

is the normalized autocorrelation of the time-sampled power, at intervals of mT_s (multiples of the pulse repetition time). A similar equation can be formulated for the variance reduction factor due to the averaging of correlated range samples, in which case the normalized autocorrelation of the range sampled power is used.

Equations for the variance reduction factors of the linear and logarithmic detectors have also been computed (Walker et al., 1980 and Doviak and Zrnic, 1984). It was found that although the logarithmic receiver decorrelates the output samples most, the quadratic receiver produces the least error of the three receiver types, for equal k_I.

The time to independence which is proportional to the wavelength and inversely proportional to the velocity variance, is another measure used to test the independence of sampled data. It is often defined as the time required for the autocorrelation to fall to 0.01 (Battan, 1973). As $\sigma_V^2 = 1\ m^2\ s^{-2}$ is a value commonly used for the velocity variance, the time to independence can be given by:

$$\tau_{0.01} = 1.71\lambda \times 10^{-3}\ \text{sec} \tag{2.26}$$

where λ is in cm.

Sirmans and Doviak (1973) summarized some of the statistics of averages obtained from the three common receiver types. These are shown in Table 2.2. As indicated by Doviak and Zrnic (1984) the biases in the expected averaged values for the linear and logarithmic receivers, are functions of the number of independent samples averaged, for k less than about 30. Similarly, the variance reduction formulas for the linear and logarithmic receivers are approximate equations for asymptotic large k (k greater than about 10).

Table 2.2 Comparison of expected mean values and standard deviation of estimates from the three receiver transfer functions when averaging a large number of independent samples (Sirmans and Doviak, 1973).

Receiver Transfer function	Typical dynamic range	Expected averaged value	Standard deviation (unbiased)
Linear	10^3	$\pi\overline{P_i}/4$	$1.05\overline{P_i}/\sqrt{k}$
Quadratic	10^6	$\overline{P_i}$	$\overline{P_i}/\sqrt{k}$
Logarithmic	6	$0.56\overline{P_i}$	$1.28\overline{P_i}/\sqrt{k}$

From Table 2.2 it can be seen that averaging the output from a quadratic receiver provides an unbiased estimate of mean received power. The standard deviation of the averages is also the smallest of the three receiver types. For a logarithmic or linear receiver a bias correction of 2.5 dB and 1.05 dB has to be applied to the averages when averaging is done over a large number of samples - as when the variance is reduced to 1 dB. The bias between averages obtained from two different receiver responses has also been used to provide additional information on the scatterers in the sampled volume and to discriminate between precipitation and ground clutter (Scarchilli et al., 1986; Gorgucci et al., 1986).

A logarithmic receiver is often used due to the large range of transfer function values. This is the case for all weather radars used in South Africa. Averaging range samples from a logarithmic receiver in regions where a reflectivity gradient over range occurs can cause a significantly larger bias than that expected due to Rayleigh fluctuations of the scatterers alone (Rogers, 1971; Schaffner, 1978). It is generally accepted that the reflectivity gradient problem is less significant with azimuth-time averaging at relatively slow scan rates (and wide antenna beamwidths). This limitation of the logarithmic receiver provided some of the motivation for the research that is reported in this thesis.

2.4 RADAR RAINFALL MEASUREMENTS

2.4.1 The Z-R relationship

As discussed in section 2.2, when precipitation particles are small with respect to the wavelength, the backscattered power is proportional to the reflectivity factor, Z. Empirical studies have shown a relation between Z and the rain rate, R in mm h^{-1}. This implies that radar can be used to estimate rainfall.

Probably the best known empirical relationship between Z and R is that of Marshall and Palmer (1948) who found, based on measurements of Z and the drop-size distribution (DSD), that:

$$Z=200\,R^{1.6} \qquad (2.27)$$

An exponential DSD - often a good approximation for precipitation is given by:

$$N(D) = N_o \exp -(\Lambda D) \tag{2.28}$$

where

$$N_o = 0.08\ cm^{-4} \tag{2.29}$$

and

$$\Lambda = 41 R^{-0.21} \tag{2.30}$$

The fact that Z-R relationships, based on exponential DSDs, have been widely investigated is reflected in Battan (1973). A list of more than 60 of these relationships are given. These Z-R relationships were obtained in different parts of the world, using different equipment and for various rainfall types. The large variety of Z-R relationships is partially due to the fact that reflectivity alone does not describe a precipitation dropsize distribution explicitly. It will be shown in Chapter 6 that the Marshall-Palmer Z-R relationship provides remarkably accurate radar-rainfall measurements in South Africa using a well calibrated S-band radar. It will also be argued that other factors, not related to the DSD, have a much larger effect on errors in radar-rain-gauge comparisons.

2.4.2 Multi-parameter radar measurements of rainfall

The measurement of precipitation using radar requires the interpretation of the back-scattered reflectivity resulting from the transmitted pulse. The reflectivity is related to the quantity of water in a targeted volume. Vital to the interpretation of radar measurements to obtain rainfall estimates is the composition of the cloud, its temperature and accompanying wind shears. These all interfere with the natural equilibrium of an exponential DSD. Horizontal winds slant the precipitation, causing a sorting of the drops. Turbulence can cause the lighter drops to be suspended aloft and low temperature can cause freezing of the precipitation. Thus techniques are being developed to minimise or at least measure these variations.

a. Attenuation and dual-wavelength measurements

Assume that the reflectivity is measured at two wavelengths. The one causing Rayleigh scattering (eg. S-band) and the other wavelength short enough that Mie-scattering occurs for the larger drops (eg. X-band). The difference in measured reflectivity can be used to deduce additional DSD parameters and provide information on the phase of the precipitation (Doviak and Zrnic, 1984; Wexler and Atlas, 1963). Eules (1979) computed R using remote measurements of K, the attenuation rate, from dual-wavelength radar data and a modified K-R relationship (Atlas and Ulbrich, 1974). It was found that rain rates computed in this manner were more accurate than using Z. Two simultaneous equations containing N_0 and Λ, and the back-scattered power at the two wavelengths can also be obtained (Goldhirsh and Katz, 1974).

The use of dual-wavelength techniques has been suggested for hail detection (Wexler and Atlas, 1963). Versions of this technique are widely used in the former USSR in their hail suppression experiments.

Prerequisites for dual-wavelength methods are well matched antenna beam patterns for the two wavelengths and accurately calibrated equipment. The processing of the data also requires methods that will not introduce unnecessary bias. An assumption is also made that the rain rate is constant over the resolution volume.

b. Dual-polarization measurements

This method also attempts to estimate two parameters of the DSD. It relies on the echo intensity of two orthogonally polarized waves, the one being transmitted and detected vertically and the other horizontally (Atlas, 1951; Seliga and Bringi, 1976). The basis for the dual-polarization method is the fact that raindrops fall as oblate spheroids. The ratio of the major axis (horizontal) to the minor axis (vertical) of these spheroids is a function of the dropsize (Green, 1975). The measurement of interest is called the differential reflectivity, Z_{DR}, defined as by:

$$Z_{DR} = 10 \log(Z_H/Z_V) \qquad (2.31)$$

with Z_H the horizontally polarized reflectivity and Z_V the vertically polarized reflectivity.

The method requires calculation of a small quantity which is the difference between two large measured quantities. It therefore requires unbiased estimates of Z_H and Z_V. The antenna beam patterns for vertical and horizontal polarizations must be well matched. The switching between polarizations, when using a common transmitter-receiver, requires a fast switching device that can handle the transmitter power. Alternatively, well matched dual transmitter-receiver units are required (Mueller et al., 1995).

Advantages of this method, compared to dual-wavelength techniques, include:

- Measurement of rain rate in the resolution volume without requiring the rain rate to be constant over the volume.
- The method has improved the ability to differentiate between the ice and liquid phase of water.

2.4.3 Other techniques

a. The Area-Time Integral (ATI)

The storm area can provide a fair estimate of rainfall from convective storms (Dennis et al., 1975; Smith et al., 1982). Doneaud et al. (1984) showed that better results can be obtained through a combination of storm area and duration. This method is called the Area-Time Integral (ATI). The principle involved is based on the observation that over a fairly large area (>> 100 km^2) an integral, over time and space, of those storm areas above a set rain-rate threshold is related to the area rainfall. In effect it means that over a storm's lifetime (or instantaneous over

many storms in different stages of their lifetimes) a rain-rate threshold exists above which area is related to rainfall (Atlas et al., 1990; Rosenfeld et al., 1990). It is a useful method due to its simplicity. It can be used as a simple check on other estimates of rainfall amounts. The ATI's applications in satellite measurements of rainfall have also been investigated.

b. Neural networks

Xiao and Chandrasekar (1995) showed, using Neural Network techniques, that the root mean square error between radar and gauge measurements of rainfall over four days were reduced by a factor of three, compared to results from a Z-R relationship. Using reflectivity and Z_{DR} as input to the neural network resulted in a further (smaller) improvement.

Neural network techniques are ideally suited for radar-rainfall comparisons. It is a technique that can be used to indicate magnitudes of improvement in rainfall estimates due to the introduction of additional radar parameters.

In the next chapter the research infrastructure of the Bethlehem area will be discussed. The focus will be on the radars used, their upgrades and the tests conducted to verify their performance. Reference is also made to the rain-gauge networks in the area.

CHAPTER 3

THE BETHLEHEM RADARS AND SUPPORTING INFRASTRUCTURE

3.0 INTRODUCTION

The first section of this chapter deals with the Bethlehem research area, its orography and the location of the hydrometeorological infrastructure. The infrastructure includes the MRL-5 dual-wavelength radar, the Enterprise C-band radar and two networks of tipping-bucket rain gauges. The main network covers the Liebenbergsvlei River catchment. Detailed run-off information is collected for this catchment by the Department of Water Affairs and Forestry (DWAF).

In the second section, the in-house developed radar data acquisition system (RDAS), the manner in which the antenna is controlled and the receiver data processed and stored are described. Information on the software developed to assist in radar calibrations is also given.

The third section deals with the detail characteristics of the Enterprise and MRL-5 radars, how the RDAS was interfaced to these radars and the manner in which they are routinely operated. In the last section of the chapter some of the performance tests performed on the two radars will be described.

3.1 THE STUDY AREA AND HYDROMETEOROLOGICAL INFRASTRUCTURE

The Bethlehem research area is located in the north-eastern Free State province of South Africa. This area has formed the base for the precipitation research effort of the Weather Bureau since the early 1970's. The region forms part of the South African Highveld, which is characterized by rolling hills, on average 1600 m above sea level. The area rises to the south where the mountain Kingdom of Lesotho is located. The Drakensberg escarpment reaches altitudes of more that 3000 m above sea level at Mont-aux-Sources. Towards the east, the Highveld comes to an abrupt end where the escarpment forms the border with the province of KwaZulu-Natal. Several other minor mountain ranges are foothills to the mountains in the south. These include the Rooiberge, Witteberge and Malotis. The region forms an important source region for the country's main rivers. The Tugela River, Malibamatso River (called the Orange River down-stream) and the Wilge River (a major tributary of the Vaal River) all originate in the area. Two of the country's most ambitious programmes for re-routing water across watersheds are also situated in the area. The Tugela-Vaal Scheme transfers water from the Tugela river (in KwaZulu-Natal) into the Vaal River system via the Wilge River. The Woodstock and Sterkfontein Dams form part of this scheme. The Highland Water Scheme will in the near future transfer Orange River water (from the Malibamatso River in Lesotho) into the Vaal River system via the Liebenbergsvlei River. These expensive projects, designed to meet the growing demand for water in the industrial and mining areas around Johannesburg, clearly indicate the increasing pressure that is being exerted on the country's water supplies. Figure 3.1 shows the north-eastern Free State and surrounding areas and the location of the radars and rain-gauge networks.

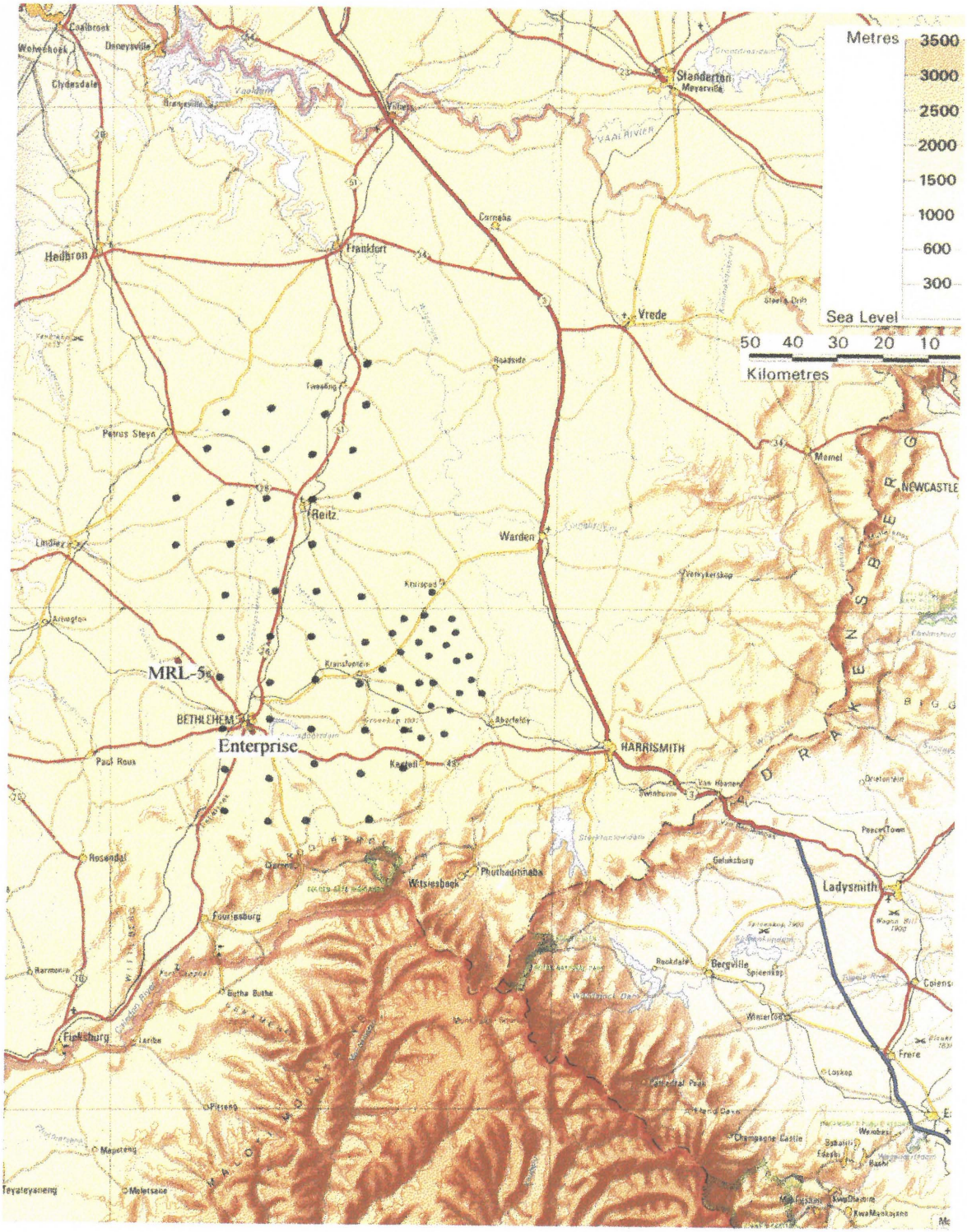

Figure 3.1 Map of the north-eastern Free State showing the radar sites and rain gauges.

Rainfall occurs mainly during the summer months, October to March. The annual rainfall in the area is about 700 mm. The winters are cold and dry. During summer, a significant portion of the rainfall occurs in the form of thunderstorms, although general rain conditions do develop during favourable synoptic conditions. The thunderstorms are mainly thermally triggered (Mather and Terblanche, 1993) but the complex orography of the area plays an important role in organizing the storms. This is an area with some of the highest frequencies of convective storm development, lightning and hail in South Africa. These high frequencies of occurrence are some of the reasons why this area was selected for thunderstorm research and cloud seeding experiments.

The rain-gauge network covering the Liebenbergsvlei River catchment of 4650 km^2 consists of 45 rain gauges on a 10 km grid. Tipping-bucket rain gauges with a 0.2 mm resolution are used. The tipping events are logged, with the date and time, on in-house developed loggers. The network was installed in October 1993 and has since provided in excess of 98 % usable data. The other network, known as the Vaalbankspruit network, in situated to the south east of the main network. It consists of 26 rain gauges with an approximate spacing of 4 km. More information on the networks, loggers and the performance testing of the rain gauges is given by Mather and Terblanche (1996). In the case studies presented in Chapter 6, data from the Liebenbergsvlei network will be used. Software was developed to arrange the rain-gauge data in time intervals that correspond to the radar volume-scan times.

3.2 THE RADAR DATA ACQUISITION SYSTEM - RDAS

A radar data acquisition system (RDAS) was developed for more flexible processing of radar data and control over the radar antenna. Being PC based, it uses a user-friendly platform with all the options of modern PC-based graphics, C programming and networking. Apart from the control and display software, which is written in C with Assembler routines, the RDAS consists of custom built interface cards which plug into the PC mother board. One card is the antenna monitoring and control card and the other the video processing card. Data are stored on EXABYTE cassettes. The system is described in detail by Terblanche et al. (1994) and only those features relevant to this thesis, concerning the video processing, will be summarized.

The original radar video processor card (RVPC-1) is a 16 bit DSP (Digital Signal Processing) card custom built to perform analog to digital (A to D) conversions of the video signal at 12 bit resolution and up to 1 MHZ in sync with the radar trigger (PRF). On-card memory is used to store the processing algorithm for averaging the digitized receiver output. Many of the card's features are software configurable. This card forms the basis for data processing on all weather radars in South Africa.

A new version of the processor card (RVPC-2) is being developed, incorporating enhanced features and processing power. Experience gained through the use of the RDAS and RVPC-1, using the processing methods which will be described in this thesis, formed the basis for the improvements introduced on the new card. This card is a general DSP based processor, designed in a way that a modular front-end, which plugs onto the card, is user defined. For our applications the front-end consists of signal conditioning and A to D conversion for two video channels. Circuitry for closed-loop antenna control, both in azimuth in elevation, is also provided

making a separate antenna monitoring and control card unnecessary. The processing power and speed of the card is much enhanced through the use of the latest DSP and memory components. Up to 4 MB of on-card memory is available. One of the advantages of RVPC-2 is that it simplifies the RDAS software as more processing is now done on the card. The fact that antenna control and video processing is done on the same card opens many new options for synchronizing the two signals.

Software was developed to simplify radar calibrations using the radar equation given in (2.19) and (2.20). Prerequisites to a proper radar calibration are radar components in sound physical condition and thorough knowledge of the radar characteristics, including the system losses and gains. The software requires input of these parameters from the user and as a first step produces a table, in 5 dB increments, consisting of received powers (in dBm), reflectivity values at 100 km range (dBZ) and the signal generator power settings (in dBm) to simulate the received powers. During the next step, the user sets the required power levels on a signal generator, simulating a pulse 50 μs wide with a delay so that the pulse is centred at a range of 100 km, and then injects these into the receiver. During this process the antenna is pointed towards a quiet section in the sky - we use the South Celestial Pole which is found by setting the antenna azimuth to true south and the elevation to the value of the radar's latitude. The software produces a graph of the receiver slope in which dBZ (at 100 km) is displayed on the x-axis and the averaged video processor value (12-bits VP value) on the y-axis. The user can then specify two points on this curve that will define a straight line approximating the calibration curve (See Figure 4.2). The software then automatically compiles the site specific table to be used by the RDAS software. Parameters in this table include the radar constant and the power and video processor values which define the calibration slope. As some of the values must be specified as integers (required by the data storage format), the software automatically compensate for the rounding off by adjusting the radar constant accordingly. A computer record is kept of the calibration information in a spread-sheet format. The software, in use on all weather radars in South Africa, simplifies calibrations and contributes towards calibrations being done in a systematic manner. Additional look-up tables as required by the signal processing method that will be described in Chapter 4, and which will be called *displacement* tables, are also compiled. These are used by the new DISPLACE processing algorithm.

3.3 THE ENTERPRISE AND MRL-5 RADARS

3.3.1 The Enterprise C-band radar

The Enterprise WSR-81 C-band radar was commissioned at the Bethlehem Project (28° 15' S, 28° 20' E) during 1982. This system replaced the previous Mitshibushi C-band radar and introduced digital recording to the project. This greatly assisted in the processing and analyses of data. The siting of the radar at the airport in Bethlehem ensures very little ground echo contamination at ranges in excess of 20 km, but partial beam blocking occurs at low elevations in certain sectors. During the 1980's this system was operated in volume-scan mode controlled by hardware. Data storage was done using two Kennedy tape drives. The radar is one of the oldest Enterprise systems still used by the Weather Bureau and has collected the most data of any weather radar system in South Africa. In general the system has been found to be reliable, although the antenna pedestal bearings are under-designed, requiring routine replacement.

The basic characteristics of this radar are summarised in table 3.1. In the early 1990's the system's antenna control, signal processing, data display and storage was upgraded using the RDAS. This upgrade and the tests that were conducted to verify the performance of the system are well documented by Terblanche et al. (1994). Using RDAS, the system is operated in programmable volume-scan mode using eighteen elevation steps with the base-scan at 1.5°. Data processing compiles 224 range bins, each 600 m long, covering an area between 14 and 150 km range. With the elevation steps in use, the closest range for data collection corresponds to a range where data at 16 km above ground level are collected at the highest elevation. The averaging is performed over 32 samples using both range and time-azimuth averaging (4 range samples over 8 PRF pulses). The antenna rotation speed is set to 5.2 rpm. This angular speed (and the PRF of 250 s^{-1}) ensures that the antenna rotates through its own 3 dB beamwidth during an averaging sequence and that averaged data for each degree in azimuth is available. During the period 1991 to 1996 this radar played a central role in the evaluation of the hygroscopic flare randomized cloud seeding experiment described by Mather and Terblanche (1993 and 1996).

Table 3.1 Characteristics of the Enterprise WSR-81 radar.

	C-Band
Receiver Sensitivity	-107 dBm
Receiver dinamic range	78 dB
Transmitter frequency	5.655 GHz
Pulse duration	2 μs 0.5 μs
Peak transmitter power	250 kW
Pulse Repetition Frequency	250 Hz ± 2%
Pulse coincidence	within 0.1 μs
Antenna gain	44 dB
Side lobes	> 22 dB down
Polarization	Horizontal
Beamwidth	1.0° at 3 dB one-way points

3.3.2 The MRL-5 dual-wavelength radar

The dual-wavelength MRL-5 radar which operates at S- and X-band is of Russian origin. It was originally designed to assist in the extensive hail research and suppression efforts which are conducted in many states of the former USSR. Two versions of the MRL-5 radar are available, one for permanent siting and the other a mobile version. The system operates at S- and X-band through a unique antenna system designed to match the beam patterns at the two wavelengths. Although many of these radars are in use in Eastern Europe, their applications in the West have been limited. An MRL-5 system was used in the multi-national Precipitation Enhancement

Programme (PEP) in Spain organized by the World Meteorological Organization during the 1980's. During PEP the rugged construction and suitability for extended operations of the system were demonstrated.

The need for a more specialized radar system to be used as part of the precipitation enhancement research and as the basis for developing radar-based rainfall and flood monitoring systems for South Africa has been known for a number of years. Financial considerations ruled out state-of-the-art radar systems available in Europe and the USA. After thorough investigations the WRC bought a new mobile-version MRL-5 radar in 1994. The system was installed approximately 20 km north west of Bethlehem (28° 05' S, 28° 10' E) on a site that provides much improved coverage of the research area. The characteristics of the MRL-5 radar are summarized in Table 3.2.

Table 3.2 Characteristics of the MRL-5 radar.

	X-Band		S-Band	
Receiver Sensitivity	-104 dBm		-106 dBm	
Receiver dynamic range	70 dB		70 dB	
Transmitter frequency	9.603 GHz		2.954 GHz	
Pulse duration	2 μs	1μs	2 μs	1 μs
Peak transmitter power	200 kW	200 kW	600 kW	600 kW
Pulse Repetition Frequency	250 Hz ± < 5 %	500 Hz	250 Hz ± < 5 %	500 Hz
Pulse coincidence	within 0.2 μs		within 0.2 μs	
Antenna gain	40 dB		39 dB	
Side lobes	> 22 dB down		> 22 dB down	
Polarization	Vertical		Horizontal	
Beamwidth	1.5° at 3 dB one-way points		1.5° at 3 dB one-way points	

An option available on the MRL-5 radar is to use the X-band with the 4.5 m antenna. This results in a 0.5° beamwidth and a antenna gain of 49 dB. An 18 dB two-way gain and improvement in performance is achieved. The antenna system of the MRL-5 radar is shown in Figure 3.2.

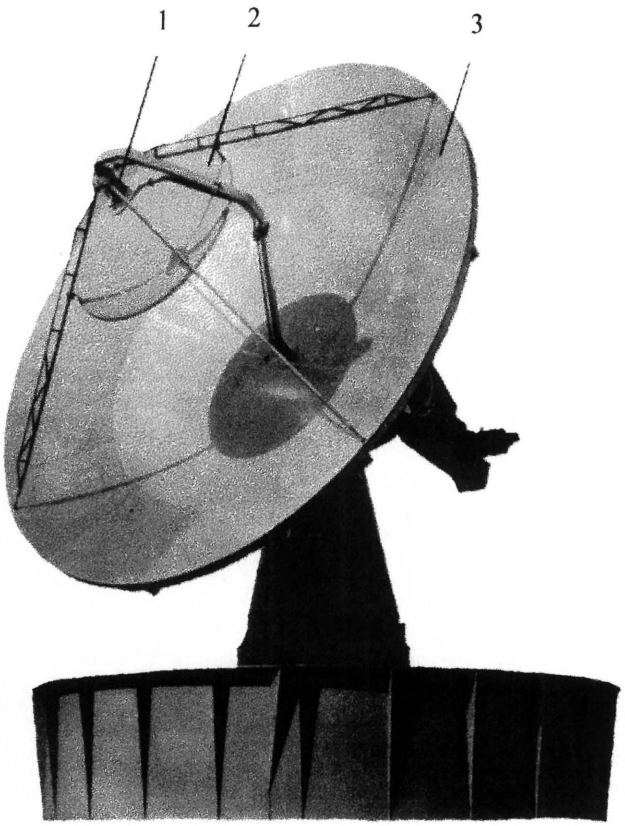

Figure 3.2 The MRL-5 antenna system showing: 1.The combined feedhorn, 2. The 1.5 m diameter X-band antenna and, 3. The 4.5 m antenna for X- and S-band use.

The RDAS was adapted to process, display and store data from both the X- and S-band sections of the MRL-5 radar in addition to controlling the antenna for volume-scan operation. This upgrade was completed by October 1994 and made the inflexible Russian built APOS unit (antenna control and data processing unit) redundant. Data processing methods and formats of the MRL-5 radar are compatible to those of the Bethlehem Enterprise radar (and to all radar data in South Africa) with all the flexibility inherent in the design of the RDAS. All the software tools developed to simplify calibrations procedures etc., are also in use on the MRL-5. The system is programmed to collect volume-scan data in exactly the same manner as the Enterprise radar, the only difference being that the wider beam width allows slightly larger elevation steps. The rotation speed is also set to 5.2 rpm.

A rack-mount 486 PC was acquired in May 1995 to replace the standard 486 PC previously used for the RDAS on the MRL-5. This new computer is more suitable for sustained operations and provides the necessary space for additional cards which may be needed for future expansion. A schematic diagram of the RDAS (using RVPC-1) and its interfaces with the MRL-5 radar is shown in Figure 3.3. The following cards (indicated in the figure) are housed in the 486 enclosure:

- Antenna Control Card (ACC)
- Radar Video Processor Card (RVPC-1; one for S-band and one for X-band)
- Radar Control Card (RCC)

A total of 5624 volume scans of data were recorded with the MRL-5 during the 1994/1995 season. This corresponds to about 20 gigabytes (400 hours). Most of these data were collected during March 1995. Towards the end of 1995 an uninterruptable power supply system integrated with an automated diesel generator was commissioned to solve the problem of electrical interruption at the site. Facilities for remote controlling and system monitoring were developed (Radar Control card - RCC). A 128 kBits s^{-1} microwave link was installed for data transfer to and from the Bethlehem offices towards the end of 1995. During the 1995/96 summer season these developments resulted in the collection of about 2000 hours (100 gigabyte) of volume-scan data. All the main rain events of the season were captured, the system proving its reliability and stability.

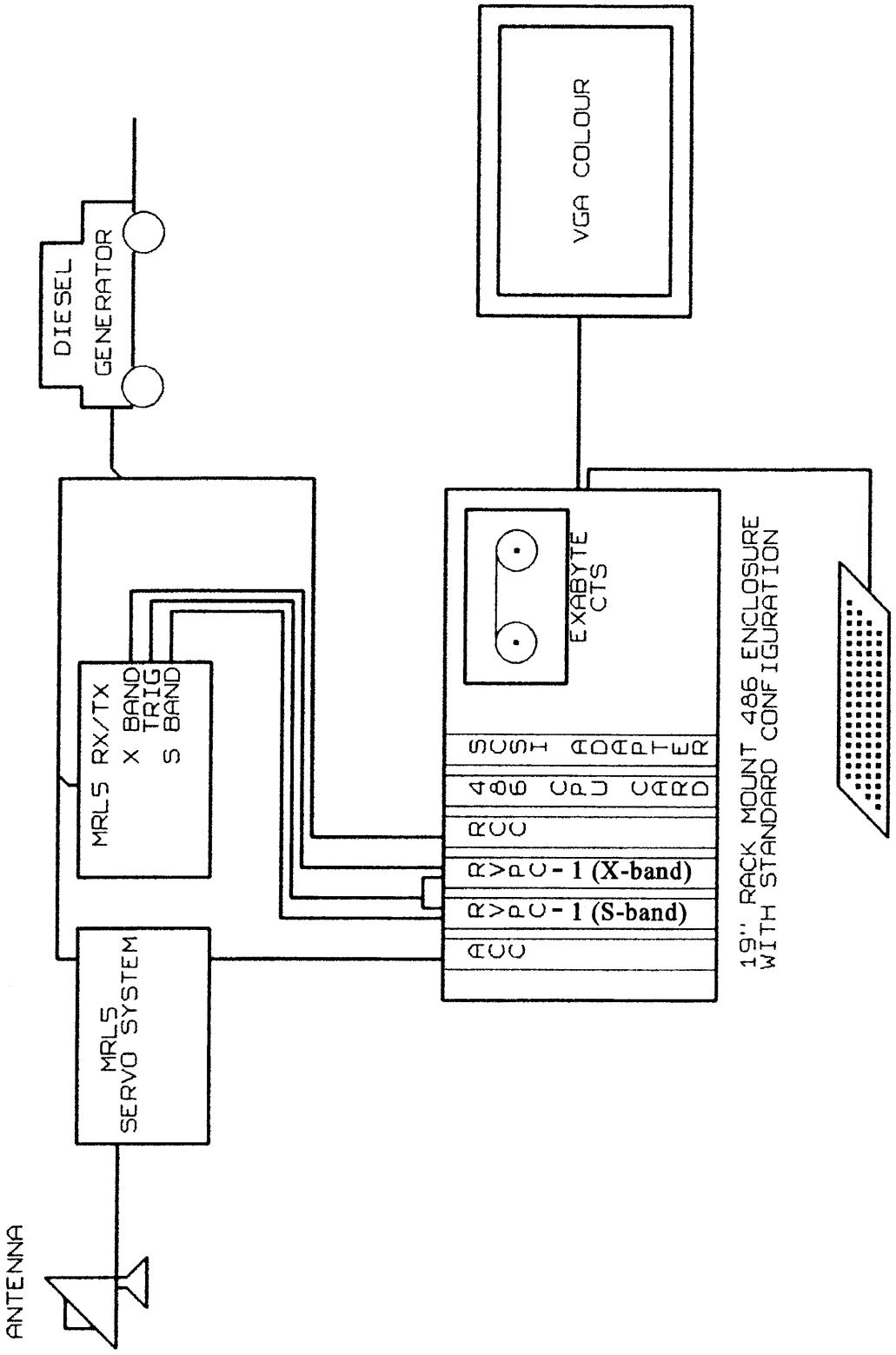

Figure 3.3 Schematic diagram of the MRL-5 radar's RDAS and its interfaces.

3.4 PERFORMANCE TESTS

Thorough performance tests were conducted on both the Enterprise and MRL-5 radars. Some of the tests on the Enterprise radar, using an optical reflector of known characteristics (Atlas and Mossop, 1960), were described by Terblanche et al. (1994). For the MRL-5 radar, the emphasis was on determining the antenna beam characteristics as the matching of the S- and X-band beam patterns are crucial to the optimum use of the radar's dual-wavelength facility. These measurements are highlighted in Mather and Terblanche (1996). Figure 3.4 shows the S-band horizontal one-way beam pattern in power ratios relative to the power in the centre of the beam. It can be seen that the side lobes are well within specification.

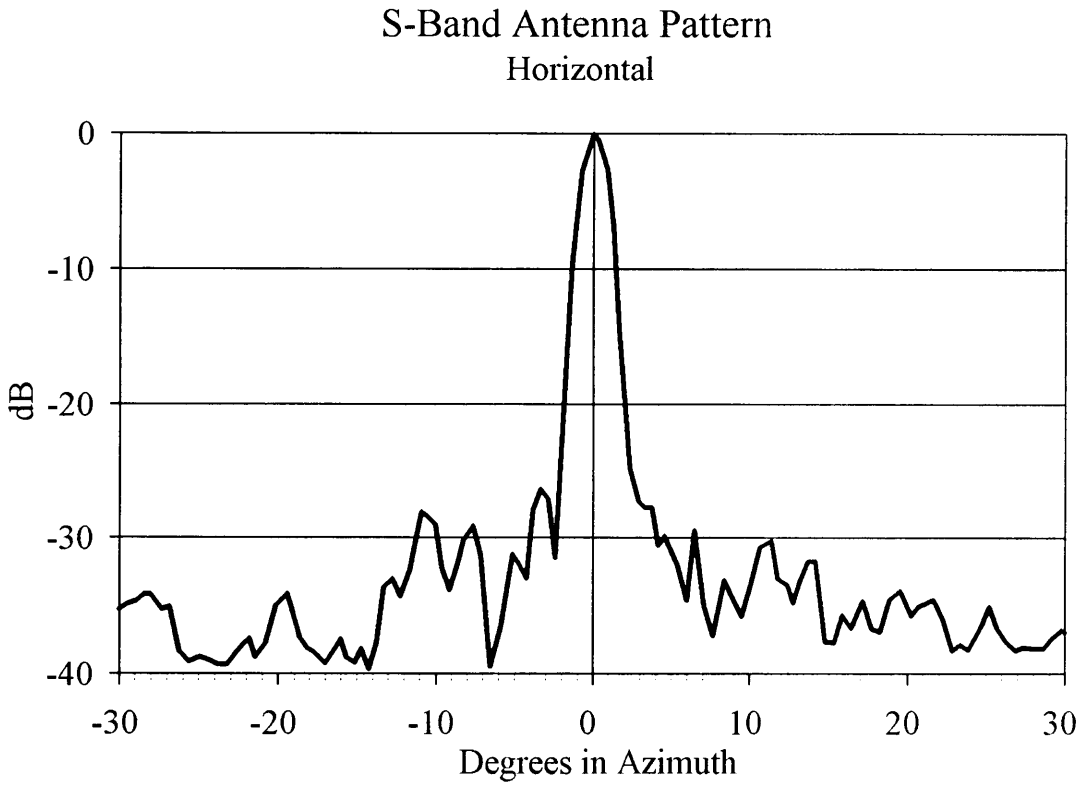

Figure 3.4 Horizontal one-way beam pattern of the MRL-5 radar's S-band.

In this section, tests relating to the characteristics of the received signals will be discussed briefly. Apart from being another way to verify the radar calibration slope (Gorgucci et al, 1989), the fluctuations of echo amplitude are used in what follows.

Digitized receiver samples were collected for precipitation echoes and ground clutter from both the Enterprise C-band and MRL-5 S-band radars using RDAS and RVPC-2. The radar antennae were kept stationary. Using one thousand precipitation echo samples (four seconds) from this record, the quadratic-to-logarithmic bias was computed. The bias is approximately 2.5 dB for both C-and S-band. The values indicate correctly calibrated receiver slopes as the digitized

video signals show the decibel fluctuations characteristic of precipitation echoes. The samples were also used to compute autocorrelation coefficients, at different delays, to check the decorrelation of the pulse-to-pulse echoes. Only echoes with reflectivities exceeding 25 dBZ were considered. The data were converted to values that correspond to linear detection before calculating the autocorrelations. In this manner the DC and AC power components of the echoes can be determined. Theoretically, the mean to AC power ratio for precipitation echoes, using independent samples, is 4.66 (6.68 dB) (Tatehira and Shimizu, 1978). This implies that the AC component represents about 21 % of the mean precipitation echo power and the DC component the remaining 79 %. For ground clutter this ratio is much larger as almost all the power is represented by the DC component. This principle forms the basis of a ground clutter filtering scheme and will be dealt with in more detail in Chapter 5.

As predicted by theory, the C-band precipitation echo samples decorrelate faster than those at S-band. In both cases, the autocorrelation coefficient decreases exponentially to about 0.75 for precipitation echoes as the delay is increased. This means that about three-quarters of the mean power is contributed by the DC component. At a delay of 4 ms (1 pulse repetition period) there is still some correlation evident, especially at S-band. The ground clutter results indicate slow decorrelation and the dominance of power from the DC component, even at relatively long delays.

The tests described in this section are simple to perform and do not require any special equipment other than RDAS. When observing precipitation echoes, it provides a measure of the system performance as any significant deviation from the expected value of the quadratic-to-logarithmic bias or the mean to AC power ratio, indicates a problem. It can easily form part of the post-calibration performance testing of the meteorological radars in the South African network.

In previous chapters the background on radar theory was given. Chapter 3 describes the Bethlehem research area and the infrastructure relevant to the studies that follow. Special emphasis is given to the two weather radars, their upgrades, mode of operation and the performance tests. In Chapter 4 the DISPLACE processing method will be developed, followed in later chapters by examples of its applications.

CHAPTER 4

THE *DISPLACE* METHOD

4.0 INTRODUCTION

The DISPLACE method (an acronym for Digital Signal Processing for Logarithmic, Linear and Quadratic Responses) was developed by Terblanche (1995 and 1996) to facilitate the averaging of digitized logarithmic receiver output. Later, the method was found to be ideally suited for many other processing applications, as will be discussed in Chapter 5. The limitations imposed by the radar-data acquisition and networking systems in use in South Africa (Terblanche et al., 1994; Visser and le Roux, 1993) were kept in mind during development. These limitations necessitated meeting the following criteria:

- During processing, all values had to be accommodated within a 16 bit word size.
- The computational efficiency of the method had to be comparable with the existing conventional averaging method.
- Modifications to radar formats and user software had to be avoided.

4.1 THE BASIC DISPLACE CONCEPT

The basis for the DISPLACE method can be explained by the following identity:

$$\log[(a+b)/2] = \log(a+b) - \log 2$$

$$= \log a + \log(1+b/a) - \log 2$$

$$= \log a + \mathbf{\log(1 + 10^{-(\log a - \log b)}) - \log 2} \qquad (4.1)$$

Therefore, if only the logarithm of each value in a pair is known, the logarithm of the average of the pair can be determined. The bold section in (4.1) represents a correction (or a *displacement*) which must be applied to log a. These *displacements* can be pre-computed and loaded into a look-up table as the value is only a function of (log a - log b). By successively computing averages over pairs, the average over 2^i , i=1,2,...,n values can be obtained. The advantages of this procedure are that (1) no division is necessary to determine the final averaged value, (2) the absolute values of the *displacement* is smaller than the larger of the pair values, and (3) only a single look up is needed for each pair of values.

4.2 DISPLACE VARIATIONS

Consider two samples (either in range or time), taken from a logarithmic receiver. These are proportional to 10 log P_1 and 10 log P_2 where P_1 and P_2 are the returned powers in mW.

Analogous to (4.1) but for the more general case we can write:

$$10\log[(P_1^a+P_2^a)/2]^{(1/a)} = 10\log P_1 \mathbf{-(10/a)\{log2-log[1+0.7943282^{a(10logP1-10logP2)}]\}} \quad (4.2)$$

From (4.2) it is clear that unbiased averages, over pairs, in dBm can be determined corresponding to receiver transference functions of the general form P^a, using the output from a logarithmic receiver.

From (4.2), the following applies for a linear response:

$$10\log[(P_1^{0.5}+P_2^{0.5})/2]^2 = 10\log P_1 \mathbf{-20\{log2-log[1+0.8913^{(10logP1-10logP2)}]\}} \quad (4.3)$$

and for a quadratic receiver we can write:

$$10\log[(P_1+P_2)/2] = 10\log P_1 \mathbf{-10\{log2-log[1+0.7943^{(10logP1-10logP2)}]\}} \quad (4.4)$$

A similar equation can also be compiled for a logarithmic response:

$$[10\log(P_1)+10\log(P_2)]/2 = 10\log P_1 \mathbf{-0.5(10logP_1-10logP_2)} \quad (4.5)$$

Therefore, the DISPLACE method can be used to obtain the pair averaged values (in dBm) corresponding to a logarithmic, linear or quadratic receiver when only logarithmic receiver outputs in dBm are known. This is achieved by using the same algorithm but with the appropriate *displacement* values. The *displacement* values in (4.3), (4.4) and (4.5), as a function of $10\log P_1$ - $10\log P_2$, are shown graphically in Figure 4.1.

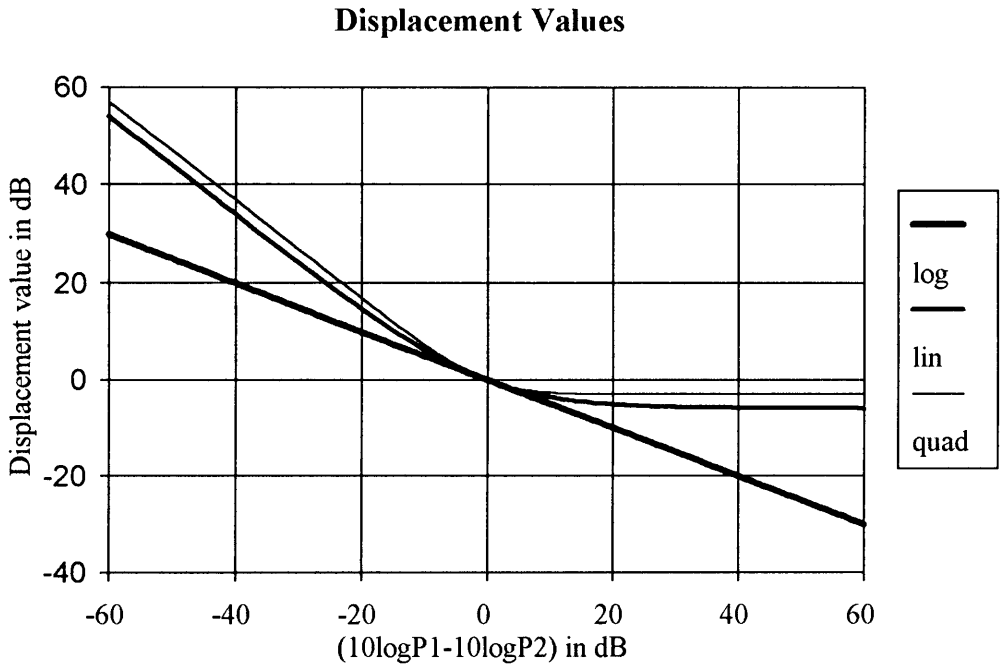

Figure 4.1 *Displacement* values for a logarithmic, linear and quadratic response.

The application of the DISPLACE method is not restricted to conventional pair averaging. Weighted averages over pairs, as done during interpolation, can also be computed, for which the following applies in the general case:

$$10\log[bP_1^a+(1-b)P_2^a]^{(1/a)}=10\log P_1+\mathbf{(10/a)\log b+(10/a)\log[1+0.7943^{a(10\log P1+(10/a)\log b-10\log P2-(10/a)\log(1-b))}]}$$

for $0 \leq b \leq 1$ (4.6)

In (4.6) an adjustment, related to the specific (non-constant) weighting factor b, must be applied to each sample before the averaging is performed on the modified samples. In the case of constant b, the entire bold section in (4.6) can be precompiled as a *displacement* value table. Whatever the case, the DISPLACE method ensures, in contrast with conventional methods, that only addition and subtraction is done between the weighing factors and the data values.

For the difference between a pair we can write the following for the general case:

$$10\log[P_1^a-P_2^a]^{(1/a)} = 10\log P_1+\mathbf{(10/a)\log[1-0.7943^{a(10\log P1-10\log P2)}]} \quad (4.7)$$

It is now possible - using the calibration relationship of a specific radar - to scale the above equations and to pre-compile tables of *displacement* values (in bold) for the difference between the digital values representing 10 log P_1 and 10 log P_2. The slope of the solid line in Figure 4.2, approximating the MRL-5 radar's S-band calibration slope (which is indicated by the dashed line), determines the scaling factor (digital change per dB) to be used.

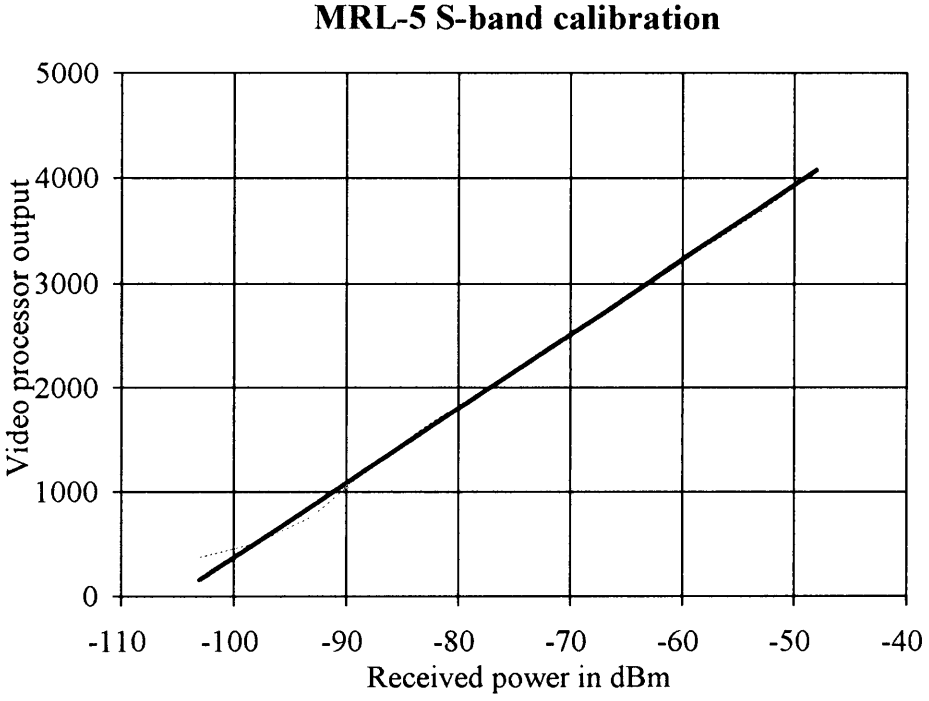

Figure 4.2 Calibration slope of the S-band receiver of the MRL-5 radar.

Whenever the calibration changes, new *displacement* tables need to be compiled. The specific *displacement* value relating to the required operation must now be subtracted from (or added to) the digital value corresponding to 10 log P_1. By arranging the pair of samples in a manner where 10 log P1 $\geq$ 10 log P2, the size of the look up table can be halved at the expense of more arithmetic. In this case a *displacement* table consisting entirely of zeros, will result in obtaining the maximum value while a table consisting of the values 10 log P_1 - 10 log P_2 will result in the minimum value of the pair (or the 2^i, i=1,2,.....,n samples under consideration).

Referring to Figure 4.2, it is evident that the solid line approximates the radar's calibration well, except at lower power levels. At these power levels, the measured power is overestimated while the variance in power is underestimated. This occurs at reflectivities that correspond to negligible rain rates.

Note that the averages are obtained with the DISPLACE method without division and products are obtained without multiplication. When rounded off, the *displacement* values and all other values obtained during the computation remain integers of the same magnitude as the larger of the two samples both numerically and in terms of computer word size. This is in contrast with other methods in which each digitized sample is converted to a received power equivalent using a look-up table before averaging is done (Chandrasekar et al., 1989), in which case the time consuming divisions must still be done. For more detail on the derivations of the DISPLACE equations in this chapter, see the Appendix.

In the next chapter the implementation of the basic DISPLACE algorithm in the RDAS and the tests done to verify its performance are discussed. Specific applications of the DISPLACE variations to radar data processing are also developed.

CHAPTER 5

THEORETICAL STUDIES AND APPLICATIONS

5.0 INTRODUCTION

In this chapter the DISPLACE equations derived in the previous chapter are tested and implemented. In the first section emphasis is placed on the computational efficiency of the averaging of logarithmic receiver output to simulate averages obtainable from a quadratic receiver. It is shown that the basic DISPLACE algorithm can calculate these averages in about half the computing time of conventional logarithmic averaging. The DISPLACE algorithm and its computation time also remains constant regardless of the receiver transfer function that is simulated. The implementation of DISPLACE averaging on the two versions of the in-house developed radar video processor cards (RVPC-1 and RVPC-2) are described. Tests are done, using artificially generated Rayleigh-distributed amplitude samples, to verify the method's accuracy.

In the second section, the problem of ground clutter is addressed, highlighting some of the methods used to deal with the problem. A DISPLACE equation is developed to implement a ground clutter filtering scheme that uses the pulse-to-pulse echo fluctuations to estimate the echo strength of precipitation echoes, even in the presence of ground clutter.

The third section deals with the application of DISPLACE in the generation of CAPPIs. This new approach makes it possible to produce CAPPIs in averaged digitized receiver bit-values, without any of the time consuming unit conversions and interpolations that are normally necessary. The method is computationally efficient and offers new possibilities for real-time CAPPI generation.

In the fourth section, other uses of the DISPLACE method, such as multi-parameter radar data processing, are highlighted.

5.1 PERFORMANCE TESTING AND IMPLEMENTATION

Independent Rayleigh-distributed amplitude samples were generated, using $(A_1^2+A_2^2)^{0.5}$ with A_1 and A_2 Gaussian-distributed random numbers around zero, as described by Marshall and Hitschfeld (1953). After applying the 10 log transformation to the square of these samples, they were converted to twelve bit integers using the MRL-5 radar's S-band calibration relationship (Figure 4.2). The corresponding logarithmic, linear and quadratic *displacement* tables were then compiled. The DISPLACE method was evaluated on 71680 of these samples using (4.3) (4.4) and (4.5), calculating averages over 32 samples, over an interval sufficient to obtain the equivalent of 2240 range bins.

The logarithmic DISPLACE method realized results comparable to those obtained by conventional averaging. Depending on whether the integer *displacement* values are rounded-off or truncated, the DISPLACE method provides averages either within 2 counts (<0.028 dB) above or below the average obtained in the conventional way. To minimize errors, it is necessary to

digitize the receiver output at a relatively high resolution.

Referring to Chapter 2, the quadratic-to-logarithmic bias (in dB) for averaging over an asymptotically large number of independent samples is -2.507 dB ($10\log(e^{-\gamma})$, with $\gamma = 0.577215$, the Euler constant). The quadratic-to-linear bias is -1.049 dB ($10\log(\pi/4)$). The average quadratic minus linear and quadratic minus logarithmic bias using the DISPLACE method was found to be -1.03 dB and -2.49 dB, with standard deviations of 0.229 dB and 0.605 dB. This corresponds well to the theoretical values when averaging over 32 samples. Figure 5.1 shows the bias frequency distributions obtained during this test.

The DISPLACE method was incorporated into RVPC-1, by replacing the EPROM containing the averaging algorithm and utilizing the on-card memory for the *displacement* values. As the on-card memory is limited, the algorithm includes the test to determine which value in each sample pair is the largest, whereby the size of the *displacement* table can be halved (Section 4.2). The success of this step was verified by developing a simulator to replace the 12 bit A to D converter. This permitted the computation of averages, as if in real time, but using the artificially produced sample values. A cascading scheme is used for averaging over 32 samples, 4 in range and 8 in time-azimuth, to obtain the averaged range bin values. A schematic diagram of this scheme is shown in Figure 5.2.

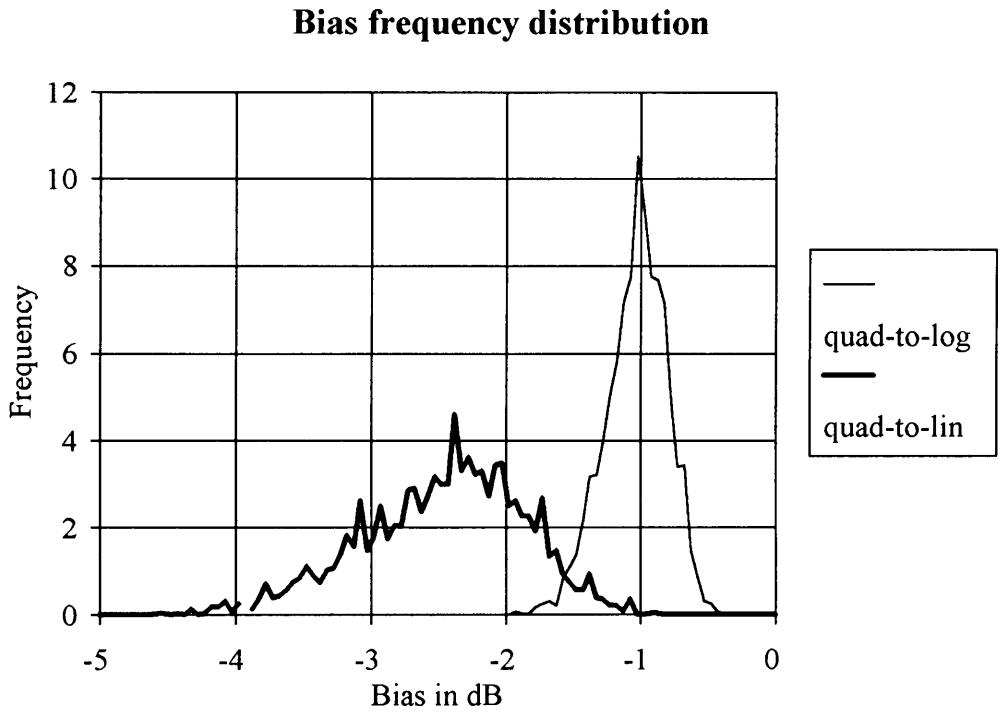

Figure 5.1 The frequency distribution of the quadratic-to-logarithmic and quadratic-to-linear biases obtained with the DISPLACE method.

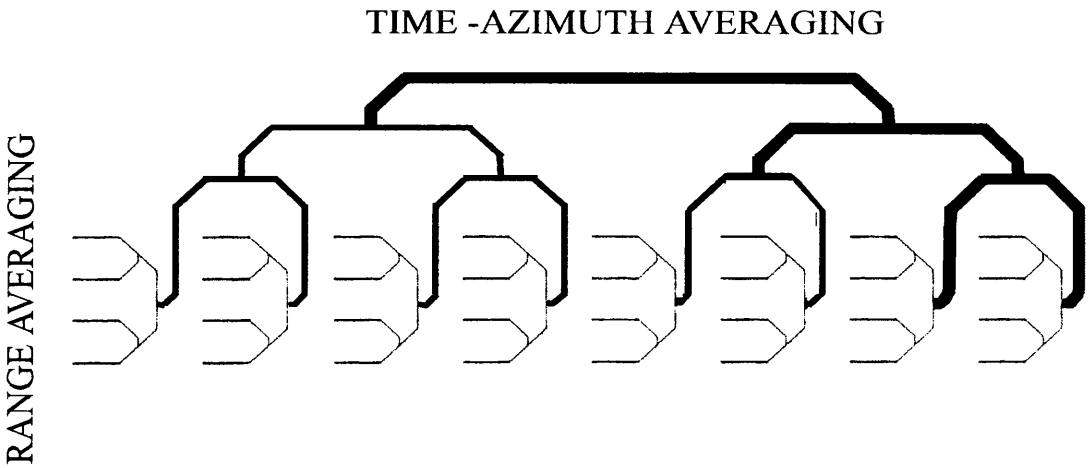

Figure 5.2 The cascading scheme to realize averages over 32 samples (4 in range and 8 in time-azimuth) using the DISPLACE method for pair-wise averaging. The thin lines indicate the pair averages for range averaging. The solid lines indicate the pair averages for time-azimuth averaging on the eighth PRF pulse (RVPC-1 algorithm) and the thick solid lines those for each PRF pulse (RVPC-2 algorithm).

The DISPLACE algorithm introduced on RVPC-1 completed the range averaging after each PRF pulse (thin lines in Figure 5.2). The 896 digitized samples from the receiver were first reduced to 448 values (by 448 DISPLACE operations) and then to 224 values. The range averaging therefore required a total of 672 DISPLACE operations per PRF pulse. All the time-azimuth averaging (indicated by the solid lines in Figure 5.2) were done after the range averaging of the eighth PRF. Apart from the 672 DISPLACE operations for range averaging on the eighth PRF pulse, the time-azimuth averaging entailed a further 1568 DISPLACE operations. Therefore, on each eighth PRF pulse a total of 2240 DISPLACE operations are done to obtain the 224 averaged range bin values. Even so, an improvement in computational efficiency of approximately 25% was achieved between the maximum DISPLACE processing time and that required by conventional averaging. This time saving was further improved in the algorithm for the RVPC-2.

On RVPC-2 the larger on-card memory permits the loading of the full *displacement* table, making the test to determine the largest in a pair redundant. On each PRF pulse the range averaging is done, as before (672 operations), but the time-azimuth averaging is arranged in a manner in which averaged output for the 224 range bins is available after each PRF pulse. By using circular buffering, only the minimum time-azimuth averaging is done after each PRF. These averages are used to output the averaged range bin values and are also stored for later use (the algorithm's time-azimuth averaging is indicated by the thick solid lines in Figure 5.2). In this manner the time-azimuth averaging remains constant at 672 operations for each PRF pulse. Therefore, the total number of DISPLACE operations per PRF pulse is 1344, representing a further 40% time saving compared to that needed for the eighth PRF of the RVPC-1 algorithm. It is noteworthy that an efficient DISPLACE algorithm will ensure that averaging is done in about half the time required to compute conventional averages. Furthermore, the processing time is constant regardless of the receiver transfer function being simulated. When calculating quadratic averages, for example, the time saving will be even greater as DISPLACE avoids the antilog conversions (or look-ups) that are necessary before normal averaging.

5.2 GROUND-CLUTTER FILTERING

There are several methods to filter ground clutter from weather radar data. A radar with a Doppler facility provides information on the radial velocities of the scatterers in the sampled volume. In the case of ground echoes these velocities have a narrow spread and an average radial velocity close to zero. It is therefore possible to filter out the returned power components of scatterers with these characteristics. In conventional radar the simplest approach is to compile a so-called average "clutter map" during a period when no precipitation is present, and to subtract these Z values from the values obtained under conditions when precipitation echoes are present. In this manner some information on the strength of those precipitation echoes that exceed the clutter reflectivities is obtained. However, the signal strength from the ground echoes is effected by several factors including ground moisture and vegetation. Furthermore, the antenna beam path through the atmosphere is affected by vertical gradients in moisture and temperature (anomalous propagation). The antenna rotation is normally not synchronized with the receiver output processing. These factors result in the target not being illuminated in exactly the same manner for each sweep. Although widely in use, and also a feature of the TITAN software (Dixon and Wiener, 1993), this procedure provides only limited quantitative improvement in precipitation echo measurement in the presence of ground clutter.

Another approach is to use the difference in the fluctuations between the pulse-to-pulse echo samples received from a volume filled by precipitation scatterers and those effected only by ground clutter (Geotis and Silver, 1976). A meteorological target consists of precipitation particles which are in continuous random motion and the received signal from such a volume exhibits a large pulse-to-pulse variation and rapid decorrelation. The received signal from a ground target on the other hand, has a decorrelation time approaching infinity, and the received signal shows a small pulse-to-pulse variance. Using this characteristic difference in the pulse-to-pulse fluctuation of the received signal, it is possible to set a fluctuation threshold that makes it possible to eliminate most range bins affected significantly by ground clutter while retaining most of the range bins containing information from precipitation scatterers. This technique is an improvement on the "clutter map" technique as it addresses the variation in the clutter field on a real-time basis. However, most of the problems of the "clutter map" technique remains unsolved.

By developing these principles further, Tatehira and Shimizu (1978) developed a method to obtain quantitative information on the power of the precipitation scatterers in range bins which are effected by fairly strong ground clutter returns. Their technique is based on the fact that the variance of the linear detected received signal from a target consisting of precipitation scatterers is related to the average received power from that sampled volume. In a sampled volume where both precipitation and ground echoes exist, the received power contribution from meteorological scatterers alone can be estimated from the variance of the linearly detected composite signal, as the contribution to the variance by the ground clutter is almost negligible. As this technique assumes that the same sample in space is monitored continuously, range averaging before filtering, and fast antenna rotation speeds are generally ruled out as these will contribute towards the measured variance.

Based on the work of Marshall and Hitschfeld (1953), Tatehira and Shimizu (1978) have shown that the following relationship between mean received power, $\overline{P_{rx}}$ and linear detected variance, $\sigma_x^2 = \overline{P_{rx}} - \overline{(P_{rx}^{0.5})}^2$, applies for precipitation echoes:

$$\overline{P_{rx}}/\sigma_x^2 = 1/(1-\pi/4) = 4.66 \qquad (5.1a)$$

In terms of decibels this can be written as:

$$10 \log \overline{P_{rx}} - 10 \log \sigma_x^2 = 6.68 \text{ dB} \qquad (5.1b)$$

Both $\overline{P_{rx}}$ and σ_x^2 have dimensions of power and can also be referred to as the mean and AC power. If σ_x^2 is measured, the mean power of the precipitation echo can be determined from (5.1 a or b). Using a C-band radar with a PRF of 250 s^{-1} and with the antenna stationary, Tatehira and Shimizu (1978) found that observed values of (5.1) conform well to theoretical values. For ground clutter measurements the authors found that the mean to AC power ratio was 522.5 (27.2 dB), indicating a clear distinction between echoes produced by the two scattering phenomena.

Tatehira and Shimizu (1978) further showed that for a composite received signal (ground clutter and precipitation echo), the mean weather to composite AC power ratio is given by:

$$\overline{P_{rx}}/\sigma_y^2 = f[\overline{P_{rx}}/\overline{P_{rg}}] \qquad (5.2)$$

where $\overline{P_{rg}}$ is the power contributed by the ground clutter and 3.01 dB $\leq f[\overline{P_{rx}}/\overline{P_{rg}}] \leq$ 6.68 dB. Therefore, a value of 4.85 dB will result in an error of at most 1.84 dB in the estimation of $\overline{P_{rx}}$. It is clear that the filtering of ground clutter will be limited to only about 20 dB, which is considered insufficient. However, as the frequency of fluctuation in the received signal from ground clutter is significantly slower than that of precipitation, this difference can be used to further improve the performance of the filtering procedure. The introduction of a filter which compares the change in the received signal between the latest sample to those prior, will eliminate a large portion of the low frequency AC component of ground clutter. A simple filter will consist of a single delay line canceller which subtracts the previous sample value from the present value. The variance, σ_d^2, of the output from this filter is related to the composite variance, σ_y^2, of the linear detected signal by:

$$\sigma_d^2 = 2\sigma_y^2(1-\rho(mT_s)) \qquad (5.3)$$

where $\rho(mT_s)$ is the dispersion-normalized autocorrelation coefficient with mT the delay line period, normally chosen as multiples of the pulse repetition period.

Tatehira and Shimizu (1980) and Tatehira (1980) concluded by showing that if the 0.7th power of the linear detected signal is used as input to the filter, a further improvement in the suppression ratio of the filter can be obtained. A flow diagram of their final ground echo filtering technique is shown in Figure 5.3.

Using the DISPLACE method the concepts discussed above can be implemented in a simple, computationally efficient digital form. Referring to the flow diagram and (4.7), the first five steps (and step 7) of the procedure can be simulated by the following equation:

$$10\log[(P_2^{(0.7/2)}-P_1^{(0.7/2)}]^{(2/0.7)} = 10\log P_2 + \mathbf{14.2857\log[1 - 0.9226^{(10\log P2-10\log P1)}]^2} \qquad (5.4)$$

where 10 log P_2 and 10 log P_1 are two samples at constant range, separated in time by a delay time of mT_s. From (5.1b) and (5.3) it follows that a correction still needs to be applied to (5.4) to compensate for the average bias between the modified AC power and the total power from precipitation scatterers.

The *displacement* values computed from (5.4) are depicted in Figure 5.4. Whenever the difference between 10 log P_2 and 10 log P_1 is small, as is the case for well correlated samples, a large *displacement* value must be subtracted from the 10 log P_2 value. Samples having a large pulse-to-pulse variation will be affected to a lesser extent. The smallest *displacement* value is set to -60 dB to limit the range of values.

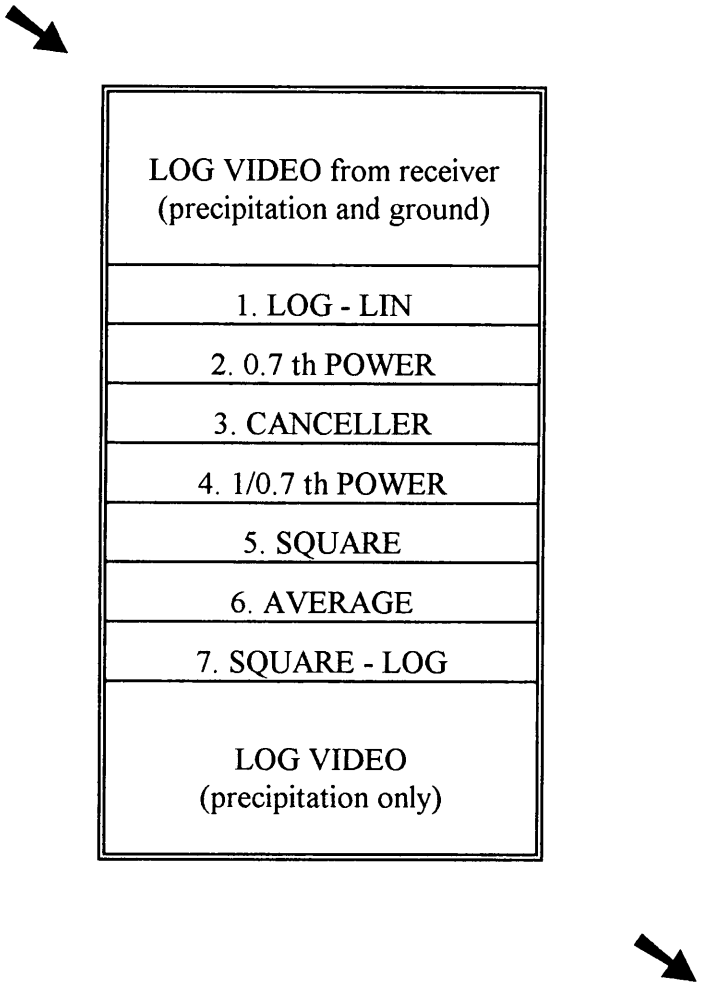

Figure 5.3 Flow diagram for ground clutter suppression (Tatehira, 1980)

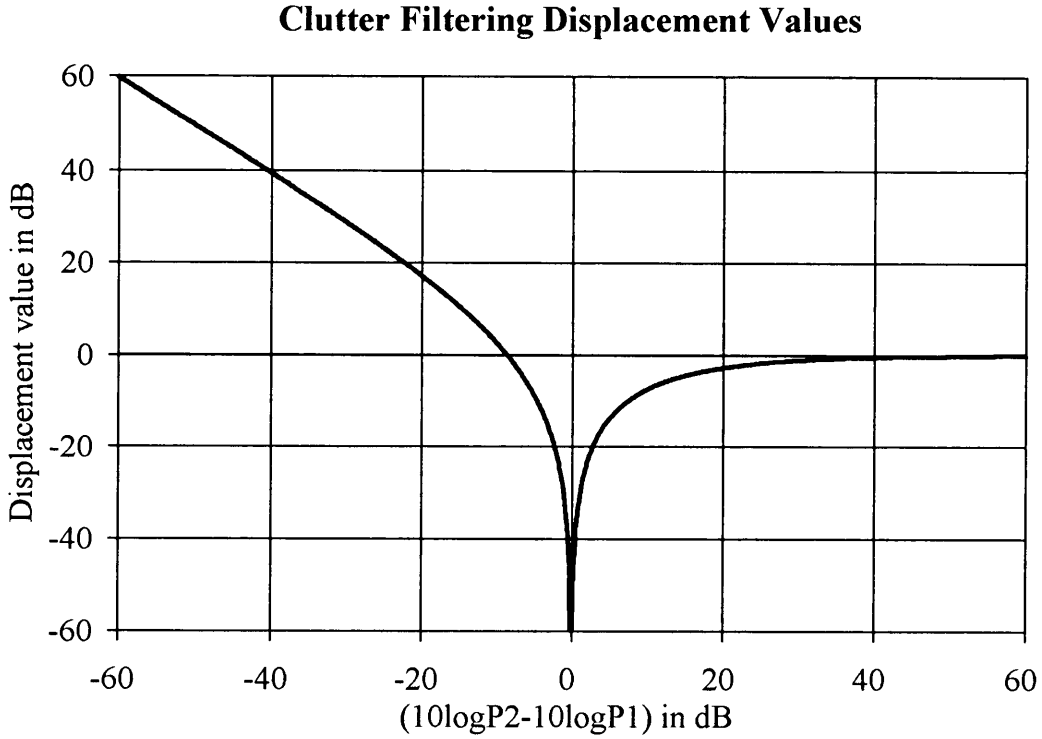

Figure 5.4 Ground clutter filtering *displacement* values computed from (5.4).

The final steps of the procedure are achieved by applying the normal quadratic averaging procedure as discussed in section 5.1 using (4.4), The difference being that the output of (5.4) at each range sample and on each pulse repetition pulse, is used as input to the standard range and time-azimuth averaging algorithm. Introducing the ground filtering algorithm requires an additional 896 operations per PRF pulse, resulting in a total of 2240 DISPLACE operations on each PRF pulse. Referring back to Section 5.1 this number of operations is exactly the same as the number needed after the eighth PRF pulse of the RVPC-1 averaging algorithm. Therefore, introducing ground clutter filtering still means that processing is 40 % faster than conventional averaging.

The performance of this application of the DISPLACE method was verified using artificially generated independent sample values and it was found that the ratio of $\overline{P_{rx}}$ to σ_d^2 was 7.34 dB. This value is larger than the one specified in (5.1b) as the 0.7 th power of the linear detected signal is used. Using the linear detected signal, the theoretical value is determined. However, it is important to keep in mind that this correction value will have to be optimized for physical data, especially in terms of the wavelengths used (affecting the correlation between samples) and the antenna rotation speeds (which introduces additional variance to the samples). Examples of the results from this method are given in Chapter 6.

5.3 GENERATING INTERPOLATION CAPPIs

Mittermaier and Terblanche (1996) reported on the use of the DISPLACE method to compute weighted averages during the conversion of radar data from spherical coordinates to Cartesian coordinates to compile CAPPIs (Constant Altitude Plan Position Indicator). It was found that the time efficiency of the process was improved by about 50% compared to conventional methods which employ the conversion to Z-values followed by normal interpolation. This improvement was achieved through the DISPLACE method's use of subtraction and addition in the place of multiplication and division and through avoiding the many conversions between units that are characteristic of conventional CAPPI calculations. This application of the DISPLACE method made it possible to compute accurate CAPPI's in real time, eliminating the need to rely on projection techniques to compute CAPPI's (Seed, 1992; Dixon and Wiener 1993). With the new method, which has been implemented to generate CAPPI's in real-time at the MRL-5 radar site for transmission to the Bethlehem, it is now possible to accumulate radar-rainfall measurements over variable timescales, even in light general rain conditions. The rings of discontinuities, which are characteristic of projection CAPPIs at ranges where changes occur in the elevations, are eliminated in these CAPPIs.

To compute the new CAPPI's, the first step is to apply the range correction term in the radar equation directly to the averaged range bin 12-bit values using a look-up table. After applying the 20 log r values, scaled by the calibration slope, modified range bin values are obtained that are directly related to the reflectivity factor (dBZ = 10 log Z).

To facilitate the use of the same quadratic correction value table that is applicable when averaging logarithmic receiver output, (4.6) can be rewritten as:

$10\log[(bZ_1+(2-b)Z_2)/2] =$

$$10\log Z_1+\mathbf{10\log b+10\log[1+0.7943^{(10\log Z1+10\log b)-(10\log Z2-10\log(2-b))}]-10\log 2} \qquad (5.5)$$

where the weighing factor, b, will now be between 0 and 2. The terms 10log b and 10log (2-b) represent decibel weighing factors that must be added to $10\log P_1$ and $10\log P_2$. Thereafter, the procedure is exactly the same as the pair averaging of the quadratic version of the DISPLACE method. The terms 10logb and 10log(2-b) have values between minus infinity (for practical purposes set to -80 dB, corresponding to a weighing factor of 10^{-8}) and 3.0103 dB. These factors must also be scaled by the receiver slope. As the difference between ($10\log P_1$ + 10log b) and ($10\log P_2$ + 10log(2-b)) can span a large range, it is practical to arrange the values in a manner where ($10\log P_1$ + 10log b) is the larger of the pair.

The interpolation CAPPI method requires interpolations in range, azimuth and between elevation steps. Using (5.5) the conventional interpolations (in Z) are replaced by the simple DISPLACE calculations which are done directly on averaged 12-bit video processor (VP) values. For the interpolation between a pair of range corrected VP values (VP_1 and VP_2), the procedure requires the following:

- Add the appropriate dB weighting factors to VP_1 and VP_2 to obtain VP_1' and VP_2'.

- Calculate the difference between VP_1' and VP_2'.
- Use the difference as a pointer in the *displacement* table.
- Subtract the *displacement* value from VP_1' to obtain the weighted average.

It is also possible to do the required interpolations in rain rate, where $R= (Z/200)^{1/1.6}$, or any other Z-R relationship of this general form, by rewriting (5.5) as follows:

$$10\log[(bZ_1^{1/1.6}+(2-b)Z_2^{1/1.6})/2]^{1.6} =$$

$$10\log Z_1+\mathbf{16\log b+16\log[1+0.8660^{((10\log P1+16\log b)-(10\log P2-16\log(2-b)))}]-16\log 2} \qquad (5.6)$$

Using this formula, the weighted averages are calculated as if the conversions to rain rate were done prior to the calculation. In this case the terms 16 log b and 16 log(2-b) range between minus infinity (for practical purposes again set to -80 dB) and 4.8165 dB, clearly showing the difference in the way the interpolations are done. The DISPLACE method can be used in a similar manner to do the averaging of raw logarithmic receiver samples, as if it is done in rain rate, but without any of the conversions that are normally necessary.

5.4 OTHER APPLICATIONS

5.4.1 Exponentially weighted running averages

A first-order recursive filter which provide an exponentially weighted running average is often used to average the raw receiver samples (Doviak and Zrnic, 1984). This averaging method has the advantage of providing an averaged output for each pulse and was in general use (in analog form) for the continuous displays on CRTs. Zrnic (1977) has shown that the means and the variances of the input power estimates obtained are almost identical to those obtained from a uniform average of n samples if n = (2-b)/b. From (4.6), the DISPLACE equation applicable in the case is:

$$10\log[bP_1^a+(1-b)P_2^a]^{(1/a)}=10\log P_1+\mathbf{(10/a)\log b+(10/a)\log[1+0.7943^{a((10\log P1+(10/a)\log b)-(10\log P2+(10/a)\log(1-b))}]}$$

for $0 \le b \le 1$ (5.7)

where a is the power law of the receiver to be simulated.

To achieve exponential averaging corresponding to a quadratic receiver and using the standard table, (5.7) reduces to:

$$10\log[bP_1+(2-b)P_2] = 10\log P_1+\mathbf{10\log b+10\log[1+0.7943^{a((10\log P1+10\log b)-(10\log P2+10\log(2-b))}]-10\log 2}$$

(5.8)

where b must again represent a value between 0 and 2. The procedure to be followed is much the same as that described in section 5.3.1 for the weighted averages in the CAPPI application with the simplification that in this case b is a constant. In terms of processing, this application of DISPLACE requires 896 DISPLACE operations to achieve the range and time-azimuth averaging described previously.

5.4.2 Processing dual-polarization data

The measurement of differential reflectivity (Z_{DR}), utilizes the receiver powers at vertical and horizontal polarization from the same sampling volume, as proposed by Seliga and Bringi (1976). Z_{DR} has shown great potential in improving the accuracy of rain-rate estimates and in identifying hydrometeors, such as hail. Many meteorological radars now have this capability (see Chapter 2).

When logarithmic receivers are used in a dual-polarisation radar it is desirable to average the antilogarithms of their output prior to computing differential reflectivity, Z_{DR}. Chandrasekar et al (1989) has shown that by averaging the antilogarithms, the variance in the estimate of Z_{DR} can be reduced to almost that obtained when using quadratic receivers. The DISPLACE method therefore provides an efficient method to achieve this improvement in differential reflectivity measurements while using logarithmic receivers.

5.4.3 Processing dual-wavelength data

Doviak and Zrnic (1984) state that, although the attenuation at S-band is negligible, X-band suffers attenuation that is approximately 100 times larger, since at X-band the precipitation particles often result in Mie scattering (see Chapter 2).

When sampling the same volume of precipitation particles at a non-attenuating and an attenuating wavelength, the attenuation rate at the shorter wavelength can be determined by using the measurements at the longer wavelength as reference. On the MRL-5 radar, which operates at S- and X-band, the antennas were designed to match the beam patterns at the two frequencies. The DISPLACE method provides a simple way of determining the attenuation of the shorter wavelength in real time. After the *range bin* averages for every *ray* have been determined for both channels using the quadratic version of DISPLACE, the difference in VP counts (corresponding to a dB difference) is calculated for each *range bin* using the DISPLACE equation given by (4.7). The table used is a modified quadratic difference *displacement* table which incorporates the differences in slopes between the two receivers. After obtaining these differences, the same algorithm is used with the standard quadratic difference *displacement* table to compute the difference between range bin i+2 and i for i=1,2,...,n-2. In this manner digital values which corresponds to the dB attenuation over the distance of two range bins are obtain for range bins 2 to n-1. The procedure is simplified and can be achieved in real time if the digitizing and averaging of both channels are done on the same processor card. The version RVPC-2 described in Chapter 3 allows this.

The inclusion of attenuation measurements in a radar-rainfall relationship provides an additional parameter of the dropsize spectra (Wexler and Atlas, 1963). Hail can have a significant effect on measurements with a dual-wavelength radar. Eccles and Atlas (1973) suggested a

method to use this effect in a hail detection algorithm. These authors used the range derivative of the logarithm of the ratio of the average echo powers at the two wavelengths as a hail indicator. The use of attenuation measurement alone has previously been investigated as an indication of hail but resulted in an unacceptable false alarm rate. Eccles and Atlas (1973) argued that the false alarm rate could be lower significantly by using the range derivative, as this derivative only becomes negative at the trailing edge of a hail shaft. When only rain or cloud liquid water is present the derivative will always be positive. This results from the fact that the wavelength dependancy of the equivalent reflectivity factor of hail is different from that of rain, and normally considerably higher at S- than at X-band. Hail will often lead to almost complete Mie scattering at X-band while Rayleigh scattering will still be significant at S-band.

Adapting the DISPLACE procedure to obtain the range derivative of the attenuation in real time necessitates one additional step. For the ray of attenuation values, the quadratic DISPLACE difference is taken between consecutive range bins, again using the standard *displacement* table. This will result in the range derivative of attenuation over the distance of two range bins for range bins 3 to n-2.

However, this hail detection approach has been discredited by subsequent information on the attenuation by wet hail (Battan, 1973).

5.4.4 Rainfall accumulation

For hydrological purposes the accumulated radar-rainfall field over varying periods of time is of particular importance. The rain-rate weighted averaging version of DISPLACE (see (5.6)) can be used to obtain these fields as follows:

$$10\log\{[(m-1)/m]Z_1^{1/1.6}+(1/m)Z_2^{1/1.6}\}^{1.6} =$$

$$10\log Z_1+\mathbf{16\log((m-1)/m)+16\log[1+0.8660^{((10\log Z1+16\log((m-1)/m))-(10\log Z2-16\log(1/m)))}]-16\log m} \quad (5.9)$$

for $m \geq 2$. The Z_1 values represent those from the latest CAPPI over which this accumulation is done. The weighting factors; (m-1)/m and 1/m; represent the weighting of the latest CAPPI to be added to the weighting of the CAPPIs that have already been accumulated (m being the total number of CAPPIs). In this manner a running accumulation of radar rainfall is obtained while all the values remain in, and calculations are done on, video processor (VP) values. The radar-rainfall field can then be obtained by converting the VP values to rain rate (using a lookup table) and then multiplying by the time interval in hours over which the accumulation is done. Therefore, the conversions from VP values to rain rate will only take place at the end of an accumulation period.

In the next chapter data collected with the MRL-5 radar's S-band, using quadratic DISPLACE averaging, will be compared to data averaged and corrected for the average bias in the conventional manner. Throughout the case studies, CAPPI's will be used which are compiled with DISPLACE for the interpolations. The ground clutter application of DISPLACE will also be evaluated in more detail.

CHAPTER 6

CASE STUDIES AND RESULTS

6.0 INTRODUCTION

The RDAS linked to the MRL-5 radar provided the ideal means for collecting S-band data, averaged in both the conventional way and using the quadratic DISPLACE method, in real-time. The DISPLACE algorithm, with the appropriate quadratic *displacement* table, was introduced into the video processor card normally used for X-band data collection and the S-band video signal was also fed to this card. The A to D convertor on this card was calibrated with a high precision analog source to be equivalent to that on the S-band card and the correspondence was verified on a regular basis. During the period 25 February to 25 March 1995 the radar was operated in volume-scan mode.

When data collection for the new season commenced in October 1995, S- and X-band data were archived, both being processed using the quadratic DISPLACE method. By this time the Enterprise C-band radar's RDAS was also using DISPLACE averaging. The X-band data collected on the MRL-5 radar during the 1995/96 season was of an experimental nature and is not used in this thesis.

This chapter deals with case studies illustrating the use of the DISPLACE method. In Section 6.1 the emphasis is on convective storms. The first example is 13 March 1995. A thorough treatment of differences between the quadratic DISPLACE and conventional data is given in terms of radar-rain-gauge comparisons, the storm properties derived using objective storm-tracking software and beam broadening effects. The second example in this section is 24-25 January 1996. During this period, slow moving storms produced heavy rainfall leading to a flash flood in the Liebenbergsvlei River catchment. The quadratic DISPLACE data are compared to the rain-gauge network data in terms of the rain-rate distribution and accumulated area rainfall. The MRL-5 S-band data are compared to that collected by the Enterprise C-band radar to show the severe attenuation that can occur under these conditions.

In Section 6.2 the emphasis is on general rain conditions. Firstly, a comparison between quadratic DISPLACE and conventional data is done using data collected on 25 March 1995. This event is also a good example of the detrimental effect that the 'bright band' can have on area rainfall measurements. Secondly, the floods during the seven day period 9 to 16 February 1996, are discussed using the rain-gauge network, stream flow and quadratic DISPLACE radar data for the Liebenbergsvlei River catchment.

In Section 6.3 attention is turned towards ground clutter filtering. The performance of the clutter filtering procedure discussed in Section 5.2 is verified using data collected with the MRL-5 radar's S-band section. Studies are performed for precipitation echoes, in the presence and absence of clutter. The effect of antenna rotation speed is also investigated.

Throughout this chapter examples of the new CAPPIs are used. As indicated in Chapter 3, these interpolation CAPPIs also make use of the DISPLACE method.

This chapter deals with the real-time applications of the DISPLACE methods already implemented in South Africa and those planned for the immediate future. The examples show the uses of DISPLACE processing and also provide a clear indication of the excellent performance and reliability of the MRL-5 radar and the rain-gauge networks. This bears testimony to the dedication of the technical members of the NPRP. The hydro-meteorological applications of the data for both the rainfall stimulation research effort, which is moving towards area experiments, and for severe weather warnings and reservoir management under flood episodes, are clear.

6.1 CONVECTIVE STORM STUDIES

6.1.1 13 March 1995

A study of 13 March 1995 is presented to illustrate the differences obtained between data collected from the MRL-5 S-band using the conventional and quadratic DISPLACE averaging methods in real-time when intense convective storms are observed. These differences can be seen as corrections made by the quadratic DISPLACE method as it provides an unbiased estimate of the average received power even in the presence of reflectivity gradients within a radar range bin.

a. Reflectivity

During the afternoon of 13 March 1995, intense convective development occurred in the northern sector of the MRL-5 radar area. In Figure 6.1a the 15:01 reflectivity field obtained using the quadratic DISPLACE method at the 2.5° elevation scan is shown as a range/azimuth plot. It was verified that this sector is not affected by ground returns and only reflectivities above a 20 dBZ threshold are shown. The maximum reflectivity of 59.7 dBZ occurred in the western sector of the storm with areas of steep reflectivity gradients facing the radar. Figure 6.1b shows the decibel differences between the quadratic DISPLACE results and those obtained using the conventional averaging method after applying the 2.5 dB averaging correction. Differences were only computed in regions where both the field shown in Figure 6.1a and that obtained using the conventional method indicated reflectivities in excess of 20 dBZ, and only positive differences are shown. The negative differences that did occur were relatively isolated and small, the largest being -1.6 dB. The positive differences clearly follow the areas of steep reflectivity gradients. A maximum difference of +13.5 dB occurred in a range bin across which a reflectivity gradient in excess of 50 $dB.km^{-1}$ occurred. This value agrees with theoretical values and differences observed by other investigators (Sirmans and Doviak, 1973). For the total storm area shown in Figure 6.1a, the average difference between the results of the two methods was +1.29 dB, which corresponds to an average range bin underestimation in returned power of 25.7 %.

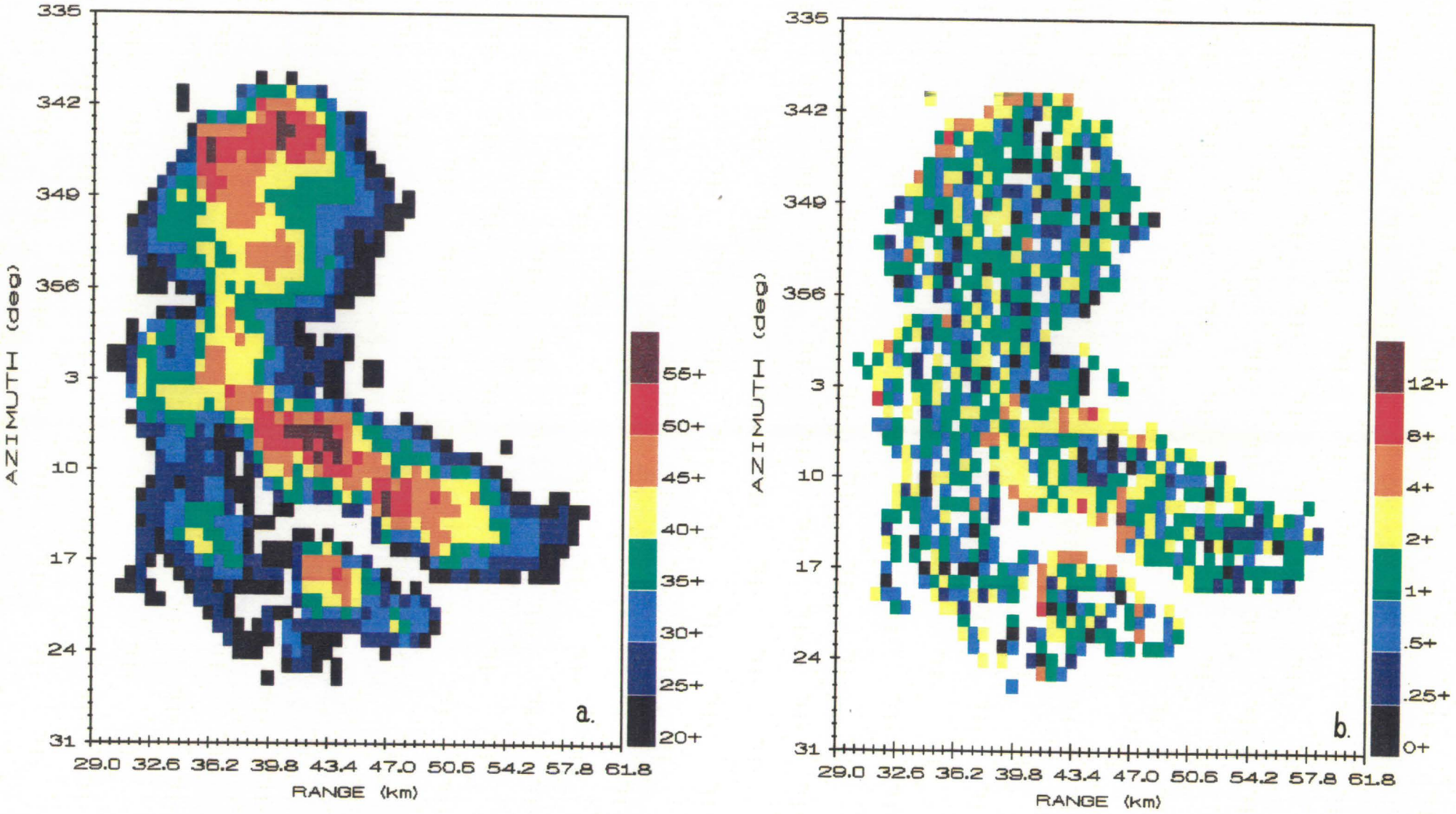

Figure 6.1 15:01 on 13 March 1995: a. Reflectivity field (dBZ) at 2.5 degree using the quadratic DISPLACE data as a B-scan plot, b. The corresponding dB difference between the reflectivity field obtained using quadratic DISPLACE and conventional averaging.

b. Rain rates and area rainfall

S-band radar data for the Liebenbergsvlei River catchment (4650 km^2), which is equipped with 45 tipping bucket rain gauges on a 10 km grid, is used to compare the radar and rain gauge rainfall measurements. An approach similar to the so-called "probability matching" technique (Rosenfeld et al., 1993; Seed et al., 1996) is used in the rain-rate comparisons. The radar completes a volume scan in between 4 to 5 minutes. This volume-scan period is used as the time interval to process both radar and rain-gauge data. The 0.2 mm resolution of the rain gauges results in discrete rain-rate intervals of approximately 3 mm h^{-1} in the volume-scan period. The radar data which have a one km resolution in CAPPI format (2 km above ground), is converted to rain rates using the Marshall-Palmer Z-R relationship. Both the radar and rain-gauge data are then sorted into the following intervals:

[1;4) mm h^{-1} [4;7) mm h^{-1} [7;10) mm h^{-1} [10;13) mm h^{-1} etc.

where [is an inclusive boundary and) an exclusive boundary.

During a rain event, the total number of occurrences in all the rain-rate intervals is used to calculate the percentage occurrences in each interval for both radar and rain-gauge data. Therefore, these percentages (or the exceedance probability percentages calculated from them) reflect the rain-rate distribution **during the time is was raining**. Only when the whole are is experiencing rainfall during a volume scan period, will the total number of occurrences for that volume scan be 4650 for the radar data and 45 for the rain-gauge data.

Figure 6.2 shows the rain-rate exceedance probabilities, where P(R>x) is the percentage rain rates exceeding the rain-rate value (x) on the x-axis. A good correlation between the radar and rain-gauge measurements is evident indicating that both radar and rain gauges measured close to the same rain-rate distribution for the event. Figure 6.3 shows the percentage contribution of the observed rain rates to the total measured rainfall. Again the good correspondence is evident, with possible evidence that the quadratic DISPLACE data is a closer match to the rain-gauge data. Of note in these figures is the smoothness of the radar derived curves when compared to those of the rain gauges. This is evidence of the point sampling of the rain gauges versus the smoother area averages of the radar. The total sampling area of the 45 rain gauges is about 1.5 m^2, which represents a fraction of less than 10^{-9} of the total catchment area. The rain gauges were at a distinct disadvantage in accurately determining the "time it was raining" as will be shown in area rainfall measurements as reflected in Figure 6.4.

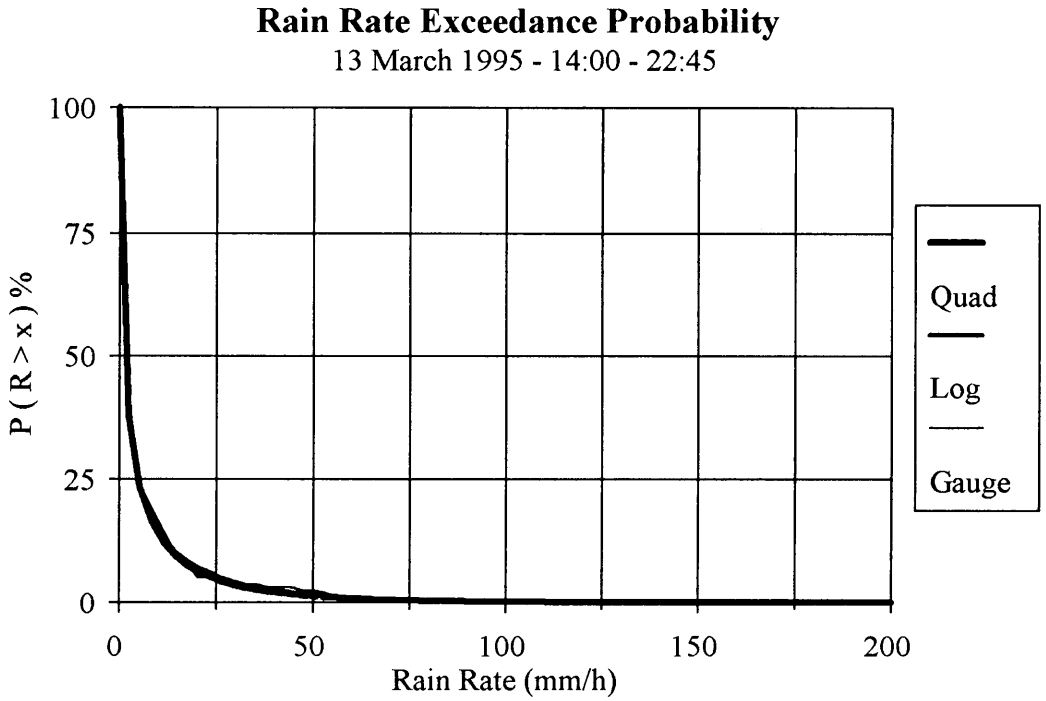

Figure 6.2 Rain rates on 13 March 1995: Exceedance probabilities.

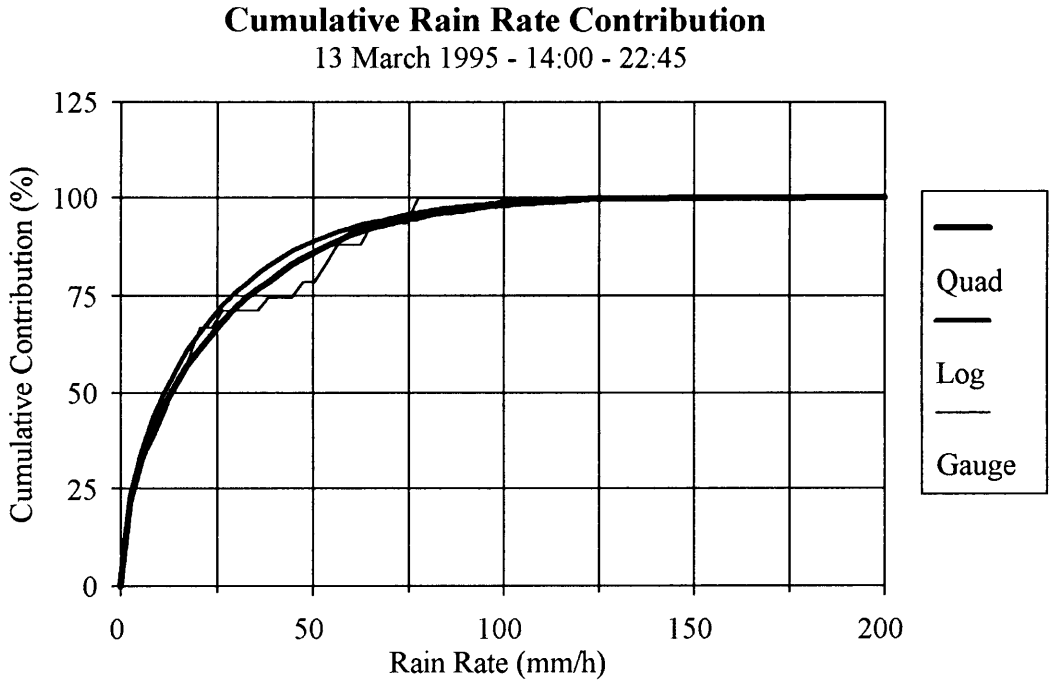

Figure 6.3 Rain rates on 13 March 1995: Cumulative contribution to the total rainfall.

The time history of accumulated area rainfall inferred from radar and the rain-gauge network is shown in Figure 6.4. The quadratic DISPLACE radar-rain-gauge ratio comes to 2.7 compared to 2.3 for the conventionally averaged radar data. Once again the smoothness of the radar derived curves are evident. Although the quadratic DISPLACE radar-rain-gauge ratio is the largest, the conditions studied in this case (intense convection) are those in which rain gauges are known to poorly sample the rainfall field. The information shown in Figures 6.2 and 6.3 is possibly a much more revealing way of comparing the radar and rain-gauge measurements under these conditions.

The 24-hour quadratic DISPLACE rainfall field for the period which ended at 08:00 on 14 March 1995, as derived from 2 km CAPPIs, is shown in Figure 6.5a. The isohyets derived from the rain-gauge network are also shown. In Figure 6.5b the difference in rainfall between the fields using quadratic DISPLACE and conventional data is shown indicating a maximum discrepancy of just over 9 mm for the day. Of note is the high spatial variability in the rainfall field which is typical for convective conditions and which gives radar a clear advantage for measuring area rainfall. The relatively high rainfalls that occurred between rain gauges led to an underestimation in area rainfall using the rain-gauge data. Many investigations blame poor radar-rain-gauge comparisons on the radar. Here is clear evidence of inadequate gauge coverage of an area, leading to serious errors in the gauge measurements of rainfall. The ground clutter in the south-eastern sector is clearly evident in Figure 6.5 a. Prominent mountain ranges are the Rooiberge, Witteberge, Malotis and the Drakenberg escarpment which rises to more than 3000 m above sea level (refer to Chapter 3).

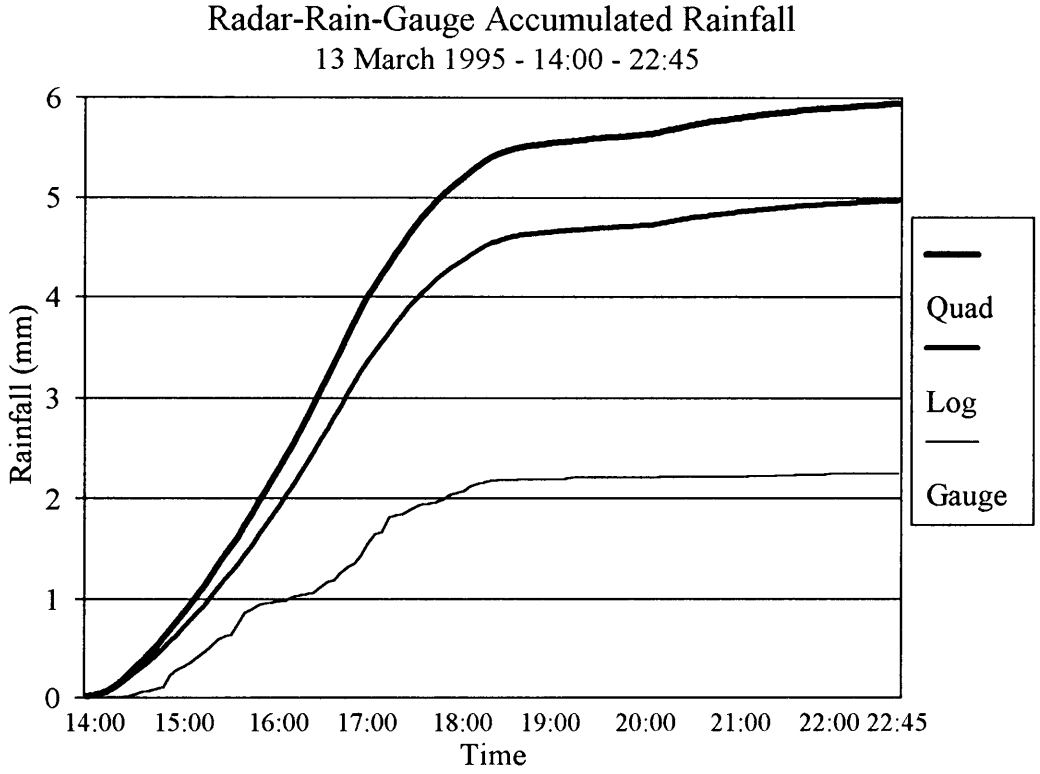

Figure 6.4 Radar (quadratic DISPLACE and conventionally averaged) and rain-gauge inferred time histories of accumulated area rainfall.

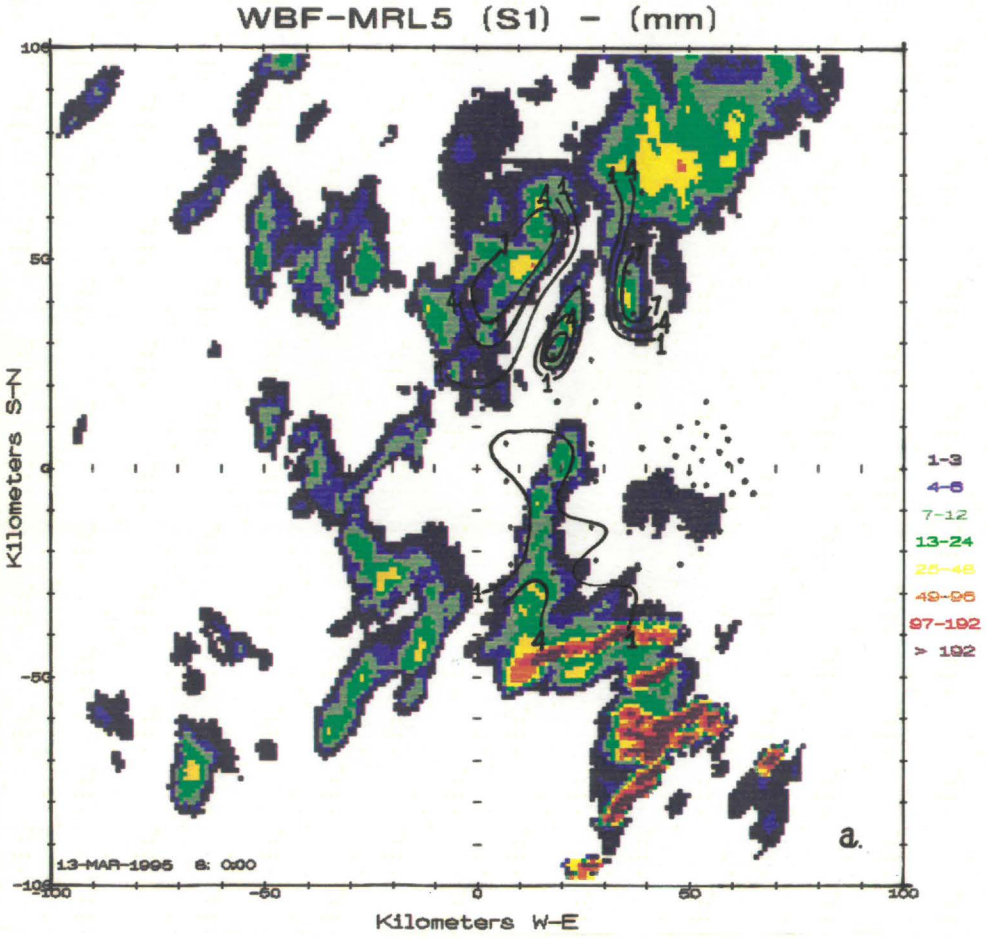

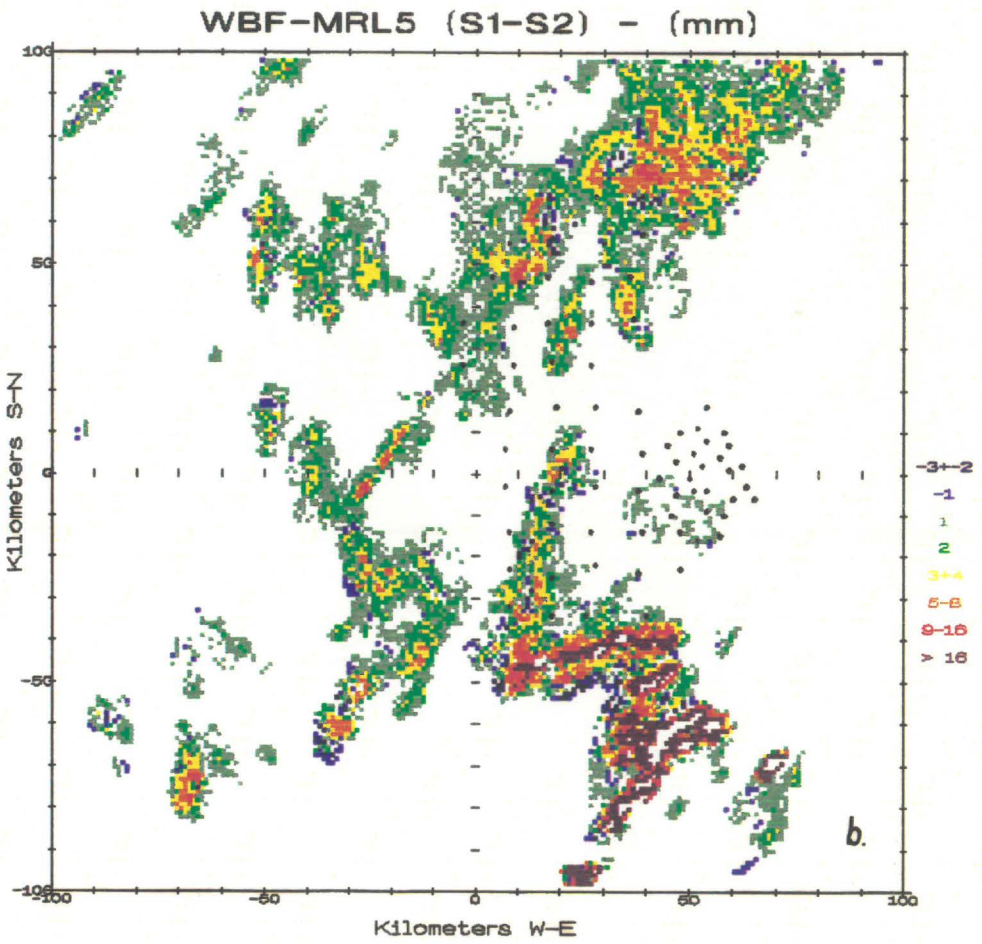

Figure 6.5 Radar-rainfall field in mm for the period studied on 13 March 1995: a. Quadratic DISPLACE based data with isohyets derived from the rain-gauge network, and b. Difference in rainfall between quadratic DISPLACE and conventional data.

c. Storm-track properties

The storm mentioned in Section 6.1.1a was tracked, using a 30 dBZ threshold, for 34 consecutive volume scans between 13:59 and 16:26 using the standard NPRP tracking software described by Dixon and Mather (1986). More information on this software can also be obtained in Mather et al. (1996). It was interesting to note that the quadratic DISPLACE data caused the software to identify only one track. When the conventional data was used, this storm was identified as two tracks. The conventional data introduced an erroneous centroid position for volume scan seven, causing the observed track jump which exceeded the specified maximum allowed centroid velocity. Table 6.1 gives a summary of the differences between some storm properties during the storm's lifetime using the two data sets.

Table 6.1 Percentage volume-scan mean and maximum differences between quadratic DISPLACE and conventionally averaged data over the lifetime of the 13 March 1995 storm.

	Volume	Storm Mass	Mean Area	Base scan Area	Rain flux per Base scan Area	Rain flux
Mean	+11.6	+21.0	+9.5	+10.5	+10.6	+21.8
Maximum	+29.0	+29.8	+28.1	+49.4	+18.1	+34.0

The ability to simulate averaging as from a quadratic receiver using the DISPLACE method - avoiding the bias introduced by conventional averaging under intense convective storm conditions - affects derived storm properties. These differences are the largest in intense convective storms and tend to zero as the reflectivity field becomes homogeneous, as under general rain conditions. It is interesting to note that the mean difference in base scan area (+10.5%) and rain flux per base scan area (+10.6%) are comparable although the maximum difference for the two properties shows a marked discrepancy (49.4% and 18.1%).

Time history plots of base scan area and rain flux per base scan area are shown in Figure 6.6a and 6.6b. The track jump that occurred after the seventh volume scan for the conventional data set is evident as a local maximum in the base scan area plot.

a.

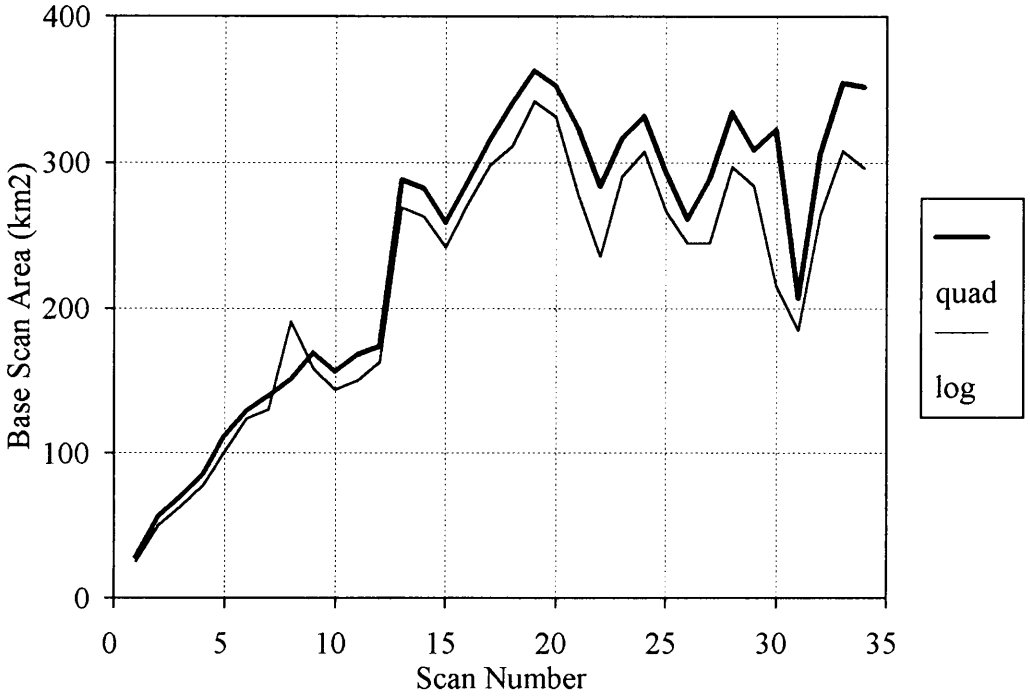

b.

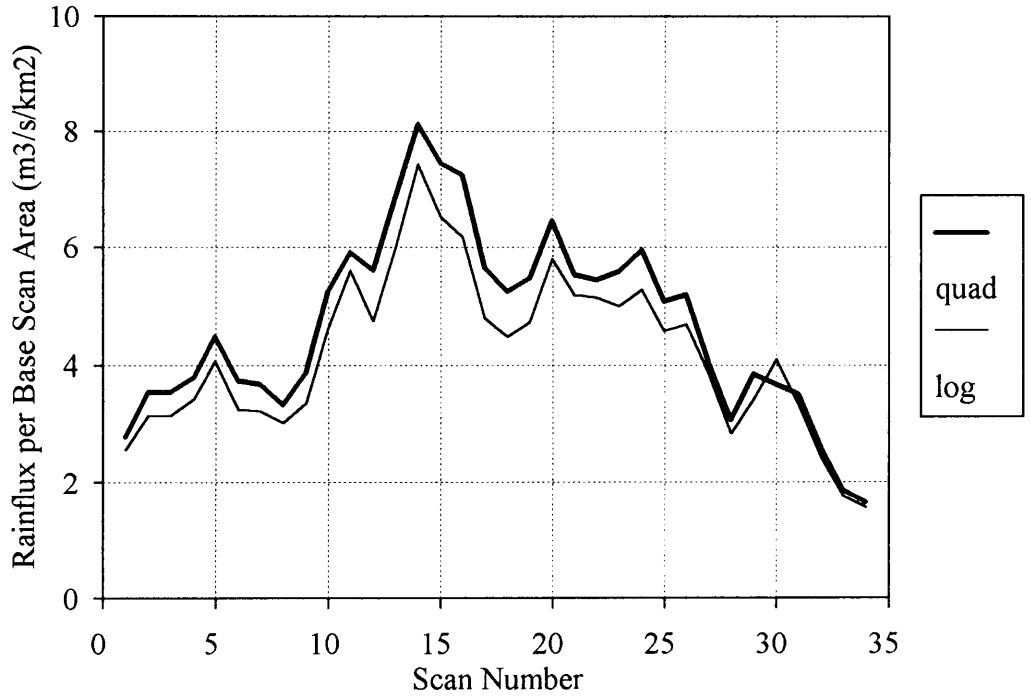

Figure 6.6 Time history plots: a. Base-scan area, and b. Rain flux per base-scan area.

Figures 6.7a and 6.7b show the time history of the differences in reflectivity between the mean and peak reflectivities of this storm. The increase in the difference of mean reflectivity from about 0.5 dB at time of origin to a peak of about 1 dB just after the fifteenth volume scan followed by a gradual decrease to a value of about 0.3 dB just before the track ends, gives a good indication of the evolution of reflectivity gradients within this storm.

a.

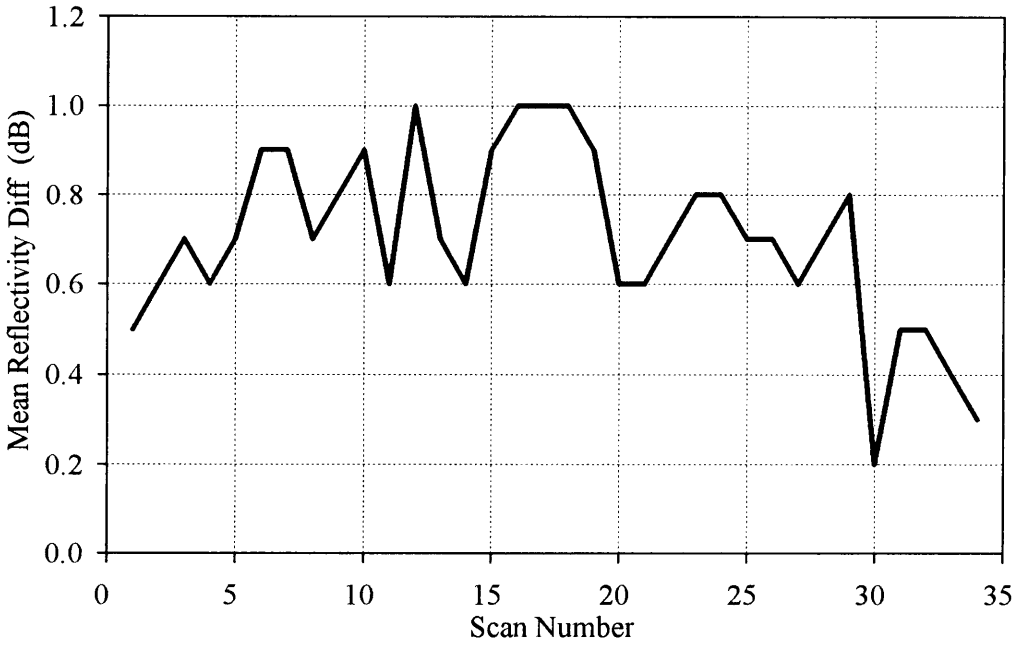

b.

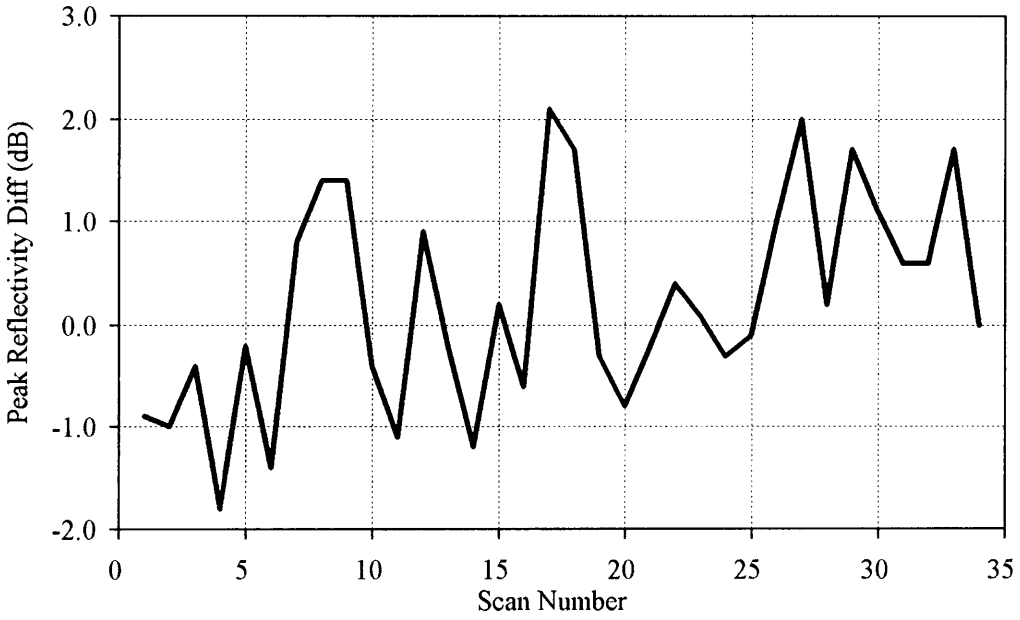

Figure 6.7 Time history plots of differences in a. Mean reflectivity and, b. Peak reflectivity.

This sequence is seen in all storms that have been investigated and can possibly be used as an objective measure of the developing stage of a convective storm. The plot for the difference in peak reflectivities shows a steady increase from about -1.5 dB to about +1 dB during the storm's life. This trend could be explained by either one of the following: (a) During the early stage of a storm's lifetime, the core of maximum reflectivity is more homogeneous (smaller gradients within a range bin) while towards the dissipation stages, this core breaks down. (b) As the storm moved towards the north, starting at a range of 20 km and dissipating at more than 70 km, the interaction between the rotating antenna and partial beam filling in the horizontal could result in this observation. The quadratic DISPLACE method provides an unbiased averaged reflectivity estimate within the sampled volume as the antenna scans through reflectivity gradients. This explanation was tested by computing the differences in rain-rate exceedance probabilities between the quadratic DISPLACE and conventionally averaged data in 10 km wide concentric annuli in the northern half of the radar area. The southern half of the area was excluded to avoid any possible contamination by ground clutter. Figure 6.8 shows the differences between the exceedance probabilities in the 10 km wide concentric rings centred on 25, 45 and 65 km ranges. The curve representing the 65 km data shows the higher rain rates derived from the quadratic DISPLACE data. Partial beam filling in the horizontal, would introduce different kinds of reflectivity gradients for the rotating antenna for the two processing methods. The quadratic DISPLACE data, in terms of the stability in the rain-rate frequency distribution, is probably usable to greater ranges.

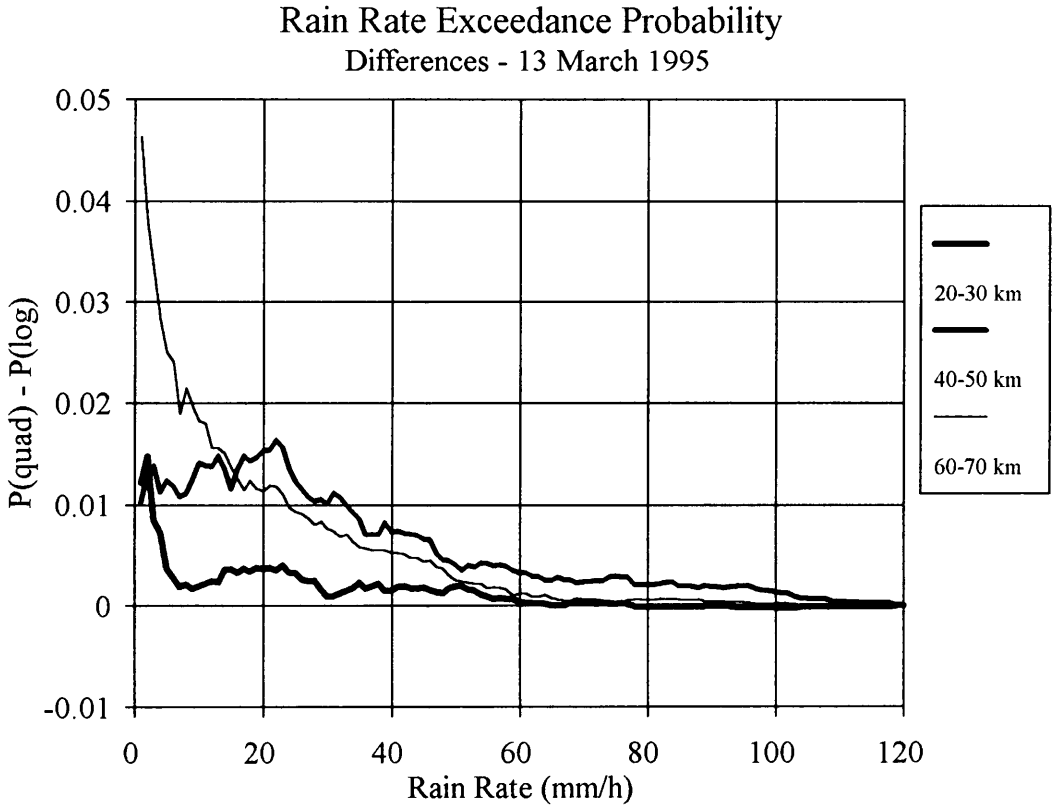

Figure 6.8 Differences between rain-rate exceedance probabilities based on quadratic DISPLACE and conventionally averaged data at different ranges.

6.1.2 24-25 January 1996

Severe thunderstorms occurred in the Bethlehem area during the late afternoon and night of 24 January 1996. The storms, showing little movement, continued throughout the night and extremely heavy falls of rain were recorded the next morning - 177 mm being the maximum at one rain gauge in the Liebenbergsvlei network.

a. Area rainfall and run-off

Only light falls of rain occurred over the Liebenbergsvlei catchment in January preceding the above event, the only exception being falls of about 40 mm over the northern parts of the catchment on January 12. The Vaal Dam was at about 100% of capacity due to the good rains that occurred towards the end of December 1995. The daily average stream flow record for January as obtained from the Department of Water Affairs and Forestry (DWAF) for the Frederichsdal gauging weir, downstream from the Liebenbergsvlei rain-gauge network, is shown in Figure 6.9. According to this record, this gauging point stopped its daily data transmissions on January 26 and stream flow figures for the Liebenbergsvlei River for the last six days of January (indicated by the thin line) were estimated from the difference between two measuring weirs in the Wilge River, one just after the confluence of the two rivers and one before. It is estimated that the increased stream flow due to the heavy rainfall of 24 January 1996, reached a 24-hour maximum of more than 700 m^3s^{-1} on the 26th. From the figure it is also evident that the stream flow response to the rainfall was almost instantaneous. The level of the Vaal Dam rose from 100.6% on the 24th to 105.1% on the 27th, mostly due to the run-off in the Liebenbergsvlei River.

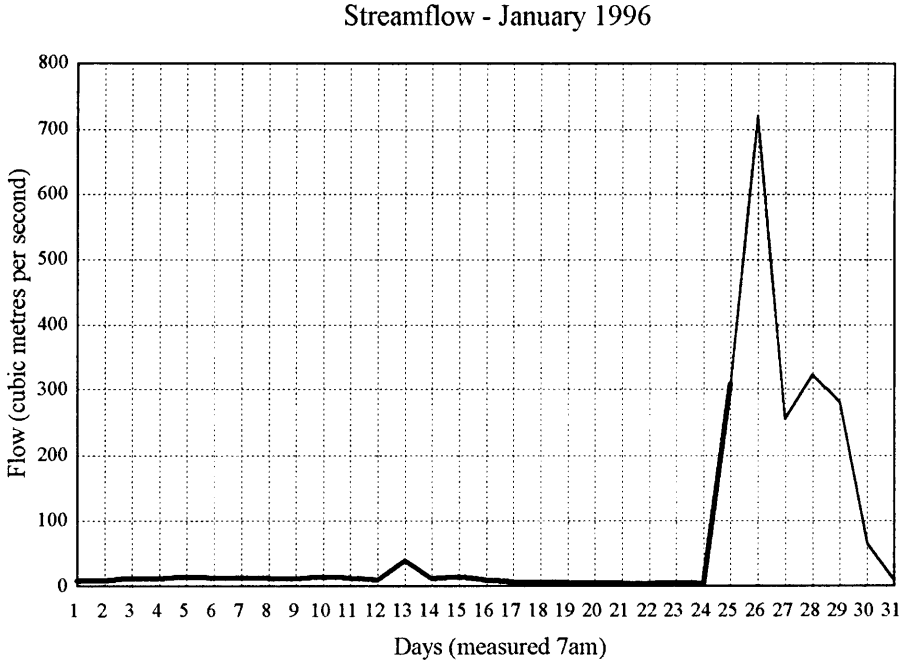

Figure 6.9 Average daily stream flow in the Liebenbergsvlei River for January 1996 as determined by the Frederichsdal gauging weir (see text).

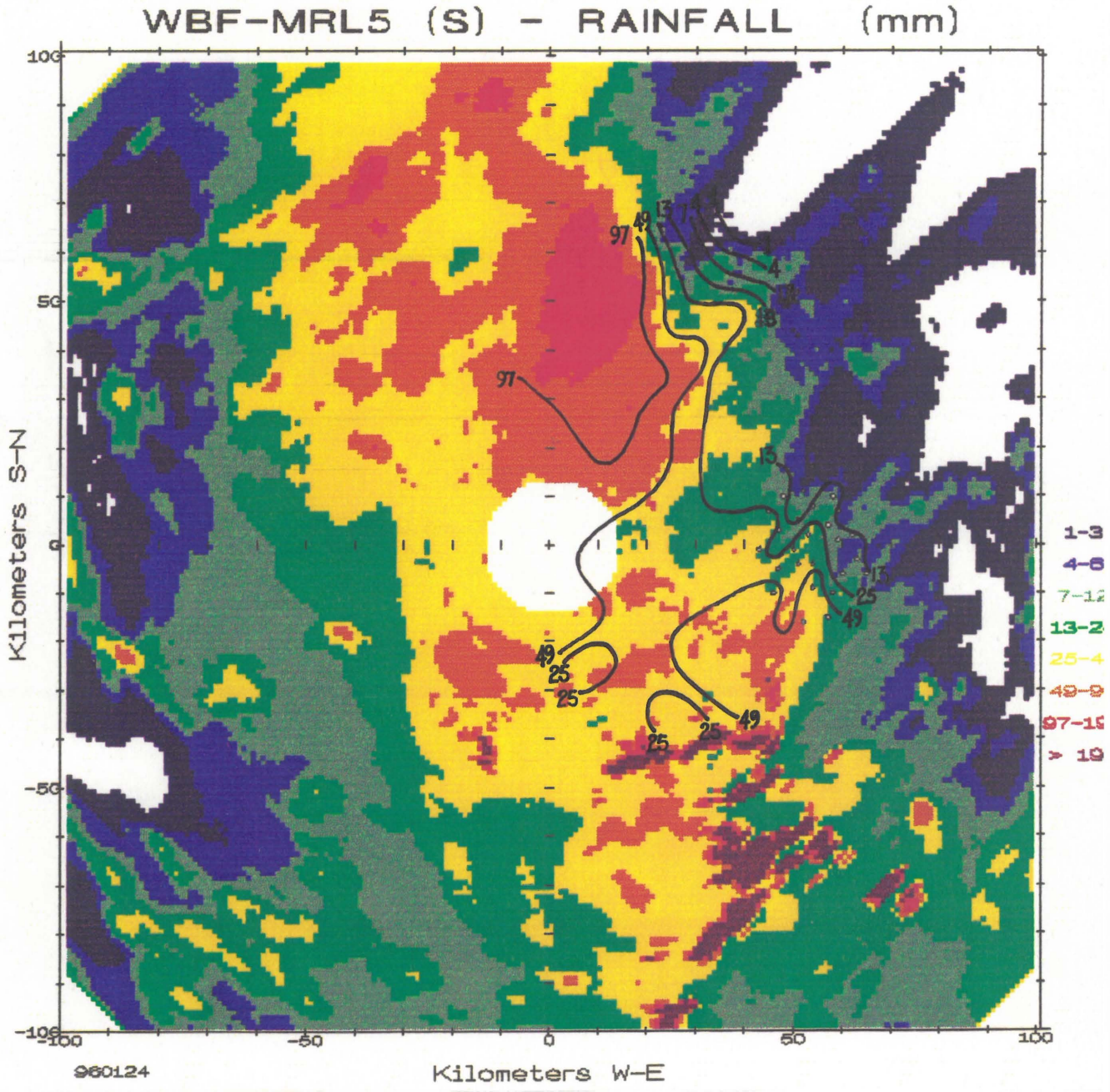

Figure 6.10 Radar-rainfall field for 24 January 1996 and the isohyets inferred from the rain-gauge network.

The MRL-5 radar collected data continuously for the entire rainfall event. The analysis was performed on data from 13:20 on 24 January to 08:00 on the 25th. The radar accumulated rainfall fields for the period, over a 200 by 200 km area centred on the radar, is given in Figure 6.10. Also shown in the figure are the isohyets computed from the rain-gauge network.

The time history plot of the accumulated area rainfall over the Liebenbergsvlei catchment using rain gauges and radar data is shown in Figure 6.11. The main rain event started at about 19:00 and continued throughout the night. The total rainfall depth for the catchment area according to the rain gauges was 62 mm and a fairly good correspondence between rain gauges and radar is evident, with a radar to rain-gauge ratio of 0.79.

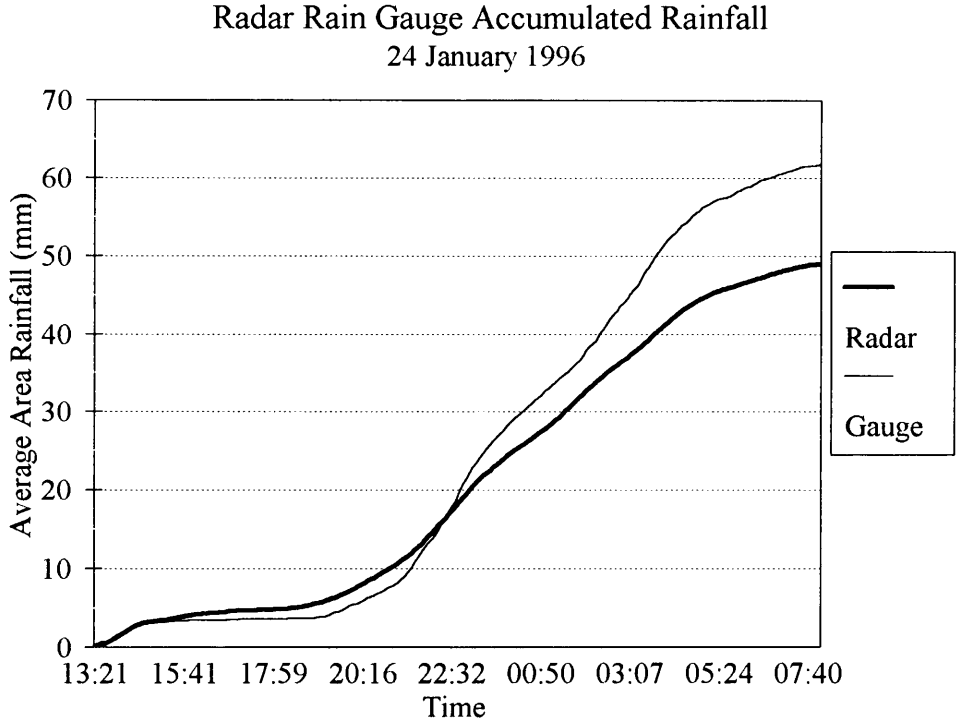

Figure 6.11 Time history of radar and rain gauge accumulated area rainfall for the Liebenbergsvlei catchment.

b. Rain rates

An analysis of the rain-rate exceedance probabilities is shown in Figure 6.12a. Using the same data sets, Figure 6.12b was compiled to indicate the cumulative contribution of different rain rates to the total area rainfall.

a.

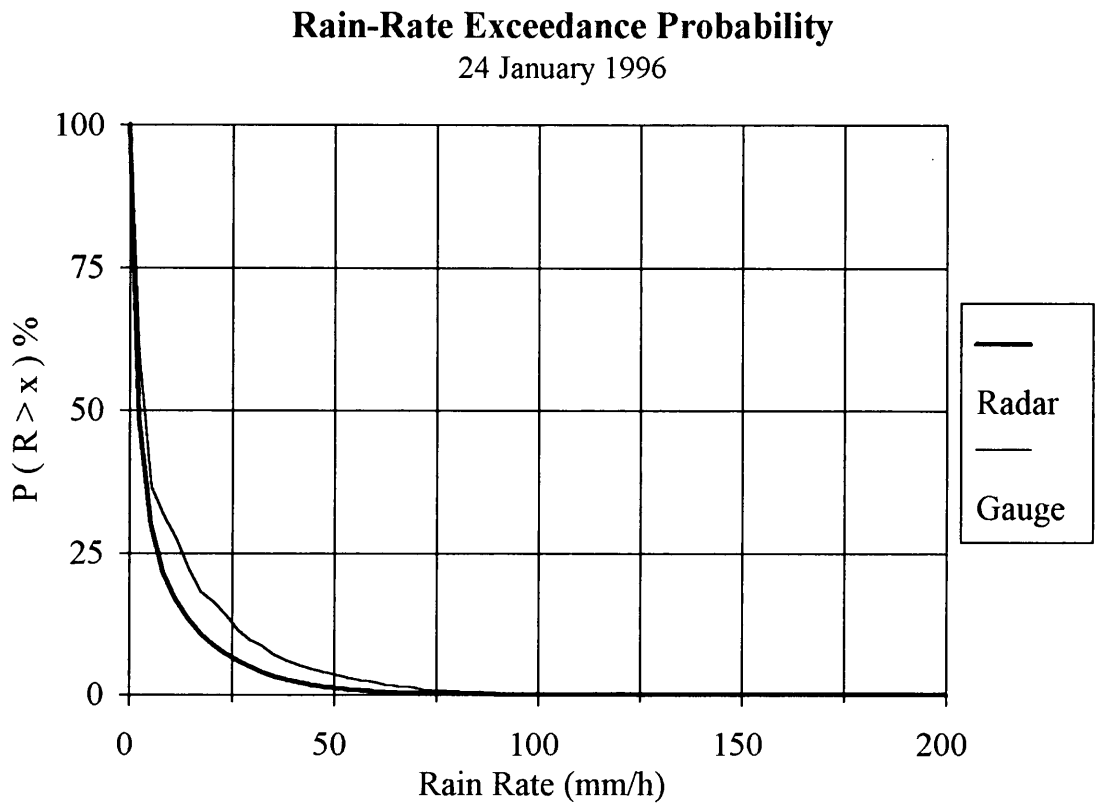

b.

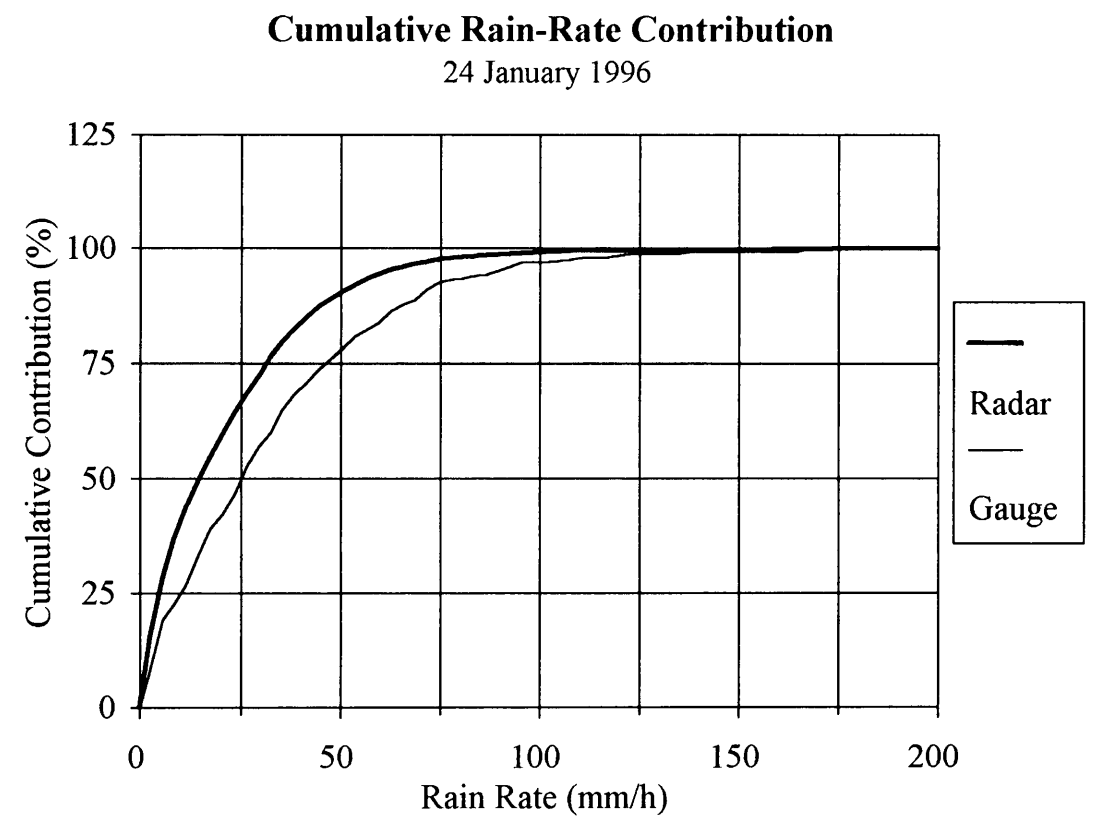

Figure 6.12 24 January 1996: a. Rain-rate exceedance probabilities as measured by radar and the rain-gauge network and, b. Cumulative contribution to the total rainfall.

According to the rain gauges, the maximum rain rate measured in a volume-scan interval was 168 mm h^{-1} compared to the radar's 108 mm h^{-1}. It can also be seen that the radar progressively under-estimated the higher rainfall rates. The sampling difference between radar and rain gauge could play a role in these discrepancies but most likely the use of the Marshall-Palmer Z-R relationship might not have been ideal for this rain event.

c. S- to C-band attenuation

This day also provided an ideal opportunity to determine the attenuation that occurs at C-band during heavy rainfall. CAPPIs were compiled from the MRL-5 S-band (22:59) and corresponding Enterprise C-band volume scans. The difference field was computed for those areas where both fields showed reflectivities in excess of 23 dBZ. The S-band reflectivity field is shown in Figure 6.13a and the S-band to C-band difference field in Figure 6.13b. Attenuation at C-band through the area of intense rainfall north of the radars reached about 20 dB, which is what one would expect from theoretical studies (Doviak and Zrnic, 1984). The much smaller areal extent of the difference field - determined by the area above 23 dBZ in the C-band data - can also be inferred from Figure 6.13. Using C-band radar for rainfall measurements under these conditions can lead to large errors.

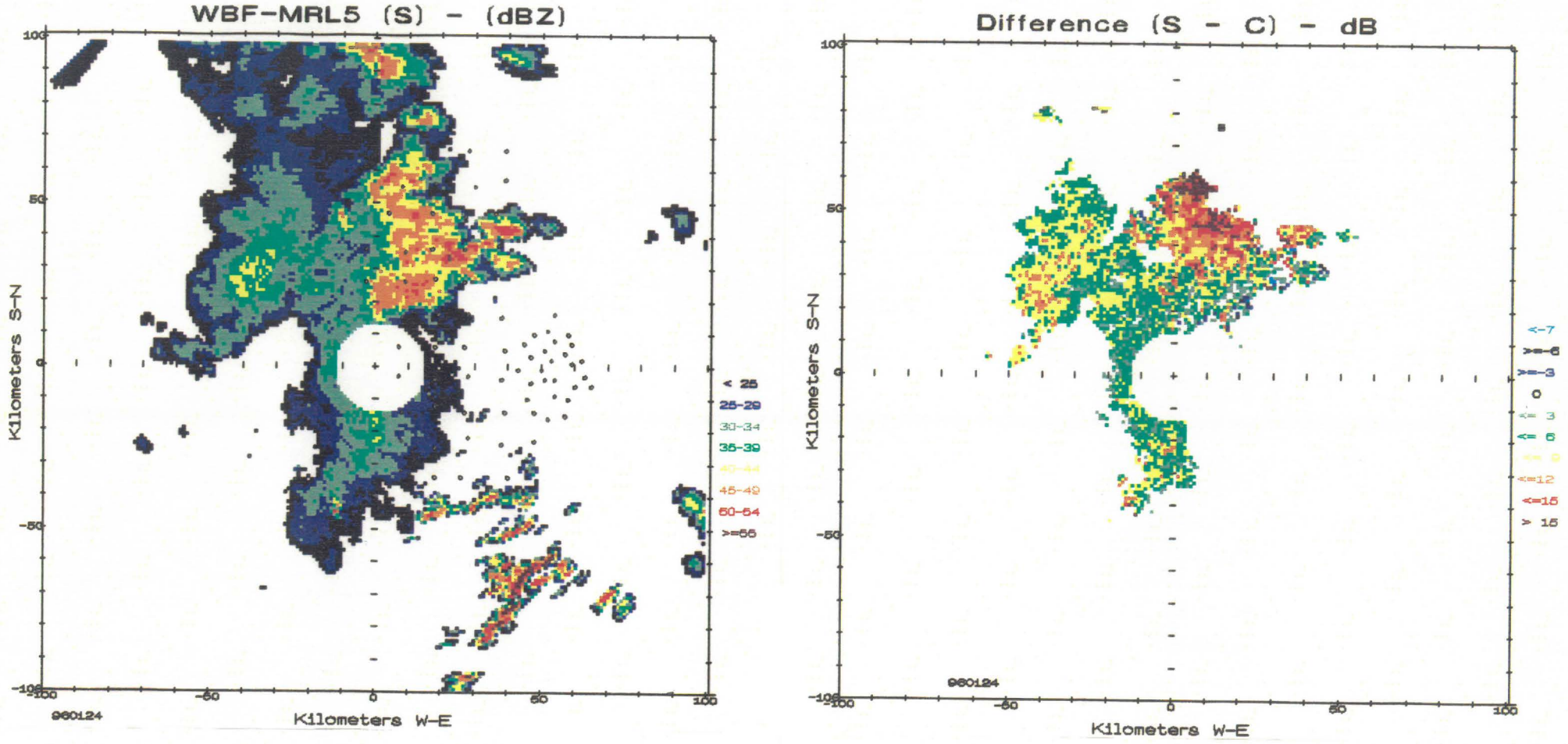

Figure 6.13 a. MRL-5 S-band reflectivity field for 22:59 on 24 January 1996.
b. S-band to C-band difference in dB for 22:59 on 24 January 1996.

6.2 GENERAL RAIN STUDIES

6.2.1 25 March 1995

Wide-spread rain occurred in the north-eastern half of the radar area during the period 02:00 to 15:00 on 25 March 1995. Although the rain continued after this time, data collection on the MRL-5 was terminated. The freezing level was situated between 2.3 km and 2.5 km AGL according to the 02:00 and 14:00 upper-air soundings at Bethlehem. The 'bright band' was clearly evident on this day, at a height where it can have a significant effect on 2 km CAPPI data.

a. Area rainfall

The accumulated Liebenbergsvlei River catchment rainfall as determined from radar (using quadratic DISPLACE and conventionally averaged data) and the rain-gauge network are shown in Figure 6.14. The radar-rain-gauge ratio for this period was about 2. As can be seen from the figure, most of the observed deviation occurred after about 07:30, the correlation between radar and rain-gauge measurements being good before this time. It is probable that the difference between radar and rain-gauge measurement of rainfall is due to the presence of the bright band, which became well defined from about 07:30, leading to enhanced reflectivities affecting the 2 km CAPPI.

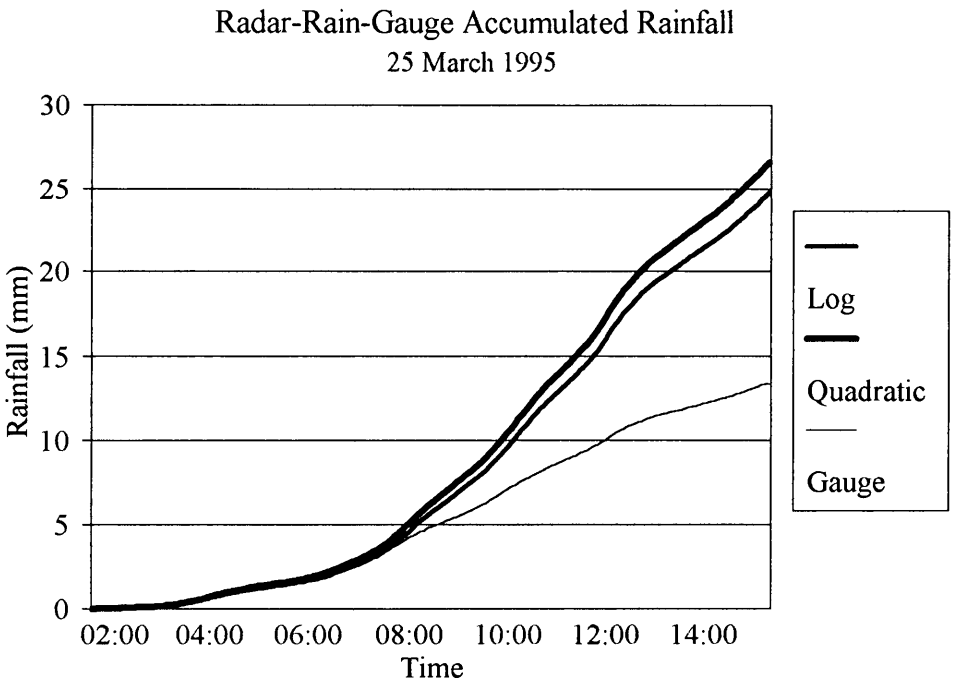

Figure 6.14 Radar and rain-gauge accumulated rainfall for the Liebenbergsvlei River catchment: 01:35 to 15:20 on 25 March 1995.

b. Rain rates

The period under investigation was divided in two parts, the period before and after 07:30 in an attempt to locate the cause of the sudden deviation between radar and rain-gauge measurements that started from about 08:00. The difference between radar and rain-gauge measurements for the two periods is shown in Figure 6.15, where the radar-rain-gauge rain-rate frequency ratios are shown as a function of rain-gauge rain rates. In the period after 07:30, this ratio approaches 4 in the 5.5 mm h^{-1} interval. In contrast to the ratios for the period before 07:30 where the ratios show an asymptotic decrease towards higher rain rates.

Figure 6.16a and b show the rain-rate exceedance probabilities, using quadratic DISPLACE and conventionally averaged radar data as well as the rain-gauge data, for the two periods. Prior to 07:30, the radar observed fewer rain rates with high values. In the period after 07:30, the radar rain-rate exceedance probabilities indicate higher rain rates than those measured by the rain gauges in all rain-rate intervals, except in the first interval. This difference is particularly large in the interval between 8 and 12 mm h^{-1}, as indicated by the rapid convergence of the radar and rain-gauge curves. These rain rates are significant contributors towards the total rainfall. They also correspond to the reflectivities that can be expected in a bright band. Visual inspection of the CAPPIs indicate that the period before 07:30 was characterized by light showers. After 07:30, general rain set in as indicated by the homogeneous reflectivities that occurred over the entire north-eastern half of the radar area.

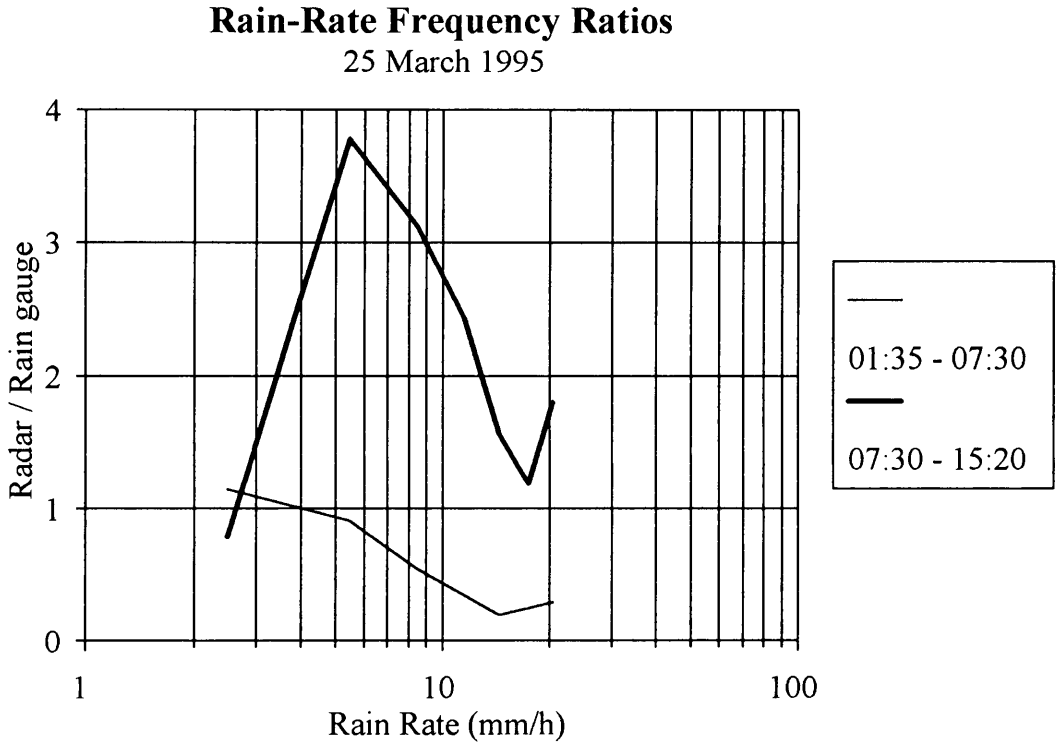

Figure 6.15 Radar and rain-gauge rain-rate frequency ratios for 25 March 1995.

a.

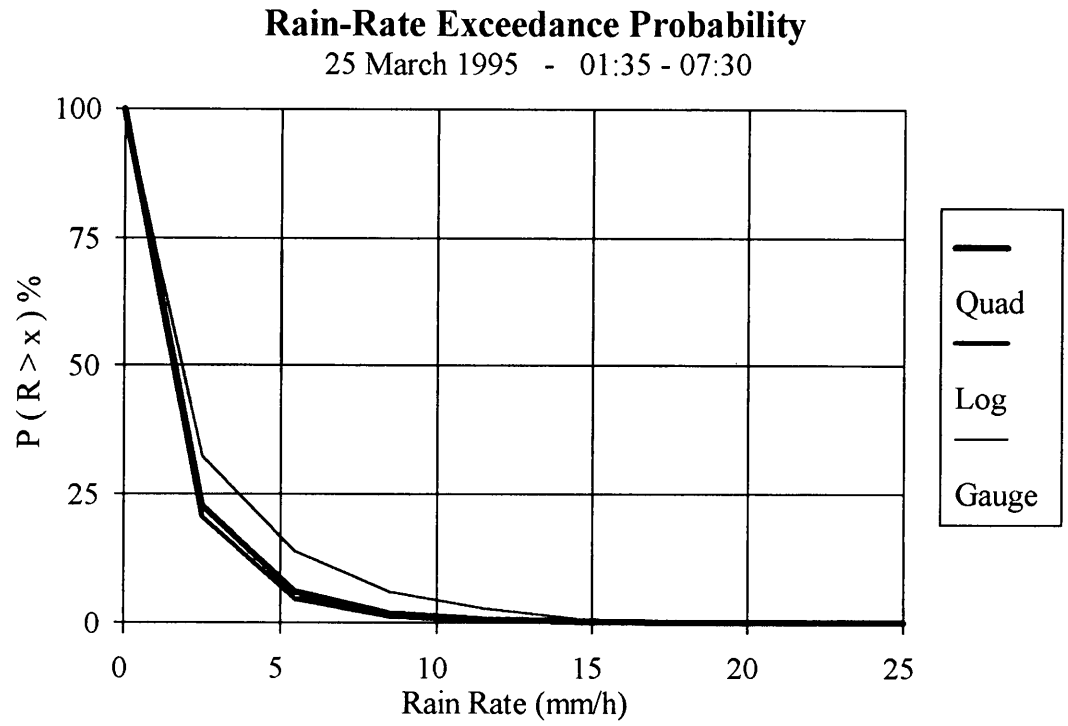

b.

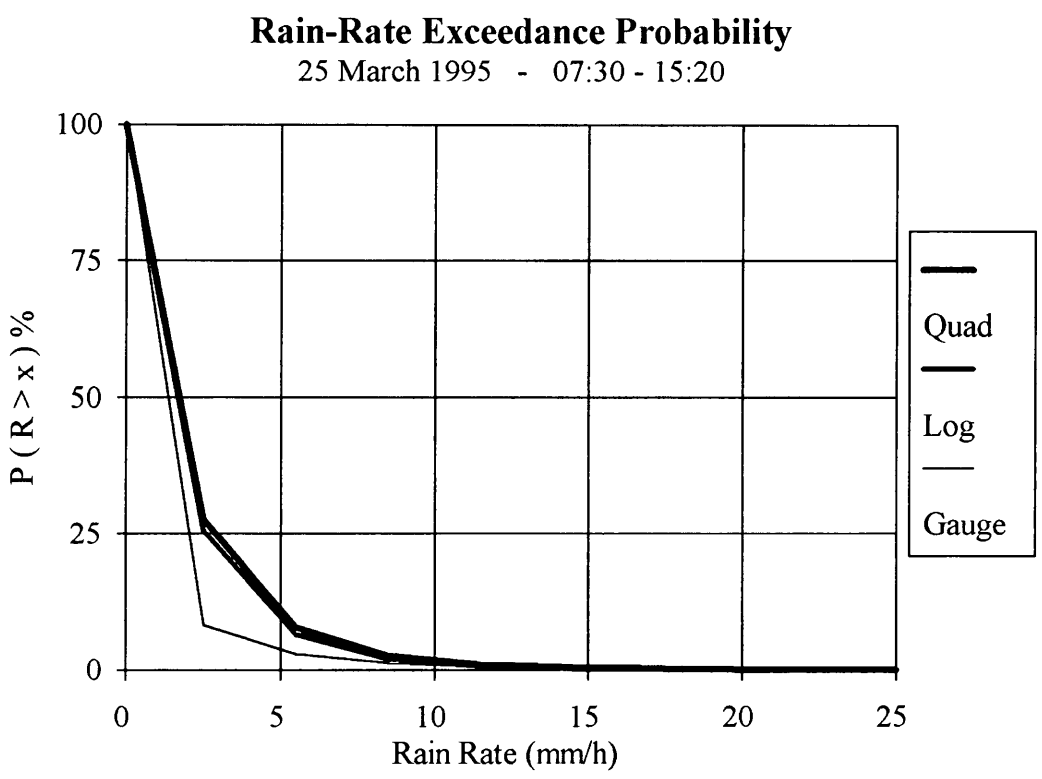

Figure 6.16 25 March 1995 : a. Radar and rain-gauge rain-rate exceedance probabilities. b. Cumulative percentage rain-rate contribution to the total rainfall.

6.2.2 9-16 February 1996

Widespread heavy rain fell over the north-eastern half of South Africa during this seven day period. Extensive flood related damage as well as loss of life occurred. According to historical stream-flow records for the Vaal River, this was one of the highest flood peaks in the past hundred years. The heavy rain occurred in a period during which the Vaal Dam was already filled to capacity, complicating the task of reservoir management. Inflow to the Vaal Dam reached a peak of 4700 $m^3 s^{-1}$ during the night of the 16 February. The level of the Vaal Dam rose from 100.75 % on the 13th to 118.32 % on the 19th despite the large number of sluice gates that were opened.

The MRL5 radar was used to collect data over the entire seven day period. Daily tape changes were the only interruption and as these were done in about ten minutes, the effect on the quality of the data was insignificant. The radar ran without problems during this period, collecting data to document a historical rainfall episode. Personnel at the Bethlehem project were in direct contact with the DWAF during the event, providing information on the rainfall distributions.

a. Area rainfall and run-off

Time histories of the hourly area rainfall as determined from radar and the Liebenbergsvlei rain-gauge network as well as the run-off at Frederichsdal are shown in Figure 6.17. The radar-rain-gauge ratio was 1.03 and the correlation coefficient between hourly measurements was 0.93. During the period considered, the run-off to rainfall ratio was in excess of 0.3. February 13 was a typical day during this rainfall episode and the 200 by 200 km radar rainfall field for the 24 hours up to 08:00 on 14 February is shown in Figure 6.18.

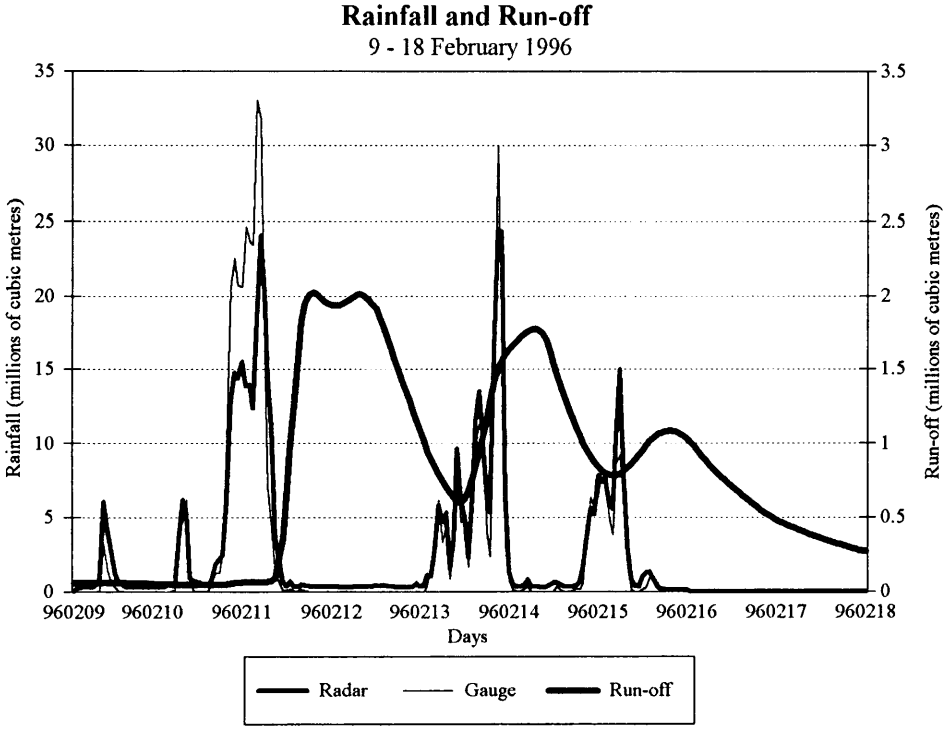

Figure 6.17 Hourly Liebenbergsvlei radar and rain-gauge rainfall and run-off.

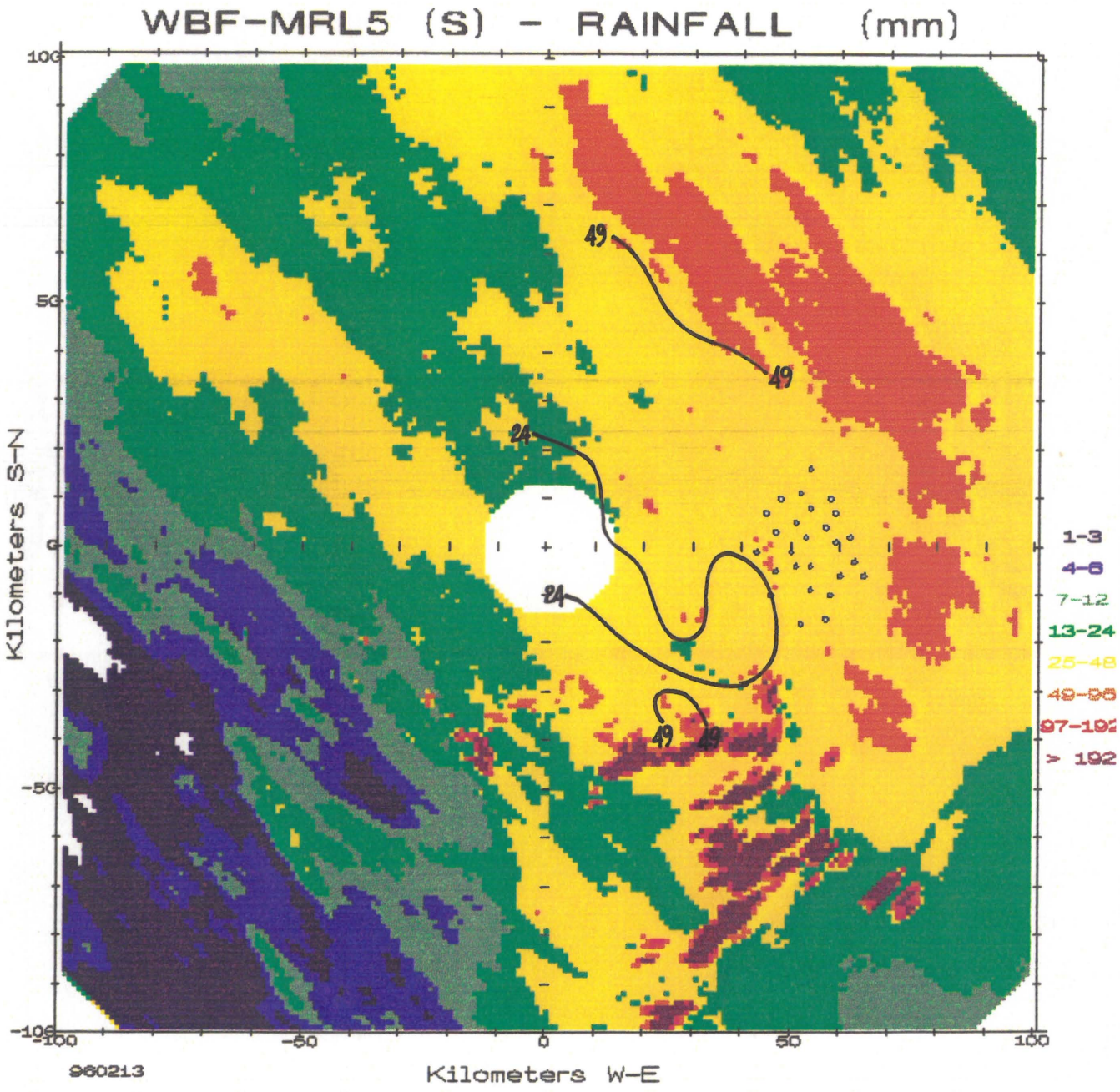

Figure 6.18 Radar-rainfall field for 13 February 1996 with isohyets inferred from the network rain gauges.

b. Rain rates

Figure 6.19a shows the rain-rate exceedance probabilities, using the Liebenbergsvlei network and the radar data for the entire period. Figure 6.19b shows the cumulative rain-rate contribution. Compared to 24 January 1996, it can be seen that the low rain rate occurred more frequently. In this case 50 % of the rainfall resulted from rain rates less than 4 mm h^{-1}. On 24 January this value was about 13 mm h^{-1}.

a.

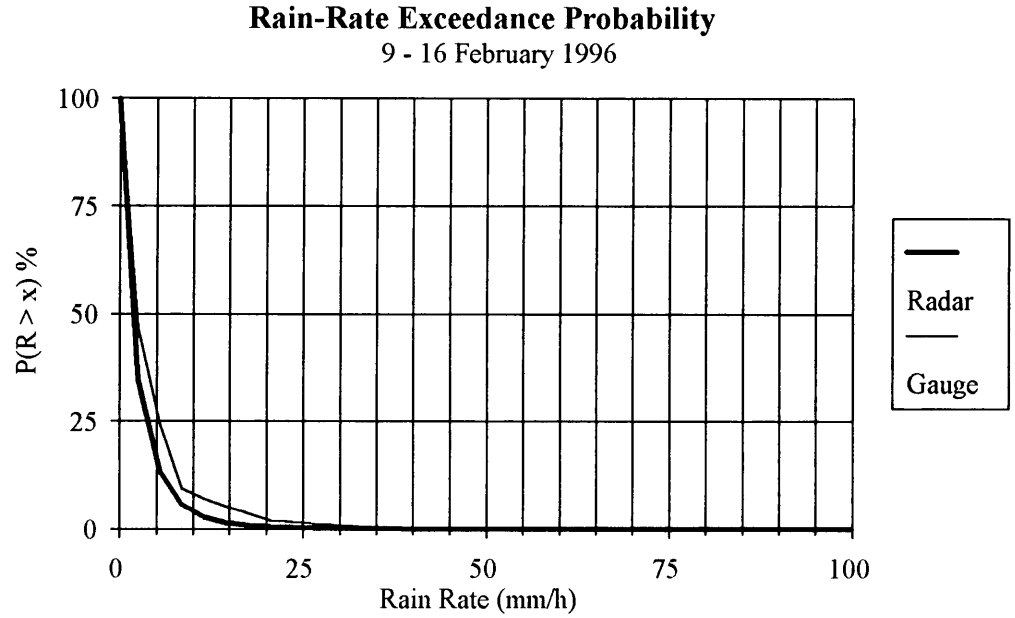

b.

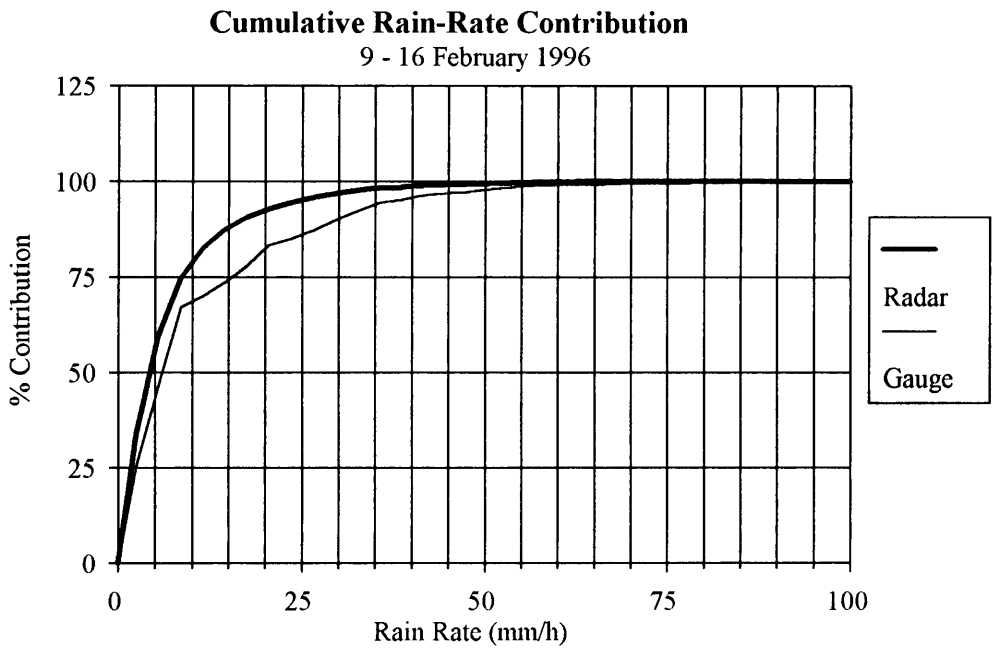

Figure 6.19 9 - 16 February 1996 : a. Radar and rain-gauge rain-rate exceedance probabilities, b. Cumulative percentage rain-rate contribution to the total rainfall.

6.3 GROUND CLUTTER FILTERING

The ground clutter in the south-eastern sector of the MRL-5 radar scan area is in a region that forms part of the Highlands Water Scheme catchment. Improved radar measurements of rainfall over this area are important as the rugged terrain complicates the deployment and maintenance of rain gauges. This sector provided the motivation to evaluate the clutter suppression routine discussed in Chapter 5. Raw digitized samples were collected from the S-band receiver of the MRL-5 radar in this sector with the antenna stationary and rotating. The cases presented here are of a preliminary nature and there is potential to further improve the performance of the scheme.

6.3.1 Studies with stationary antenna

During the afternoon of 22 October 1996 a storm moved over the radar site from the north west. By 15:15, the storm has just past the radar and was extending to the south east. Four seconds of digitized receiver output (500 samples in range over 1000 PRF pulses) was recorded with the antenna stationary at 145° azimuth and 1° elevation. The results calculated with the algorithm described in Section 5.2, were adjusted to correspond to the quadratic DISPLACE averaged reflectivity values in regions that are not effected by ground clutter. A time delay of 8 μs (two PRF periods) was used in the filter. Figure 6.20 shows the M-P rain rates calculated from the quadratic DISPLACE averaged reflectivities before and after the filtering is done.

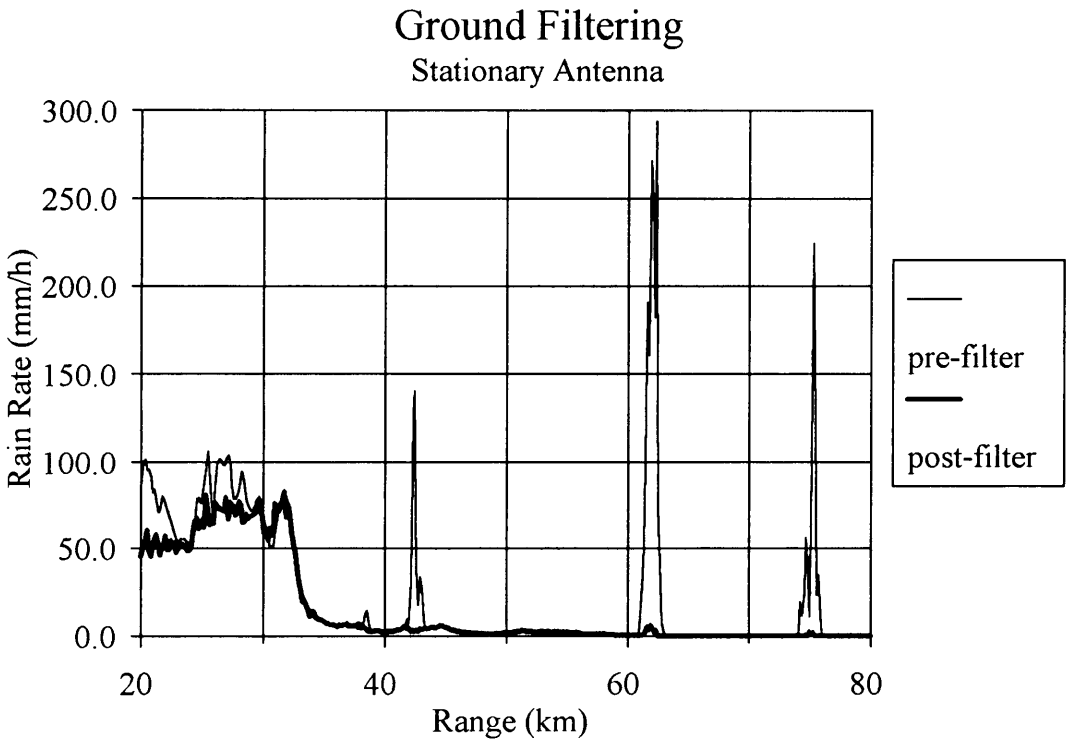

Figure 6.20 Rain rates calculated from quadratic DISPLACE averaged reflectivities before and after applying the ground clutter filter algorithm.

Fairly heavy precipitation (> 50 mm h^{-1}) occurred between 20 km and about 32 km from the radar with only light rain extending out to in excess of 50 km. Between 20 km and 30 km range the precipitation occurred in the presence of ground clutter, with areas of pronounced ground clutter evident at 42 km, 62 km and 75 km ranges.

Good correlation between the data sets is evident at ranges where the precipitation echoes are not affected by ground clutter (30 km to 40 km). The effectiveness of the clutter algorithm at ranges were ground clutter exists, even in the presence of precipitation echoes, is shown. The clutter filter effectiveness, when no precipitation echoes are present, can be seen at ranges in excess of 60 km. The clutter suppression ratio is in the order of 30 dB which is especially significant in terms of rain rates.

6.3.2 Studies with rotating antenna

At 15:20 the antenna was rotated in azimuth through a part of the south-eastern sector of the radar area at approximately 3 r.p.m. Data were collected in a similar manner to that described in Section 6.3.1. In this case a delay of 4 μs (one PRF period) was used, After filtering, range averaging was performed over four samples and time-azimuth averaging over 16 PRF pulses. The reflectivity field was again adjusted to correspond to the quadratic DISPLACE averaged data in those areas not affected by ground clutter. Figure 6.21 shows the b-scan reflectivity plots for the unfiltered and filtered quadratic DISPLACE averaged data. The area shown represents a range from about 15 to 90 km from the radar and a sector between 100° and 150° in azimuth. The clutter filtering ratio again approached 30 dB, resulting in a remarkable improvement in the visual quality of the reflectivity field. Of note is the improvement in the area of ground clutter near the centre of the figures. The precipitation echoes were hardy affected in the process.

The examples shown provided the impetus to include the clutter filtering as part of the algorithm that is being developed for RVPC-2. This will facilitate routine data collection and proper evaluation of this technique.

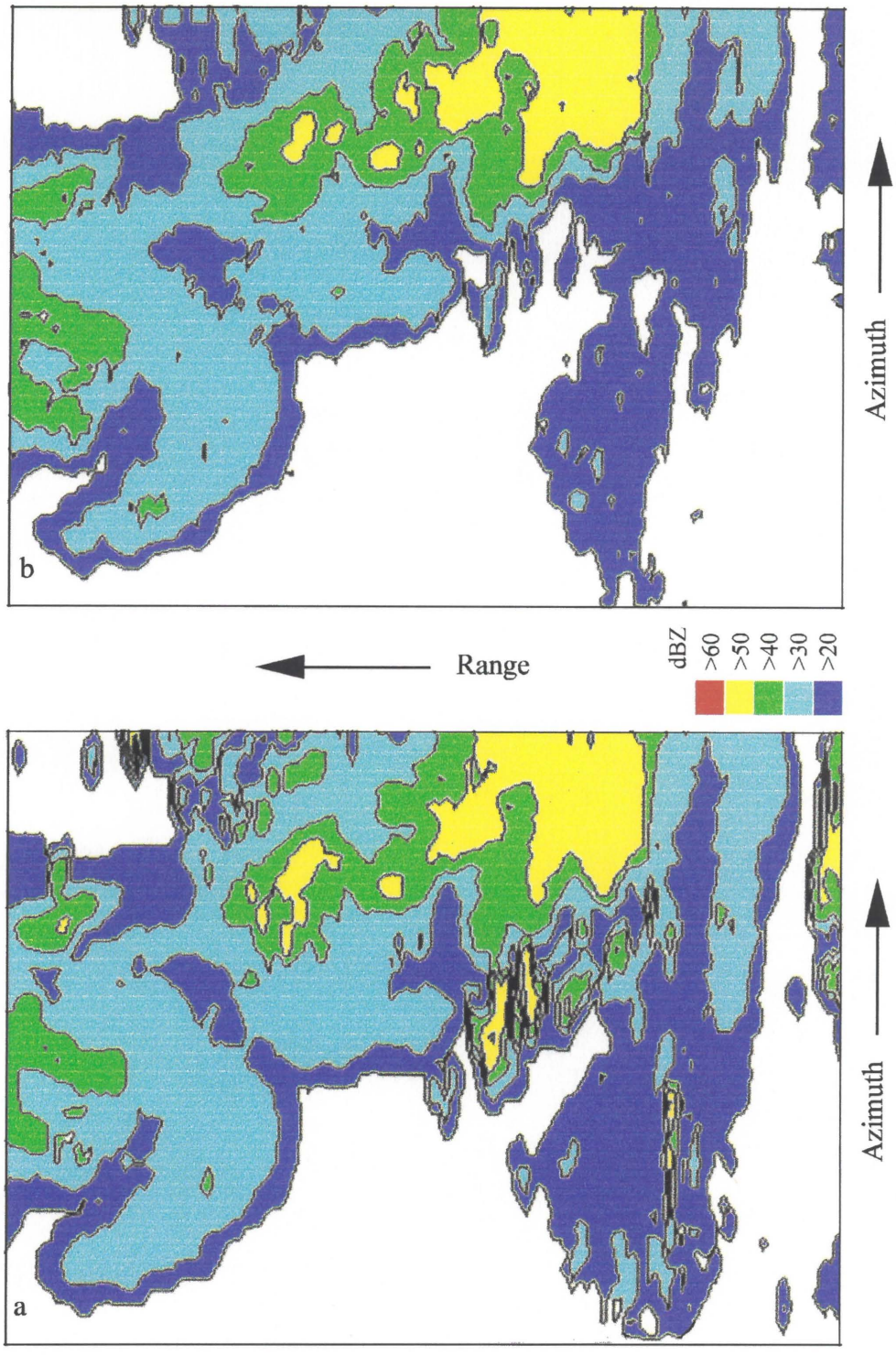

Figure 6.21 B-scan reflectivity plot: a. Unfiltered and, b. Filtered (see text).

6.4 SUMMARY

The quadratic DISPLACE algorithm eliminates the bias problems of conventionally averaged data which can lead to a difference of more than 20 % in total convective storm rainfall. The first case study in this chapter also indicates improvements in storm tracking with the use of quadratic DISPLACE averaged data. The magnitude of the observed differences in the properties, especially that of radar derived rainfall, is large. In addition to the problems associated with the limited sampling areas of rain gauges, this effect contributes significantly towards radar-rain-gauge discrepancies under intense convective conditions. The radar-rain-gauge analyses follow a holistic approach whereby radar and rain gauge data over entire rainfall events (during the time it was raining) were compared for large areas (Seed et al., 1996; Rosenfeld et al., 1993). This is in contrast to studies which focus on the spatial and temporal alignment of the data.

This chapter also provides some arguments for the use of a constant Z-R relationship in general radar-rainfall studies. There are many problems, not related to the drop-size distributions, which can lead to differences between radar and rain-gauge measurements of rainfall. These factors include insufficient sampling by rain gauges and influences by the bright band. Adjustments to the Z-R relationship will not lead to significant long term improvements in radar-rain-gauges ratios if the other factors are not addressed.

This chapter also illustrates the problems of attenuation at C-band under heavy rain conditions. This problem should be kept in mind by users of radar data, since all other weather radars in South Africa operate at C-band.

Figure 6.22 shows the radar-rain-rate probabilities (as a percentage) for all four rain events described in this chapter, plotted against the rain-gauge probabilities corresponding to the same rain-rates. Therefore, each plotted point on the graph represents a common radar and rain gauge rain rate. The data for all events align well, with the exception of those of the bright band episode on 25 March 1995. The 1:1 line is shown in addition to the regression ($R^2 = 0.95$) of the data (the bright band period is not included). A slight overestimation of the occurrence of frequent rain rates (the low rain rates that contribute significantly to the rainfall) and a more pronounced underestimation of the infrequent rain rates (high rain rates) are evident. The change occurs at those rain rates that occur about 30 % of the time. The difference between radar and rain-gauge rain-rate probabilities appear to be functionally dependent upon the rain-rate probabilities. In other words, during different rain events, the difference between radar and rain-gauge rain-rate probabilities will be similar for comparable rain-rate probabilities. These probabilities will not necessarily correspond to the same rain-rates. If this tendency can be confirmed, and the non-DSD problems of radar-rain-gauge discrepancies can be addressed, this could form the basis of an objective method of adjusting the Z-R relationship for each rain event. This should lead to better results than using the classical Marshall-Palmer Z-R.

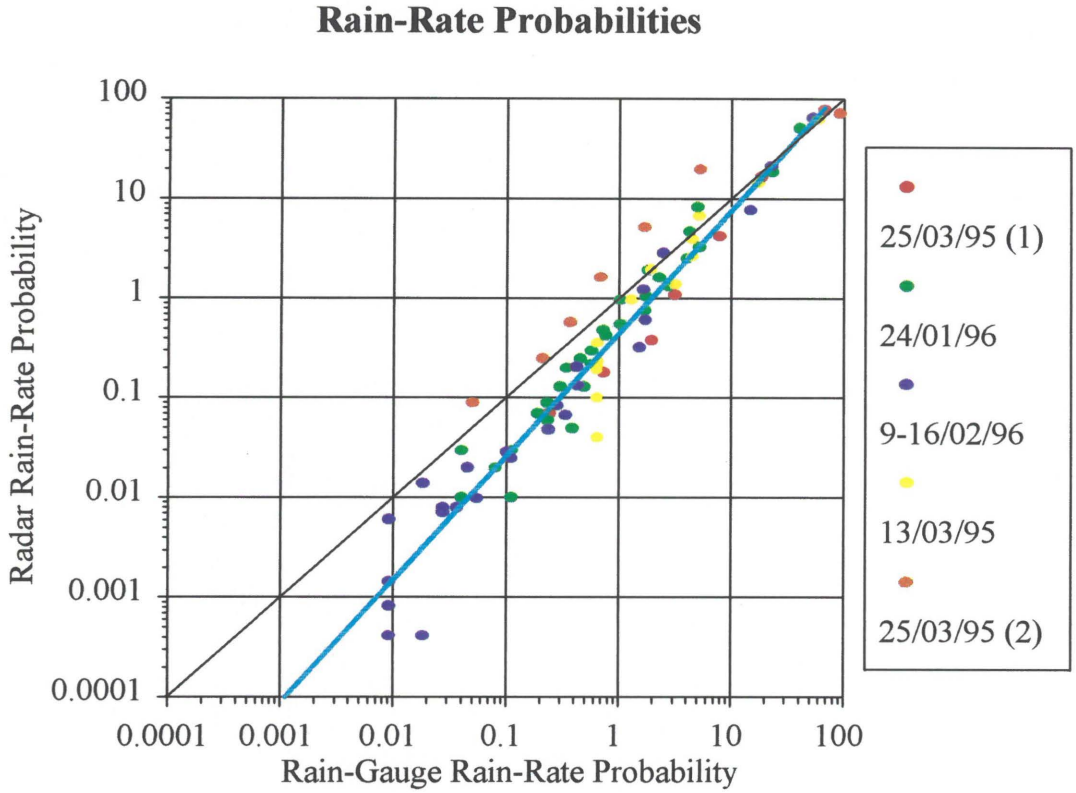

Figure 6.22 Radar-rain-rate probabilities as a function of rain-gauge-rain-rate probabilities for common rain rates. The 1:1 line is shown as well as a regression for all cases excluding the bright band period on 25 March 1995 (25/03/95 (2)).

CHAPTER 7

CONCLUSIONS AND RECOMMENDATIONS

7.1 CONCLUSIONS

A new method of processing the digitized output from a logarithmic radar receiver has been developed, tested and several of its applications implemented. The method is called DISPLACE and operates on digitized receiver data pairs, using look-up tables with pre-computed *displacement* values. The *displacement* values are dependent on the difference between the pair values and are scaled by the radar's calibration slope.

The applications of DISPLACE include:

- Processing the output from a radar's logarithmic receiver to simulate averages corresponding to general power law transfer functions. Specific applications include logarithmic, linear and quadratic responses.
- Calculating weighted averages in interpolation CAPPIs and exponentially weighted running averages.
- Processing the outputs from multi-parameter radars using logarithmic receivers.
- Facilitating ground clutter filtering in conventional weather radars using the characteristic signal fluctuations of precipitation scatterers.

The advantages of DISPLACE are:

- All calculations are integer based.
- All values remain smaller than the maximum value of the video signal's A to D conversion.
- A common algorithm is used to simulate the different receiver transfer functions.
- It requires only half the computer time of conventional averaging.
- Averaging of the video takes the same time for all simulated transfer functions.
- Using DISPLACE in interpolation CAPPIs halves the computation time by eliminating mathematical divisions and multiplications as well as the conversions between units.
- It leads to new ways of efficiently processing radar data.

The case studies presented in Chapter 6 were chosen for convective storm conditions and general rain. The rain-gauge networks were used in an integrated manner highlighting the following:

- The reliability of the equipment and the in-house developments, including the new CAPPI software.

- The quadratic displace averaged data improves the quality of storm track properties by eliminating the bias that exists after applying the averaging correction to conventionally averaged data from a logarithmic receiver.

- The over-amplified beam-broadening effects observed in conventionally averaged logarithmic receiver outputs are corrected with quadratic DISPLACE averaging.

- The Marshall-Palmer Z-R relationship works well for the conditions studied. Its use results in small overestimations at low rainfall rates and underestimations at high rainfall rates.

- Some of the major causes for deviations between radar and rain-gauge measurements of rainfall are not related to the Z-R relationship. The bright band and insufficient sampling by rain gauges are major problems.

- Comparisons of the radar and rain-gauge rain-rate frequencies over large areas, without temporal and spatial alignment of data, proved successful.

- There is a tendency for the difference in radar and rain-gauge measurements of rain rates over an area to be a function of the frequency of occurrence of rain rates during a specific rain event, rather than of the rain rates themselves.

- The potential for using DISPLACE to filter ground clutter was demonstrated.

The DISPLACE method, which simulates a quadratic receiver, has been introduced on both S- and X-band receivers of the MRL-5 radar (S-band - February 1995, X-band - October 1995), the Enterprise C-band radar at Bethlehem (May 1995) and the Pacer C-band radar at Tzaneen (October 1996). The method is also used on a C-band radar in Agen, France (June 1995) and in Mexico (June 1996). The South African RDAS is compatible with other user software (eg. TITAN) and in combination with the calibration software, contributes towards standardization of procedures and formats, improving data quality. The DISPLACE method can be introduced on the RDAS of nine other meteorological radars in South Africa without hardware changes and related expenses, contributing towards improving the accuracy of weather radar measurements.

The development of this new method has shown that the potential of conventional weather radar (with its logarithmic receiver) has not been fully exploited. The DISPLACE method, in combination with the other radar upgrades and procedures introduced in South Africa during the past few years has opened many opportunities for developing the weather radar infrastructure in South Africa to the advantage of meteorologists, hydrologists and the people of South Africa as a whole. It has stimulated renewed interest in radar meteorology in South Africa and paved the

way for young scientists and technicians to become involved.

Rainfall stimulation research in South Africa is entering a new phase. The randomized hygroscopic seeding experiment was concluded after the 1995/96 season after reaching a high level of statistical significance. The observed increases in rainfall from seeded storms must now be realized as an increase in areal rainfall, and this effect must be quantified. The work in this thesis coincides with this shift in emphases. In contrast to the importance of relative measurement between seeded and non-seeded storms of the randomized experiment, the emphasis will now shift to absolute rainfall measurements. Future work will include measuring area rainfall under convective conditions, isolating seeding signatures in treated storms and developing new and innovative ways to verify operational seeding experiments. Radar and the enhancement of its capabilities reported in this thesis will play a central role in these studies and will also provide meteorologists and hydrologists with a tool to better manage weather-related disasters.

7.2 RECOMMENDATIONS

The experienced gained with the radars in the Bethlehem area has led to the following suggestions:

- Radar data should be stored for research. In this way, feedback is established between researcher and radar engineer, thereby improving data quality. Engineers and researchers should interact closely and ideally form part of one group.

- The radar researcher should assume the role of radar forecaster when severe weather conditions occur. The arrangement whereby forecasters with little radar background are required to handle severe weather forecasts in addition to their normal work load is unrealistic.

- A radar network should not be planned and developed by administrators. It is a specialist field in which knowledgable people in South Africa, some not active in the field anymore, are often ignored.

- The administrators should rather focus their attention on training more radar specialists. Lack of trained people is the largest threat to the future of radar meteorology in South Africa. Successful use of equipment is an indication of the expertise and dedication of the people involved in using this equipment.

- For the intended use of the SAWB radar network and the limited resources available, conventional radar measurements provide ample opportunities to do research and develop practical forecasting systems. If funds are available they should rather be spent on providing uninteruptable power to the equipment. A good system will safeguard the equipment from lightning-introduced damages and will ensure that data is available when it is needed.

- A radar operated in volume-scan mode will provide data that will satisfy both the researcher and forecaster.

- The limitations of C-band radar in South African convective conditions should be kept in mind.

- The methods designed as part of this thesis indicate that radars should not be regarded as redundant purely on its year of manufacture. It is the processing of the output that is important and improvements in this regard will probably give a better return on investment. There is real danger in pursuing the latest radar technology at all costs. Many of the older radars are actually easier and cheaper to maintain than the latest equipment with their surface mounted circuitry.

- The implementation of the RDAS and its related tools and processing methods on more radars should be encouraged. This is helping to bring some order to data formats and quality of many radars. This can be of great benefit, especially within the international weather modification fraternity.

- Based on the experience gained with the Enterprise and MRL-5 sites our bias is towards the "hill-top" siting. Beam blocking is a bigger problem than some ground clutter. Logic must however prevail in the siting of radars as many other factors play a role.

- The development and implementation of methods to minimize the bright band's detrimental effect on radar-rainfall measurements should receive high priority.

- The ground-clutter filtering algorithm should be developed further to improve its performance for faster antenna rotation speeds. An approach in which the change in the DC component of ground clutter, due to the scanning of the known beam pattern is considered, has potential.

- The DISPLACE method has opened new ways of processing radar data in an efficient and flexible manner. Time should be spent on developing new applications of the method, on calibration tests and developing objective methods to filter phenomena that have a detrimental effect on radar-rainfall measurement. Little will be achieved by trying to perfect Z-R relationships.

APPENDIX

THE DISPLACE EQUATIONS

In Chapter 4 the basis for the DISPLACE method is given:

$$\log[(a+b)/2] = \log(a+b) - \log 2$$

$$= \log a + \log(1+b/a) - \log 2$$

$$= \log a + \mathbf{\log(1 + 10^{-(\log a - \log b)}) - \log 2} \qquad (4.1)$$

This can also be written as:

$$\log[(a+b)/2] = \log a - \mathbf{[\log 2 - \log(1 + 10^{-(\log a - \log b)})]}$$

Similar to the above but for the more general case we can write:

$$10\log[(P_1^a+P_2^a)/2]^{(1/a)} = 10\log[(P_1^a+P_2^a)]^{(1/a)} - 10\log(2)^{(1/a)}$$

$$= 10\log[(P_1)^a]^{(1/a)} + 10\log[1+(P_2^a/P_1^a)]^{(1/a)} - 10\log(2)^{(1/a)}$$

$$= 10\log P_1 + (10/a)\log[1+(P_2^a/P_1^a)] - (10/a)\log 2$$

$$= 10\log P_1 + (10/a)\log[1+10^{(a\log P2 - a\log P1)}] - (10/a)\log 2$$

$$= 10\log P_1 + (10/a)\log[1+10^{-(a/10)(10\log P1 - 10\log P2)}] - (10/a)\log 2$$

Using $10^{(1/10)} = 0.7943282$, we can now write:

$$= 10\log P_1 - \mathbf{(10/a)\{\log 2 - \log[1+0.7943282^{a(10\log P1 - 10\log P2)}]\}} \qquad (4.2)$$

All the DISPLACE equations are derived in this manner.

REFERENCES

Atlas D., 1951: Microwave scattering from nonspherical hydrometeors. Proc. Conf. On Water Resources, Bull. 41, Illinois State Water Survey, 269-276.

Atlas D., 1964: Advances in radar meteorology. Advances in Geophysics, Vol 10, Academic Press, New York, USA.

Atlas D., ed., 1990: Radar in Meteorology. Battan Memorial and 40th Anniversary: Radar Meteorology Conference, AMS., Boston, USA.

Atlas D. and Mossop S.C., 1960: Calibration of a Weather Radar by Using a Standard Target. Bulletin of the Amer. Meteoro. Soc., 41(7), 377-382.

Atlas D. and Ulbrich C.W., 1974: The physical basis for attenuation-rainfall relationships and the measurement of rainfall parameters by combined attenuation and radar methods. J Rech. Atmos., 8(1-2), 275-298.

Atlas D., Rosenfeld D. and Short D.A., 1990: The estimation of convective rainfall by area integrals. Part 1: The theoretical and empirical basis. J. Geophys. Res., 95 (D3), 2153-2160.

Battan L.J., 1973: Radar observation of the atmosphere. The University of Chicago Press, Chicago, USA.

Breit G. and Tuve M., 1926: A test of the existence of the conducting layer. Phys. Rev., 28, 554.

Byers H.R. and Braham R.R., Jr., 1949: The Thunderstorm. U.S. Govt. Printing Office, Washington DC, 287 pp.

Carte A.E., 1992: Stormy weather report. S. Afr. J. Sci. 88, 462-464.

Carte A.E. and Held G., 1978: Variability of hailstorms on the South African plateau. J. Appl. Met., 17, 365-373.

Chandrasekar V., Bringi V.N., Gray G.R. and Keeler R.J., 1989: Efficient Differential Reflectivity Processing Using Logarithmic Receivers. J Atmos Ocean Tech, 6, 4, 663-670.

CSIR, 1948: Artificial stimulation of precipitation: Interim progress report on experiments carried out by the CSIR, the Division of Meteorology and the South African Airforce. December 1947 to April 1948. CSIR, Pretoria, South Africa.

Dennis A.S., Koscielski D.E., Cain D.E., Hirsch J.H. and Smith P.L., 1975: Analysis of radar observations of a randomized cloud seeding experiment. J. Appl. Meteorol., 14, 897-908.

Dicks D., Hodson M.C., Held G. and Neishlos H., 1987: Initial results from the newly-developed CSIR Doppler pulse-pair processor. Abstract of the 4th Annual Conference of the South African Society for Atmospheric Sciences, Pretoria, 27.

Dixon M., and Mather G.K., 1986: Radar evaluation of a randomized rain-augmentation experiment - some preliminary results. Preprints, Tenth Conference on Planned and Inadvertent Weather Modification, Arlington, VA.

Dixon M., and Wiener G., 1993: TITAN: Thunderstorm Identification, Tracking, Analysis and Nowcasting - a Radar-based Methodology. J. Atmos. Ocean. Tech., 10(6), 785-797.
Doneaud A.A., Ionescu-Niscov S., Priegnitz D.L. and Smith P.L., 1984: The area-time integral as an indicator for convective rain volumes. J. Clim. Appl. Meteorol., 23(4), 555-561.

Doneau A.A., Ionescu-Niscov S., Priegnitz D.L. and Smith P.S., 1984: The area-time integral as an indicator for convective rain volumes. J. Climate Appl. Meteor., 23(4), 555-561.

Doviak R.J. and Zrnic D.S., 1984: Doppler Radar and Weather Observations. Academic Press, 458 pp.

Eccles P.J., 1979: Comparisons of remote measurement by single- and dual-wavelength meteorological radars. IEEE Trans. Geosci. Electron., GE-17, 205-218.

Eccles P.J. and Atlas D., 1973: A dual wavelength hail detector. J. Appl. Meteorol. 12, 847-856.

Fleischer S.L.M., 1980: Radar observationas in the BEMEX area. BEWMEX Progress Report 21, 47.

Gagin, A., D. Rosenfeld and H. Nozice, 1986: Report on the analyses of convective rain cells, in the region of Bethlehem, R.S.A. as a basis for a rainfall enhancement experiment. Report to the Water Research Commission, Pretoria, South Africa.

Geotis S.G. and Silver W.M., 1976: An Evaluation of Techniques for Automatic Ground-echo Rejection. Preprints, 17th Conf. on Radar Meteorol., Boston, AMS., 448-452.

Goldhirsch J. And Katz I., 1974: Estimation of raindrop size distribution using multiple wavelength radar systems. Radio Sci., 9(4), 439-446.

Gorgucci, E., G. Scarchilli and R.M. Leonardi, 1986: Possibility of ground echo cancellation by means of bias measurement. 23rd Conf. on Radar Meteorol., Snowmass. AMS. JP329-332.

Gorgucci E., Chandrasekar V., Scarchilli G. and Leonardi R., 1989: Radar receiver transfer function from correlated meteorological signal. 24th Conf. on Radar Meteorol., Tallahassee, AMS, 443-446.

Green A.W., 1975: An approximation for the shapes of large raindrops. J. Appl. Meteorol., 14, 1578-1583.

Harrison M.S.J., 1974: An Introduction to the Bethlehem Weather Modification Experiment. Part 1. Technical Paper No 1, Weather Bureau, Pretoria.

Held G., 1978: The probability of hail in relation to radar echo heights on the South African Highveld. J. Appl. Met., 17, 755-762.

Held G., 1982: Comparison of radar observations of a devastating hailstorm and a cloudburst at Jan Smuts Airport. Cloud Dynamics eds. E.M. Agee and T. Asai, D Reidel Publ. Co., Dordrecht.

Held G. and Carte A.E., 1973: Thunderstorms in 1971/72. CSIR Research Report 322, 1-77.

Held G. and Gomes A.M., 1992: The first case study of a thunderstorm in South Africa based on dual-Doppler radar observations. S. Afr. J. Sci. 88, 516-524.

Hewitt F.J., 1953: The study of lighting streamers with 50 cm radar. Proc. Phys. Soc. London, B 66, 895-897.

Hewitt F.J., 1957: Radar echoes from inter-stroke processes in lightning. Proc. Phys. Soc. London, B 70, 961-979.

Hewitt F.J., 1975: South Africa's role in the development and use of radar in World War 2. S.A Inst. Elec. Eng., 230-235.

Hodson M.C., 1993: An Analysis of the meteorological and volume sampling effects on the comparison of radar and raingauge measurements of rainfall. Phd thesis. University of the Witwatersrand, Johannesburg.

Hodson M.C. and Peter T.V., 1964: Observations of the ellipticity of raindrops using a polarized radar system. Preprints, 11th Radar Meteorology Conf., Boulder, AMS, 188-191.

Krauss T.W., Bruintjes R.T. and J. Verlinde, 1987: Microphysical and radar observations of seeded and non-seeded continental cumulus clouds. J. Climate Appl. Meteor., 26, 585 - 606.

Marshall J.S. and Hitschfeld W., 1953: Interpretation of the fluctuating echo from randomly distributed scatterers. Can. Jour. Phys., 31, Pt 1, 962-995.

Marshall J.S., Lagille R.C. and Palmer W.McK., 1947: Measurement of rainfall by radar. J. Meteor., 4, 186-192.

Marshall J.S. and Palmer W.McK., 1948: The distribution of raindrops with size. J. Meteorol., 5, 165-166.

Mather G.K., 1989: Estimates of Precipitation Embryo densities using measurements from a aircraft radar. J. Appl. Meteorol., 28(10), 1089-1097.

Mather G.K., Dixon M. and de Jager J.M., 1996: Assessing the potential for rain augmentation - The Nelspruit randomized convective cloud seeding experiment. Accepted for publication in J. Appl. Meteorol.

Mather G.K. and Terblanche D.E., 1993: The National Precipitation Research Programme: Final Report 1990-1992. WRC Report, Pretoria.

Mather G.K. and Terblanche D.E., 1994: Initial Results from Cloud Seeding Experiments Using Hygroscopic Flares. Proceedings 6th WMO Scientific Conference on Weather Modification, Paistum, Italy. 687-690.

Mather G.K. and Terblanche D.E., 1996: The National Precipitation Research Programme: Final Report 1993-1996. WRC Report, Pretoria (in press).

Miles V.G., 1952: Radar echoes and lightning. Nature, 170, 365-366.

Miles V.G., 1953: Radar echoes associated with lightning. J. Atmos. Terrest. Phys., 3, 258-262.

Mittermaier M.P. and Terblanche D.E., 1997: Converting weather radar data to Cartesian space: A new approach using DISPLACE averaging. Accepted for publication in Jan 1997 Water SA.

Mueller E.A. et al., 1995: CSU-CHILL radar upgrades. 27th Conf. On Radar Meteorol, Vail, AMS, 703-706.

Probert-Jones J.R., 1962: The radar equation in meteorology. Quart. J.Roy. Meteor. Soc., 88, 485-495.

Rogers R.R., 1971: The effect of variable target reflectivity on weather radar measurements. Quart. J. Roy Meteor. Soc., 97, 154-167.

Rosenfeld D., 1988: Evaporation of rain falling from convective clouds as derived from radar measurements. J. Applied Meteor., 27, 209-215.

Rosenfeld D. and A. Gagin, 1989: Factors governing the total rainfall yield from continental convective clouds. J. Appl. Meteor., 28, 1015-1030.

Rosenfeld D., Atlas D. and Short D.A., 1990: The estimation of convective rainfall by area integrals. Part II: The height area rainfall threshholds (HART) method. J. Geophys. Res., 95, 2161-2176.

Rosenfeld D.,Wolff D.B. and Atlas D., 1993: General probability-matched relations between radar reflectivity and rain rate. J. Appl. Meteor., 32, 50-72.

Ryde J.W., 1941: Echo intensities and attenuation due to clouds, rain, hail sand and dust storms. Rep. No. 7831, General Electric Laboratory, Wembley, England, 48pp.

Scarchilli G., Gorgucci E., Iacovelli P. and Leonardi R.M., 1982: Information from bias measurements. Seminar on Radar Meteorology, ERICE, WMO No 626, 152-184.

Scarchilli G., Gorgucci E., and Leonardi R.M., 1986: Theory and optimization of the excess bias measurement. J. Atmos. Oceanic. Technol., 3 (2), 217-229.

Schaffner M., 1978: Processing by data and program blocks. IEEE Trans. Comp., Vol C-27, 1015-1028.

Seed A.W., 1992: Generation of a spatially distributed daily rainfall database for various weather modification scenario. Report to the WRC, Pretoria, WRC 373/1/92.

Seed A.W., Nicol J, Austin G.L., Stow C.D. and Bradley S.G., 1996: The impact of radar and rain-gauge sampling errors when calibrating a weather radar. Meteorol. Appl., 3, 43-52.

Seliga T.A. and Bringi V.N., 1976: Potential use of radar differential reflectivity measurements at orthogonal polarizations for measuring precipitation. J. Appl. Meteor., 15, 69-76.

Sirmans D., and Doviak J., 1973: Meteorological radar signal intensity estimation. ERL-NSSL-64, NOAA Technical Memorandum, Norman, Oklahoma, 80.

Skolnik M.I., ed., 1970: "Radar Handbook." McGraw-Hill, New York.

Skolnik M.I., 1981: Introduction to radar systems. International Student Addition, McGraw-Hill, Johannesburg, RSA.

Smith P.L., 1986: On the sensitivity of weather radars. J. Atmos. Oceanic. Technol., 3, 704-713.

Smith P.L., 1995: Dwell-time Considerations for Weather Radars. Preprints 27th Conf. On Radar Meteor. AMS, Vail, 760-762.

Smith P.L. et al., 1982: Research on evolving design and evaluation of the HIPLEX program: Final technical report. Rep. 82-7, Institute of Atmospheric Science, South Dakota School of Mines and Technology, 128 pp.

Steyn P.C., and Bruintjes R.T., 1990: Convective cloud characteristics for the Bethlehem area. Water SA, 16-2, 115-118.

Tatehira R. and Shimizu T., 1978: Intensity measurements of precipitation echo superposed on ground clutter: A new automated technique for ground clutter rejection. 18th Conf. on Radar Meteor., AMS, Atlanta, 364-369.

Tatehira R. and Shimizu T., 1980: Improvement in Performance of ground Clutter Rejection. Preprints, 19th Conf. On Radar Meteor., AMS, Boston, 176-179.

Tatehira R., 1980: Operational use of echo phase by conventional radar (In Japanese). 27, 12, 3-8.

Terblanche D.E., Pienaar H.G. and de Waal K.P.J., 1993: Radar rainfall studies over the northeastern Free State. Preprints, 6th National Hydrological Symposium, Pietermaritzburg.

Terblanche D.E, Hiscutt F.O. and Dicks D.J., 1994: The upgrading and performance testing of the Bethlehem weather radar. S.A. Jour. Sci., 90, 588-595.

Terblanche D.E., 1995: Simulating Linear, Logarithmic and Quadratic Responses from a Radar's Logarithmic Receiver by a Simple Digital Signal Processing Method. Preprints, 27th Conf. on Radar Meteor, AMS, Vail, 769-770.

Terblanche D.E., 1996: A simple digital signal prosessing method to simulate linear and quadratic responses from a radar's logarithmic receiver. J. Atmos. Ocean. Tech., 13(2), 533-538.

Visser P.J.M. and le Roux E., 1993: The radar network of the Weather Bureau. Tenth Annual Conference, S.A. Society for Atmospheric Sciences, 72.

Walker G.B., Ray P.S., Zrnic D. and Doviak R., 1980: Time, angle and range averaging of radar echoes from distributed targets. J. Appl. Meteorol., 19, 315-323.

Wexler R. and Atlas D., 1963: Radar reflectivity and attenuation of rain. J. Appl. Meteorol., 2, 276-280.

Zrnic, D.S., 1977: Mean power estimation with a recursive filter. IEEE Trans. Aerospace and Electr., Vol. AES 13, 218-289.

Xiao R. And Chandrasekar V., 1995: Multiparameter radar rainfall estimation using Neural Network Techniques. 27th Radar Conf., AMS, Vail, 199-201.